Ministère de l'enseignement Supérieur et de la recherche Scientifique

وزارة التعليم العالي والبحث العلمي

Badji Mokhtar Annaba University
Université Badji Mokhtar – Annaba
Faculté de Technologie

Département Génie Civil

جامعة باجي مختار – عنابـــة

كـليـة التكنـولـوجيـا

قســم الهندسة المدنية

Thèse

Présentée pour obtenir le diplôme de

Doctorat Troisième Cycle

Filière : Genie Civil

Spécialité : Structures

Par :

BOUDEBOUDA Afaf

Thème :

Contribution to the Seismic Hazard Assessment in Northeastern Algeria

Thèse soutenue le …….. 07/07/2025 ……. devant le jury composé de :

N°	Nom et prénom	Grade	Etablissement	Qualité
01	**DJEGHABA Kamel**	Prof.	Université de Badji Mokhtar -Annaba	Président
02	**ATHMANI Allaeddine**	MCA	Université de Badji Mokhtar -Annaba	Rapporteur
03	**KEBAILI Bachir**	MCA	Université de Badji Mokhtar -Annaba	Examinateur
04	**FILALI Kamel**	MCA	Université 20 août 1955 - Skikda	Examinateur
05	**HABES Sameh**	MCA	Ecole Nationale Supérieure de Technologie et de l'Ingénierie – Annaba	Examinatrice

" المساهمة في تقييم المخاطر الزلزالية في شمال شرق الجزائر "

الملخص:

تُعرف المنطقة الشمالية الشرقية من الجزائر بنشاطها الزلزالي الكبير ضمن سياق شمال أفريقيا. يُسفر معدل النشاط الزلزالي العالي في هذه المنطقة عن مخاطر زلزالية كبيرة ، وفقًا لخريطة تقسيم المناطق الزلزالية الوطنية في الجزائرتقع المنطقة الشمالية الشرقية ضمن المناطق الأولى والثانية، التي تتميز بنشاط زلزالي منخفض إلى متوسط. ومع ذلك، يمكن أن تُسبب الزلازل ذات الحجم المنخفض نسبيًا أضرارًا كبيرة، لا سيما عندما تكون المباني ذات جودة منخفضة وبالنظر إلى الأحداث القوية الأخيرة، يتضح عدم كفاية خريطة تقسيم المناطق الزلزالية لاستيعاب الأحداث الكبيرة في المنطقة وبالتالي، يصبح من الضروري إجراء تقييم موثوق للمخاطر الزلزالية يأخذ في الاعتبار التطورات الحديثة في هذا المجال، لتعزيز تصميم المباني والحد بشكل فعّال من المخاطر الزلزالية في هذه المنطقة.

تهدف هذه الرسالة إلى تحسين تقييم المخاطر الزلزالية في شمال شرق الجزائر من خلال دمج بيانات جديدة، والنظر في مصادر الزلازل، وتوقعات حركة الأرض، ومعالجة الشكوك المتأصلة بعمق. من الإسهامات الهامة لهذا العمل هو تطوير كتالوج زلزالي جديد، والذي يُعد عنصرًا أساسياً لتحليل المخاطر الزلزالية. يتم تنقية الكتالوج باستخدام تقنيات متقدمة ومعايير واضحة. قمنا بإنشاء كتالوج لحظي موحد باستخدام علاقات التحجيم المحلية بين مقاييس الزلازل المختلفة ولحظة الحجم. سيكون الكتالوج المُعد في هذه الدراسة مفيدًا لتطبيقات زلزالية متعددة، بما في ذلك تقييم المخاطر الزلزالية، وإعداد معادلات توقع حركة الأرض ، والزلازل، والزلازل التكتونية، والتنبؤ بالزلازل في منطقة الدراسة

تم تحديد توزيع المخاطر من حيث تسارع الذروة الأرضية لموقع واحد ولعدة مواقع في منطقة الدراسة والتسارعات الطيفية لفترات مختلفة لتقييم تسارع الذروة الأرضية، تم استخدام برنامج ريسيس لتحليل المخاطر الزلزالية الاحتمالي .تم تنفيذ تحليل المخاطر الزلزالية الاحتمالية باستخدام منهجية شجرة المنطق القياسية، مما يسمح بالنظر المنهجي في الشكوك المستندة إلى النموذج وتأثيراتها على معلمات حركة الأرض المقدرة. تُعد هذه الخرائط للمخاطر الزلزالية أدوات قيمة لتقييم المخاطر المستقبلية للهياكل في المناطق المحددة.

كلمات مفتاحية: شمال شرق الجزائر ، النشاط الزلزالي ، المخاطر الزلزالية ، كتالوج زلزالي ، المخاطر الزلزالية الاحتمالية، تسارع الذروة الأرضية ، شجرة المنطق.

« Contribution a l'évaluation de l 'alea séismique dans le Nord-Est Algérien»

Résumé :

La région nord-est de l'Algérie est réputée pour son activité sismique significative dans le contexte nord-africain. Le taux de sismicité élevé dans cette zone génère un risque sismique considérable. Selon la carte nationale de zonage sismique du RPA, la région nord-est de l'Algérie se trouve dans les zones I et II, caractérisées par une sismicité faible à modérée. Cependant, même les tremblements de terre de faible magnitude peuvent causer des dommages importants, en particulier lorsque les bâtiments sont de mauvaise qualité. Compte tenu des événements récents, l'insuffisance de la carte de zonage du RPA pour tenir compte des grands événements dans la région est évidente. Par conséquent, une évaluation fiable du risque sismique, tenant compte des récents progrès dans le domaine, est impérative pour améliorer la conception des bâtiments et réduire efficacement le risque sismique dans cette zone. Cette thèse vise à améliorer l'évaluation du risque sismique dans le nord-est de l'Algérie en intégrant de nouvelles données, des considérations de sources sismiques, des prévisions de mouvements du sol, et en abordant de manière exhaustive les incertitudes inhérentes. Une contribution significative de ce travail est le développement d'un nouveau catalogue sismique, qui sert d'élément fondamental pour l'analyse du risque sismique. Le catalogue est affiné grâce à des techniques avancées et des critères clairs. Nous avons établi un catalogue unifié de magnitudes de moment en utilisant des relations d'échelle locales entre différentes mesures de magnitude et la magnitude de moment. Le catalogue préparé dans cette étude sera utile pour diverses applications sismologiques, y compris l'évaluation du risque sismique, la préparation d'équations de prévision de mouvement du sol (GMPE), la sismicité, la sismotectonique, et la prévision des tremblements de terre dans la zone d'étude. La distribution du risque a été quantifiée en termes d'accélération maximale du sol (PGA) et d'accélérations spectrales pour différentes périodes. Pour évaluer la PGA, le logiciel REASSESS V2.0 a été utilisé pour l'analyse probabiliste du risque sismique (PSHA) sur un ou plusieurs sites dans la zone étudiée. Le PSHA a été réalisé en utilisant une méthodologie d'arbre logique standard, permettant une considération systématique des incertitudes basées sur le modèle et de leurs effets sur les paramètres de mouvement du sol estimés. Ces cartes de risque sismique sont des outils précieux pour les futures évaluations des risques pour les structures dans les régions spécifiées.

Mots clés : Nord-Est de l'Algérie, Activité sismique, Aléa sismique, Catalogue Sismique, Risque Sismique Probabiliste, Accélération Maximale du Sol, Arbre Logique.

« Contribution to the Seismic Hazard Assessment in Northeastern Algeria »

Abstract:

The northeastern region of Algeria is renowned for its significant seismic activity within the North African context. The high seismicity rate in this area generates a considerable earthquake hazard. According to the national seismic zoning map of RPA, the northeastern region of Algeria falls within zones I and II, characterized by low to moderate seismicity. However, even earthquakes of relatively low magnitude can cause significant damage, particularly when buildings are of poor quality. Considering recent strong events, the inadequacy of the RPA zoning map to accommodate large events in the region is evident. Consequently, a reliable seismic hazard assessment, accounting for recent advancements in the field, is imperative to enhance building design and effectively mitigate seismic risk within this area. This thesis aims to improve the seismic hazard assessment in northeastern Algeria by incorporating new data, seismic source considerations, ground motion predictions, and thoroughly addressing inherent uncertainties. A significant contribution of this work is the development of a new seismic catalog, which serves as a foundational element for seismic hazard analysis. The catalog is refined through advanced techniques and clear criteria. We established a unified moment magnitude catalog using local scaling relationships between different magnitude measures and moment magnitude. The catalog prepared in this study will be useful for various seismological applications, including seismic hazard assessment, preparation of ground motion prediction equations (GMPE), seismicity, seismotectonics, and earthquake prediction in the study area. The hazard distribution was quantified in terms of Peak Ground Acceleration (PGA) and spectral accelerations for different periods. To evaluate the PGA, the REASSESS V2.0 software was used for single and multi-site Probabilistic Seismic Hazard Analysis (PSHA) in the area under study. The PSHA was performed using a standard logic tree methodology, allowing for a systematic consideration of model-based uncertainties and their effects on the estimated ground motion parameters. These seismic hazard maps are valuable tools for future risk assessments of structures in the specified regions.

Key words : Northeast Algeria, Seismic Activity, Seismic Hazard, Seismic Catalog, Probabilistic Seismic Hazard Analysis, Peak Ground Acceleration, Logic Tree.

Acknowledgements

First and foremost, I am profoundly grateful to God for granting me the strength, patience, and perseverance needed to complete this journey. Without His guidance and blessings, none of this would have been possible.

I would like to extend my deepest gratitude to my supervisor, Dr. Athmani Allaeddine, for his unwavering support, invaluable guidance, and continuous encouragement throughout the course of my research. His insights and expertise have been instrumental in shaping this work.

I am also immensely thankful to the members of the jury for taking the time to read my thesis and for providing their thoughtful comments and constructive feedback.

A special thanks to Mr. Formisano, Associate Professor of Structural Design in university of Naples Federico II, for his warm welcome and the enriching training period I experienced in Italy. His hospitality and mentorship were truly inspiring and greatly contributed to my professional growth.

To my parents, words cannot express how grateful I am for their endless love, sacrifices, and unwavering belief in me. Your support and encouragement have been my foundation, and I owe my accomplishments to your boundless faith and constant prayers.

To my sisters and brothers, thank you for always being there for me, providing encouragement, and sharing in both my struggles and triumphs. Your love and support have meant the world to me.

To my daughters, Sidra and Manessa, you are my greatest joy and my ultimate motivation. Your smiles and hugs have been a constant source of strength, reminding me why I strive to achieve my best.

Finally, a very special thank you to my husband, Dr. Ahmed Nasri. Your steadfast support, patience, and belief in me have been my rock throughout this journey. Thank you for standing by my side through every challenge and celebrating every success. Your love and encouragement have been my greatest source of strength and inspiration.

This thesis is dedicated to all of you. Without your love and support, this achievement would not have been possible.

Index

List of Figures

List of Tables

GENERAL INTRODUCTION

• Problem Statement and Main Contribution

The Mediterranean region is known for its seismic activity, primarily attributed to the gradual convergence of the African and Eurasian tectonic plates, which occurs at a rate of approximately 5 mm/year (Beldjoudi, 2011). This tectonic interaction is particularly pronounced in the eastern Mediterranean, resulting in significant seismic hazards (Vannoli & Console, 2023). Within this context, the northeastern region of Algeria, located between 35° and 38° N latitude and 4° to 8.5° E longitude, emerges as one of the most seismically active areas of the Mediterranean basin (Abacha et al., 2023; Hamidatou et al., 2021). Recent studies indicate that this region has recorded nearly half of Algeria's seismic events over the last 15 years, as reported by the Algerian Digital Seismic Network (Yelles-Chaouche et al., 2022).

While the national seismic zoning map of RPA (2004) classifies northeastern Algeria within low to moderate seismicity zones (I and II), the reality on the ground reflects a need for greater scrutiny. Even low-magnitude earthquakes can cause substantial damage, especially in structures lacking adequate design and construction standards (Athmani & Ademovic, 2023). Historical events, such as the 1985 Constantine earthquake (M_s = 6.0) and more recent quakes like the 2020 Mila earthquake (M_w = 5.3) and the 2021 Béjaia earthquake (M_w = 6.0), underscore the potential for catastrophic impacts from earthquakes of moderate magnitude. Thus, the inadequacy of the existing seismic zoning map is evident, particularly in light of recent strong seismic events. A comprehensive seismic hazard assessment that incorporates the latest advancements in seismic hazard analysis is imperative to enhance building design standards and effectively mitigate seismic risk in the region.

This thesis aims to fill the existing gap in seismic hazard assessment for northeastern Algeria. By leveraging updated methodologies and comprehensive data compilation, it presents a detailed and state-of-the-art probabilistic seismic hazard assessment (PSHA) tailored to this seismically active region.

• Overview of Chapters

The thesis is structured into four chapters, each addressing critical aspects of seismic hazard assessment:

1. Fundamentals of Earthquakes and Magnitude Scaling: This chapter introduces the foundational concepts essential for understanding earthquake science, covering the processes that generate earthquakes, the terminology used to describe their occurrence, and the types of seismic waves produced. It further explores the various magnitude scales and the methodologies used to convert between them, emphasizing the selection and reliability of regression methods in accurately measuring earthquake size. Together, these concepts lay the groundwork for analyzing seismic hazards with consistency and precision.
2. Earthquake Data Compilation and Development of a Unified Seismic Catalog: This chapter outlines the methodologies used to process earthquake catalogs, which serve as a foundation for seismic hazard analysis. It details the steps necessary for developing a new earthquake catalog specific to the region under study, including magnitude conversion, declustering, and completeness analysis. A critical component in preparing this catalog is the magnitude conversion law, derived using the General Orthogonal Regression (GOR) method. Recently gaining popularity for magnitude conversions, the GOR method requires careful estimation of standard deviations associated with different magnitude types to determine an accurate error variance ratio. Leveraging recent research, this study approximates these standard deviations for various magnitudes and calculates the error variance ratio based on magnitude uncertainties. This application of GOR enables effective earthquake magnitude homogenization and fills a significant research gap in Algeria by developing regional empirical relationships with appropriate error variance ratios.

3. Seismicity Analysis and Characterization of Seismic Source Zones: This chapter outlines the geographic, geomorphological, and seismotectonic context of the study area. It includes a detailed characterization of seismic sources, representing a crucial first step toward effective seismic hazard analysis.
4. Comprehensive Seismic Hazard Assessment for Northeastern Algeria: Methodologies and Regional Application: This chapter provides an in-depth exploration of seismic hazard assessment methodologies, covering both probabilistic and deterministic approaches essential for evaluating and defining seismic design parameters. Building on these fundamentals, it applies the probabilistic seismic hazard assessment (PSHA) specifically to the northeastern region of Algeria, leveraging the classical Cornell–McGuire methodology. The findings, presented through Peak Ground Acceleration (PGA), Spectral Acceleration (SA), and Uniform Hazard Spectra (UHS), are complemented by a detailed hazard map generated with REASSESS software.

Through this comprehensive approach, the thesis contributes significantly to the understanding and mitigation of seismic hazards in northeastern Algeria, providing a vital resource for stakeholders involved in earthquake risk management and infrastructure resilience.

CHAPTER I: FUNDAMENTALS OF EARTHQUAKES AND MAGNITUDE SCALING

1 Fundamentals of Earthquakes

1.1 Introduction

Earth is a dynamic planet with uncontrollable internal movements and vibrations that can lead to natural disasters. Among these, earthquakes have had the most profound impact on humanity. Today, hundreds of millions of people worldwide face significant risks to their lives and property due to earthquakes. Billions of dollars' worth of public infrastructure are perpetually threatened by earthquake damage, posing a menace to the health of local, regional, and even national economies. Since 1900, earthquakes have killed approximately 8,5 million people and caused $ 2 trillion of damage (Baker et al., 2021).

Earthquakes have been happening for millions of years and will continue indefinitely. Seismic processes are highly unpredictable and may result in very large economic and social losses. Consequently, they demand special attention and risk planning based on reliable protection and prevention plans. In the last few centuries, it has been a concern of humankind to create safer environments to live in, making time-consuming efforts to reveal how seismic activities occur and the causal relationship between earthquake properties and their destructive effects. Although the immediate consequences of earthquakes and their effects on people living in regions where seismic activity becomes significant are well known, much remains uncertain about the timing of earthquakes, the resulting ground shaking, and how structures will perform under such stress (Kramer, 1996).

Seismic hazard assessment is essential for estimating potential ground shaking in a region over a specified period. These estimates are crucial for evaluating an area's seismic vulnerability and guiding the construction and retrofitting of buildings to endure future earthquakes (Kolathayar & Sitharam, 2018). Although formal seismic hazard and risk analysis concepts have only existed for about 50 years, their continued development has made them integral to designing and assessing structures in seismic regions, ensuring that risks remain within societally acceptable limits. In order to fully understand the nature of earthquakes and their implications, it is essential to grasp several fundamental concepts. This chapter will provide key definitions and explanations related to earthquakes, including how they are produced, the terminology used to describe their locations, the types of seismic waves they generate, and how the size of an earthquake is measured.

1.2 Hazard and Risk Analysis

In assessing the potential danger posed by earthquakes, it is useful to distinguish between hazard and risk. Seismic hazard and seismic risk are fundamentally different. *Hazard analysis* involves identifying and describing the natural phenomena that occur during earthquakes. This includes examining several physical effects produced by seismic activity. In the specific sense, seismic hazard is the likelihood, or probability, of experiencing a specified intensity of any damaging phenomenon at a particular site, or over a region, in some period of interest (Thenhaus et al., 2003). Earthquakes generate seismic waves, leading to ground shaking in the surrounding areas. They also cause permanent displacements in the form of ruptures, uplifts, and folding. Ground shaking and permanent displacements are primary hazards. Earthquakes induced primary hazards can also cause secondary hazards such as, tsunamis, landslides, soil liquefaction, and floods (Baker et al., 2021). In fact, ground shaking can be considered to be the most important of all seismic hazards because all the other hazards are caused by ground shaking.

Risk analysis focuses on understanding the potential consequences of these hazards, such as structural damage, fatalities, and economic losses. Conducting a risk analysis requires a comprehensive hazard analysis as well as an understanding of exposure and vulnerability (Wang, 2009).

- Exposure: This refers to the presence and value of people, buildings, infrastructure, and other assets in hazard-prone areas. High exposure implies that many elements could potentially be affected by an earthquake. For example, densely populated urban areas with critical infrastructure like hospitals and bridges are considered highly exposed.

- Vulnerability: Vulnerability defines the degree to which exposed elements can be damaged or disrupted when subjected to earthquake effects. It depends on factors like building design, construction quality, material strength, and local soil conditions. For example, unreinforced masonry structures are more vulnerable than modern engineered buildings.

In general, seismic risk can be expressed qualitatively as (Eq.1)

$$Risk = Hazard * Vulerability * Exposure \quad (1)$$

Therefore, while hazard is an unavoidable geological fact, risk is influenced by human factors. Regions with high hazard can have low risk if they are sparsely populated, whereas areas with moderate hazard can have high risk due to dense populations and inadequate construction practices.

1.3 Earthquakes

From a geological perspective, an earthquake results from the release of accumulated energy within the Earth's lithosphere. This energy builds up due to deformations in the rock, causing stress to accumulate along fault planes. When the stress exceeds the strength of the rocks, it results in a rupture or slip along the fault line, which releases the stored elastic energy suddenly. This sudden release generates seismic waves that propagate through the Earth's crust, leading to ground shaking. An earthquake initiates at a specific point known as the focus or hypocenter, where the first seismic waves originate. The focus is located at a certain depth below the ground, known as the focal depth or hypocentral depth, while the point on the surface directly above it is called the epicenter. The distance between the observer and the epicenter is referred to as the epicentral distance, whereas the distance between the observer and the focus is known as the focal or hypocentral distance (Fig. I. 1).

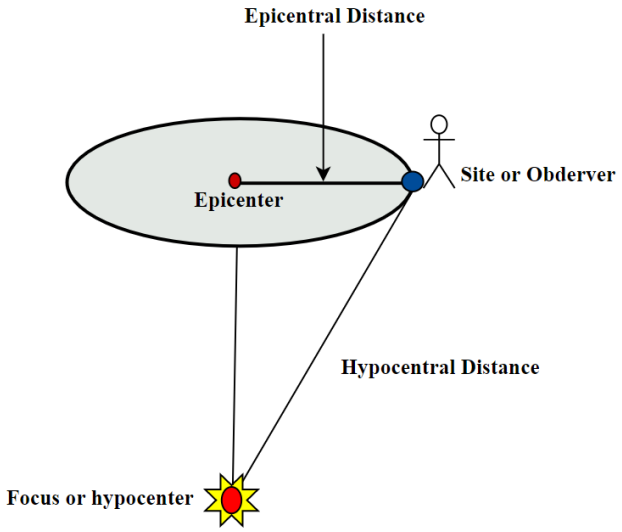

Fig. I. 1: Notation for description of earthquake location

1.4 Earth Structure and Theory of Global Plate Tectonics

The Earth is composed of several distinct layers, with the primary divisions being the thin crust, the thick mantle, and the outer and inner core (Fig. I. 2, first panel). While the Earth's surface, shielded by our atmosphere, remains relatively cool, temperatures rise dramatically toward the core. Most of the significant temperature differences occur within the mantle. Although solid, the mantle behaves like a viscous fluid over geological time scales due to the presence of convective cells formed by the thermal gradient. These cells exert shear forces on the base of the crust, driving the motion of tectonic plates (Jaeger et al., 2007). The flow within the mantle, whether converging or diverging, leads to regions of the crust being subjected to compression or tension, respectively. However, the Earth's crust is not a continuous surface; it is made up of individual tectonic plates (Wegener, 1912). The theory of plate tectonics, developed in the early 1960s, is now the dominant explanation for many geological phenomena, particularly earthquakes. The Earth's lithosphere is divided into approximately 15 large, rigid plates, which are continuously in motion due to convection currents in the mantle. Both continents and oceans rest on these plates, which once formed a single supercontinent that began breaking apart roughly 200 million years ago. The plates move at a rate of a few centimeters per year. While minimal deformation occurs within the plates themselves, significant deformation takes place at their boundaries, giving rise to earthquakes, mountain formation, volcanism, and other geological processes (Saouma & Hariri-Ardebili, 2021). Fig. I. 2 (second panel) demonstrates global plate movements. Earthquakes originate within the Earth's crust, where temperatures are cool enough to permit the brittle failure of rocks. The maximum depth at which earthquakes occur within the crust is known as the seismogenic thickness, which typically ranges between 10 and 20 kilometers, though this varies by region (Scholz, 2019).

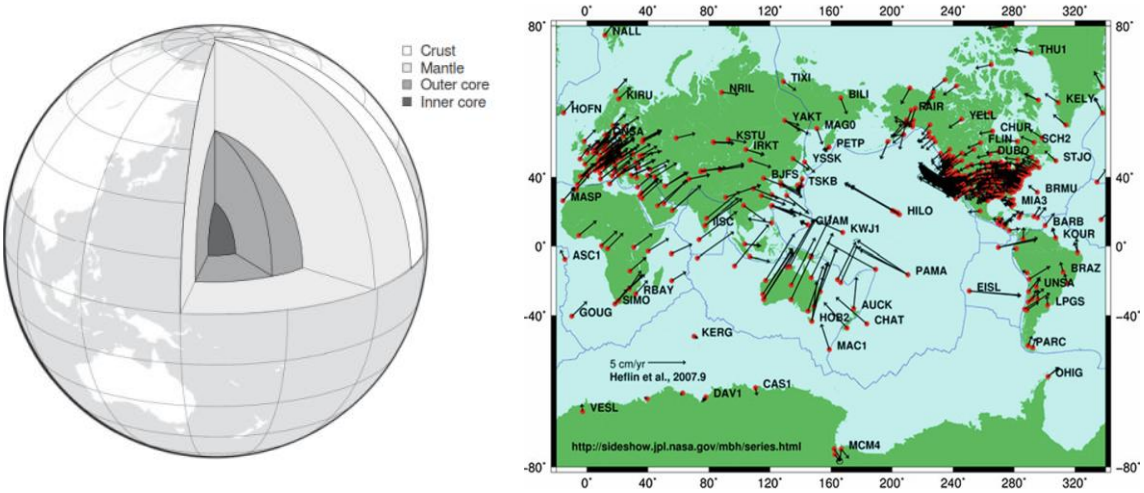

Fig. I. 2: Structure of the Earth and Vectors showing thw major direction of relative motions of the global tectonic plates http://sideshow.jpl.nasa.gov/mbh/all/images/global.jpg

The movement of tectonic plates relative to one another leads to different types of interactions at their boundaries. These interactions are shaped by both the direction of the plates' motion and the type of crust involved—whether oceanic or continental. Oceanic crust is thinner compared to continental crust, and there can be significant temperature differences between them. These variations in thickness and temperature (or buoyancy) play a key role in determining the nature of plate boundary interactions. The main types of these interactions are outlined below and illustrated schematically in Fig. I. 3

- Divergent Plate Boundaries: occur where two plates slide apart from each other in regions of the crust that experience tensile deviatoric stresses from the mantle loading. As the plates separate, mantle material rises to fill the gap, forming new crust in the process.
- Convergent Plate Boundaries: At convergent margins, two plates move toward each other. When oceanic crust converges with continental crust, a subduction zone forms. In contrast, when two continental plates collide, a collision margin is created. Subduction zones lead to the destruction of oceanic crust as it is forced beneath the continental crust into the mantle. Due to its older, denser, and cooler nature, oceanic crust is subducted, while the continental crust is uplifted, often resulting in significant coastal topography
- Transform Boundaries: These boundaries occur where two plates slide past each other laterally. This lateral movement may result from either the relative rotation or translation of the plates. A well-known example is the San Andreas Fault in California. In some cases, the movement is not purely lateral, and a convergent or divergent component may contribute to the creation of topographic features, as seen in the Alpine Fault.

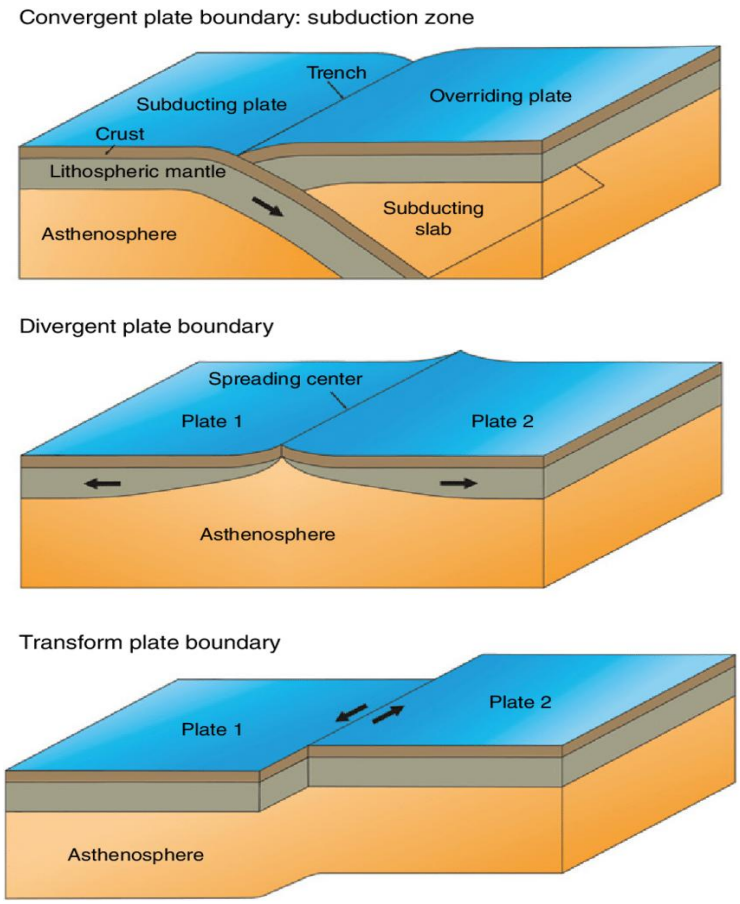

Fig. I. 3: Different types of plate boundaries

The vast majority of earthquakes worldwide occur along the plate boundaries, known as interplate earthquakes. The Pacific Ocean's perimeter, where oceanic and continental plates converge through subduction, stands out as the most active zone in this regard. Other notable regions experiencing interplate earthquakes include the Mediterranean Sea and its surroundings, the Azores islands in the Atlantic Ocean, and extensive parts of Asia. These earthquakes result from various types of plate interactions: convergent, divergent, and transform. In contrast, earthquakes that occur within plates, such as those in northeastern America, Australia, central India, and northeastern Brazil, are termed intraplate earthquakes. The mechanisms driving these intraplate earthquakes differ from those at plate boundaries. Interplate events are typically triggered by significant deformations along well-defined boundaries, whereas intraplate earthquakes occur in stable continental regions lacking such clear boundaries. Despite their lower frequency, large earthquakes in stable continental regions can still have considerable impact due to their significant magnitudes(Stein & Wysession, 2009).

1.5 Faults

A fault is a fracture or zone of fractures between two blocks of rock. Faults allow the blocks to move relative to each other. This movement may occur rapidly, in the form of an earthquake - or may occur slowly, in the form of creep. Faults may range in length from a few millimeters to thousands of kilometers. Most faults produce repeated displacements over geologic time. During an earthquake, the rock on one side of the fault suddenly slips with respect to the other. The fault surface can be horizontal or vertical or some arbitrary angle in between. Earth scientists use the angle of the fault with respect to the surface (known as the dip) and the direction of slip along the fault to classify faults. Faults which move along the direction of the dip plane are dip-slip faults and described as either normal or reverse (thrust), depending on their motion. Faults which move horizontally are known as strike-slip faults and are classified as either right-lateral or left-lateral. Faults which show both dip-slip and strike-slip motion are known as oblique-slip faults.

- Normal fault - a dip-slip fault in which the block above the fault has moved downward relative to the block below. This type of faulting occurs in response to extension and is often observed in the Western United States Basin and Range Province and along oceanic ridge systems.
- Reverse (thrust) fault - a dip-slip fault in which the upper block, above the fault plane, moves up and over the lower block. This type of faulting is common in areas of compression, such as regions where one plate is being subducted under another as in Japan. When the dip angle is shallow, a reverse fault is often described as a thrust fault.
- Strike-slip fault - a fault on which the two blocks slide past one another. The San Andreas Fault is an example of a right lateral fault.

A left-lateral strike-slip fault is one on which the displacement of the far block is to the left when viewed from either side. A right-lateral strike-slip fault is one on which the displacement of the far block is to the right when viewed from either side.

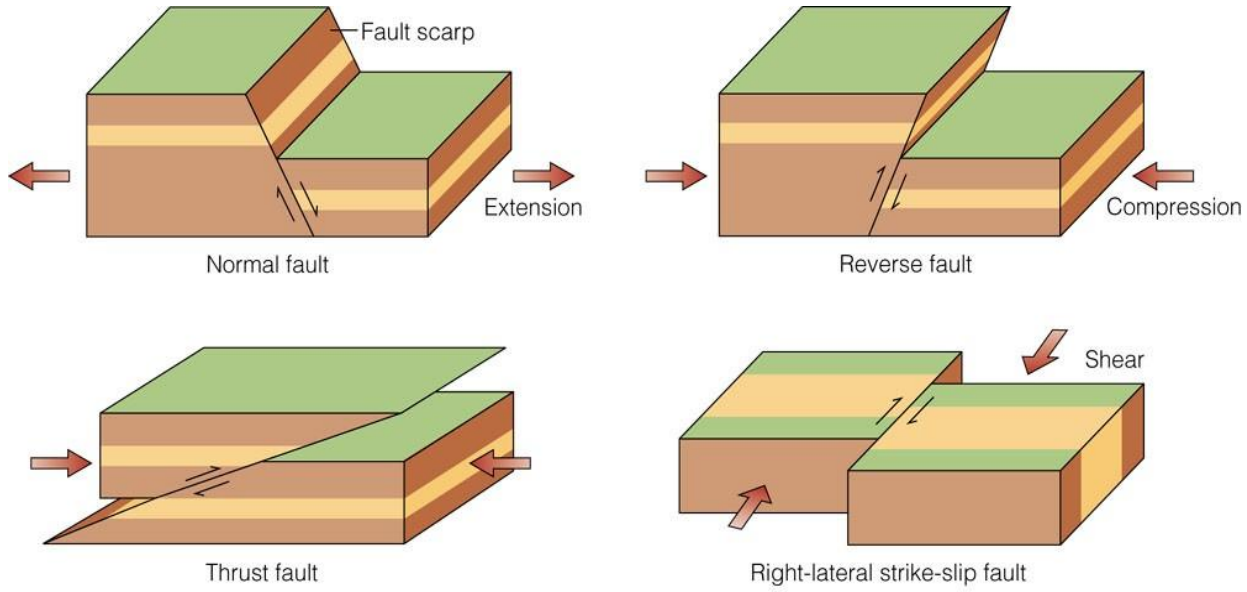

Fig. I. 4: Different types of plate boundaries

1.6 Seismic Waves

When an earthquake occurs, seismic waves propagate from the epicenter and rapidly travel through the Earth's crust. Upon reaching the surface, these waves induce ground shaking, which can endure from mere seconds to several minutes. Seismic waves produced during an earthquake are classified into body waves and surface waves (Fig. I. 4).

- Body waves, which travel through the Earth's interior, include:

- Primary waves (P-waves): compress and expand the materials they move through and can travel through solids and fluids. They are classified as longitudinal waves since the particle motion of them is in the direction of wave propagation. They travel faster and they are the first waveforms observed in seismic recordings (seismograms).
- Secondary waves (S-waves): are divided into SV waves (vertical motion) and SH waves (horizontal motion). S-waves are called as shear waves. They cannot travel through fluids. Their particle motion is in the transversal direction to the wave propagation. They are lower frequency, larger amplitude compered to primary waves

- Surface waves result from the interaction of body waves with the Earth's surface and subsurface layers, traveling along the surface with amplitudes that decrease with increasing depth. These waves become more prominent at greater distances from the earthquake source. The main surface waves of engineering importance are

- Rayleigh waves Rayleigh waves, created by the interaction of P-waves and SV-waves with the surface, exhibit both vertical and horizontal motion.
- Love waves, produced by the interaction of SH-waves with a soft surface layer, lack vertical motion. They usually travel slightly faster than Rayleigh waves (Kramer, 1996; Saouma & Hariri-Ardebili, 2021; Stein & Wysession, 2009; Sucuoğlu et al., 2014).

Seismologists use the differences in arrival times of P-waves and S-waves at multiple seismic stations to:

- **Determine the earthquake's epicenter:** The time difference between P- and S-wave arrivals (known as the S–P interval) increases with distance from the source. By measuring this time difference at three or more stations, the epicenter can be located using triangulation.
- **Estimate the focal depth:** The shape and amplitude of the seismic waves—especially body waves—provide information about the depth of the earthquake focus.
- **Calculate the earthquake's magnitude:** The amplitude of the seismic waves recorded at known distances from the source is used in magnitude scales (e.g., Richter, moment magnitude).
- **Identify fault mechanisms:** Waveform analysis and moment tensor inversion allow scientists to infer the fault type and the direction of slip during the rupture.

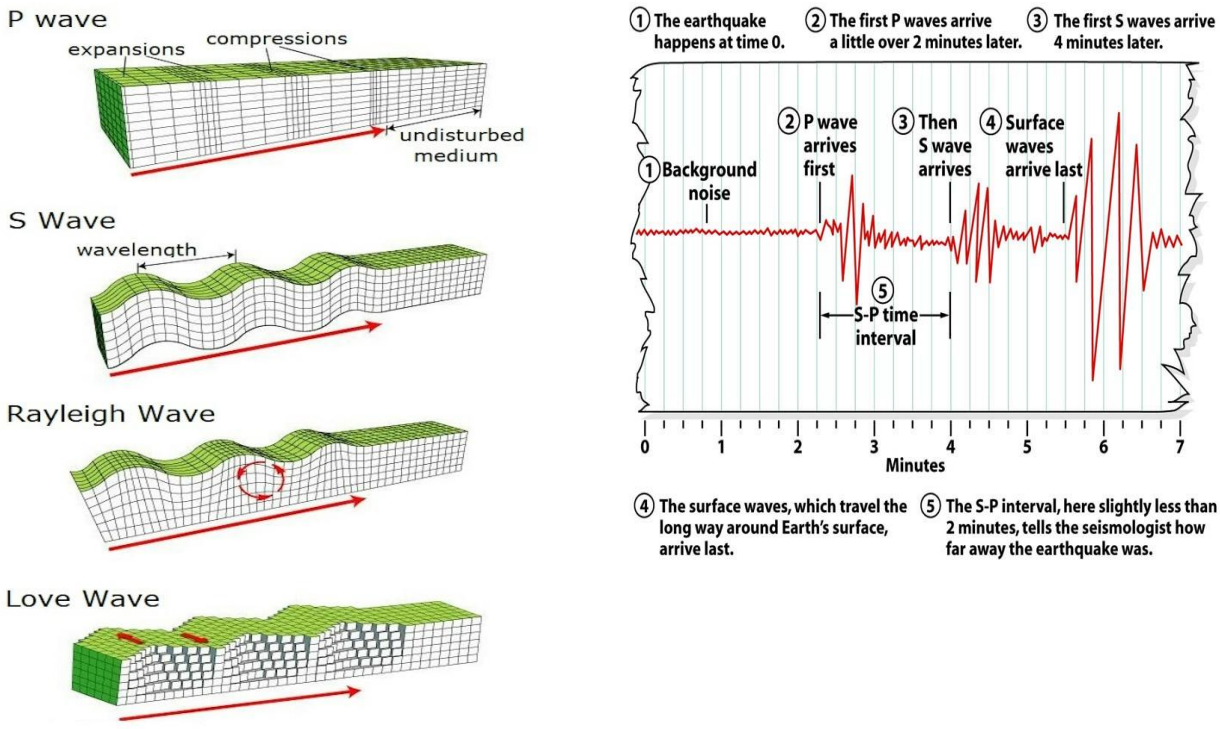

Fig. I. 5: first panel, Particle motions of body waves: a) P-waves, b) S-waves, and surface waves: c) Rayleigh waves, d) Love waves. Second panel, typical seismogram recording, clearly showing the main types of seismic waves

1.7 Earthquake Size

The size of an earthquake is a crucial parameter, and it has been characterized in various ways. Before the advent of modern instrumentation, the size of earthquakes was described using basic and qualitative observations of their effects. Nowadays, modern seismographs have enabled the development of several quantitative measures of earthquake size. Since these measures are widely used in seismology and earthquake engineering, it is important to understand the unique characteristics of each.

1.7.1 Earthquake Intensity

The oldest method for measuring earthquake size is intensity. Intensity provides a qualitative description of an earthquake's effects at a specific location, based on observed damage and human reactions. It depends on the distance from the source and the soil conditions (Bormann et al., 2013). Because these qualitative descriptions are available throughout recorded history, intensity can be used to estimate the locations and magnitudes of earthquakes that occurred before modern seismic instruments were developed (pre-instrumental earthquakes). This approach has been invaluable for determining the recurrence rates of earthquakes of varying magnitudes in different regions, which is essential for assessing seismic hazards. Additionally, intensity measurements can estimate strong ground motion levels, compare earthquake effects across different geographic areas, and aid in earthquake loss estimation(Bakun & Wentworth, 1997).
Earthquake intensities are typically gathered from interviews with observers after the event. These interviews are often conducted by mail, but in some seismically active areas, permanent observers are trained to provide rational and unbiased reports. Since human observers and structures are more widely distributed than seismological instruments, intensity observations offer valuable information about the distribution of ground shaking in a region. By plotting reported intensities on a map, contours of equal intensity, or isoseisms, can be created, resulting in an isoseismal map. The greatest intensity is usually near the earthquake's epicenter, referred to as epicentral intensity, and isoseismal maps show how intensity decreases with distance from the epicenter(Sucuoğlu et al., 2014).
The first internationally used intensity scale was the 10-point Rossi-Forel (RF) scale, developed in 1883. In 1902, **Giuseppe Mercalli** introduced a new **12-degree scale**, which underwent significant revisions. The 12-point scale Sieberg in collaboration with Gutenberg (Sieberg, 1912; Sieberg & Gutenberg, 1923) updated this scale and developed **the** Mercalli–Cancani–Sieberg (MCS) scale. Sieberg and Gutenberg (1923) work was translated into English by Wood and Neumann (1931) and named the Modified Mercalli (MM) scale. This version was thoroughly revised by Richter (1958), resulting in the Modified Mercalli Scale of 1956. In 1964, Medvedev, Sponheuer, and Karnik published the MSK scale, which was based on the MCS, MM56, and Medvedev's earlier work in Russia (Sponheuer, 1964). The MSK scale was widely used in Europe until the publication of the European Macroseismic Scale (EMS) by Grünthal (1998). The Japanese Meteorological Agency (JMA) has its own intensity scale. e. A comparison of the RF, MMI, JMA, and MSK scales is shown in Fig. I. 5.

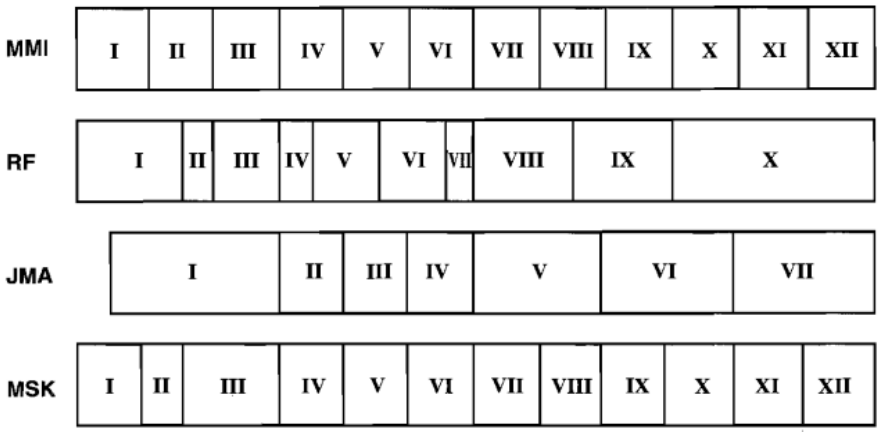

Fig. I. 6: Comparaison of intensity values from modified Mercalli (MMI), Rossi-Forel (RF), Japanese Meteorological Agency (JMA), and Medvedev-Spoonheuer-Karnik (MSK) scales.

The table below summarizes the different intensity levels and their typical observed effects, based primarily on the Modified Mercalli Intensity (MMI) scale and comparable modern intensity scales such as EMS-98.

Table I. 1 Description of Intensity Classes and Their Observed Effects (Based on MMI / EMS-98 Scales)

Intensity	Description	Typical Observed Effects
I	Not felt	Not felt except by a very few under especially favorable conditions.
II	Weak	Felt only by a few people at rest, especially on upper floors. Delicate suspended objects may swing.
III	Weak	Felt indoors by several people; feels like passing of a light truck; hanging objects swing.
IV	Light	Felt by many indoors; few outdoors. Windows, dishes, doors rattle. Vibration like heavy truck.
V	Moderate	Felt by nearly everyone; some broken dishes and windows; unstable objects overturned.
VI	Strong	Felt by all; many frightened; some heavy furniture moved; slight damage.
VII	Very strong	Damage negligible in buildings of good design; slight to moderate damage in poorly built structures.
VIII	Severe	Moderate damage in well-built structures; considerable damage in ordinary buildings. Fall of chimneys, monuments.
IX	Violent	Considerable damage even in specially designed structures; buildings shifted off foundations.
X	Extreme	Most masonry and frame structures destroyed; rails bent; landslides; ground cracks.
XI	Extreme	Few, if any masonry structures remain standing; bridges destroyed; wide ground cracks.
XII	Catastrophic	Total destruction; waves seen on ground surface; objects thrown into the air.

1.7.2 Earthquake Magnitude

The development of modern instruments for measuring ground motion during earthquakes has made it possible to obtain a more objective and quantitative assessment of earthquake size. Over the past 60 years, advances in seismic instruments and our understanding of their measurements have significantly progressed. These instruments provide an objective, quantitative measure of earthquake size known as magnitude, a concept and method introduced by Charles F. Richter in 1935. Despite some limitations, magnitude offers crucial insights into the earthquake source spectrum at the period where it is measured. Through various empirical relationships, magnitudes can be used to estimate seismic moment and the energy released by an earthquake, both of which are critical for understanding global issues such as seismic slip rates between lithospheric plates. Magnitude values also hold immense practical importance, as they populate earthquake catalogs and data banks that span long time periods—decades and, hopefully, centuries. This extensive data is essential for assessing seismic activity and related hazards across different regions of the Earth, as well as their potential variability over time and space. This information is not only of significant scientific interest but also forms the foundation for realistic long-term disaster preparedness and risk mitigation strategies.

1.7.2.1 Richter Local Magnitude, M_L

In 1935, Charles Richter used a Wood-Anderson seismometer to define a magnitude scale for shallow, local earthquakes in southern California (Richter, 1935). Richter defined what is now known as the *local magnitude* as the logarithm (base 10) of the maximum trace amplitude (in micrometers) recorded on a Wood-Anderson seismometer located 100 km from the epicenter of the earthquake. Eq.2 gives the local magnitude (M_L) expression proposed by Richter.

$$M_L = LogA - LogA_o \tag{2}$$

where A is the Wood-Anderson seismograph amplitude of the event in [mm], A_0 is the amplitude of a standard event for the same epicentral distance.

Richter (1935) provides the calibration factor -log (A_0) for epicentral distances up to 1000 km for the average conditions in southern California. The computation of M_L can also be done from the nomogram that requires P- and S-wave arrival times and the maximum amplitude readings on a Wood-Anderson seismograph. The calibration by base amplitude A_0 is embedded into the nomogram.

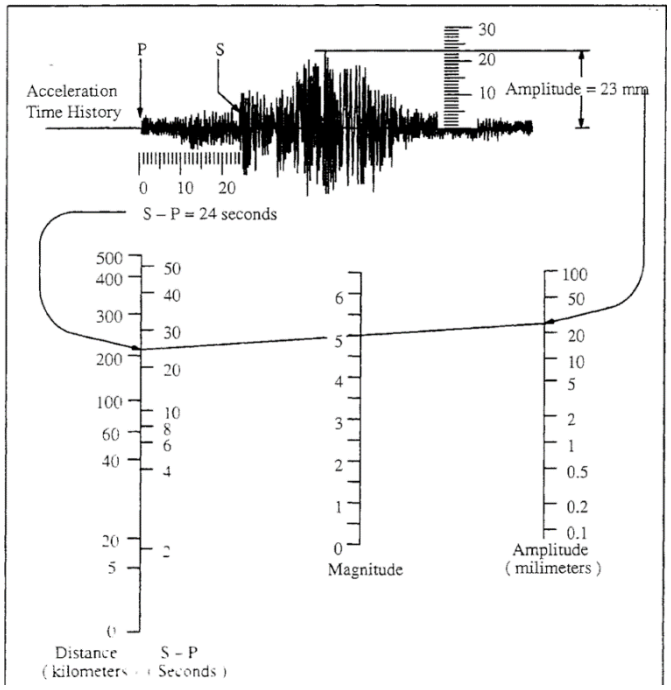

Fig. I. 7 Nomogram for Determining Local Magnitude (ML) Using Amplitude and Distance

The M_L is the best-known magnitude scale, but it is not always the most appropriate scale for description of earthquake size. Definition of M_L is based on seismic waveform amplitudes recorded by the Wood-Anderson seismograph and the amplitude calibrations that reflect the regional attenuation characteristics of southern California. Thus, the seismic networks reporting M_L should properly account for the instrumental differences if maximum waveform amplitudes are measured by another type of seismograph. The differences in regional attenuation should also be considered thoroughly by the seismic networks as the original calibrations proposed by Richter are only valid for southern California. The local magnitude proposed by Richter has limitations in application and may not provide globally consistent estimation of earthquake size if the above stated factors are overlooked by seismic agencies.

The original Richter scale for Southern California has been further developed since its invention. In its expanded form, the following relation now holds:

$$M_L = \log_{10} A_{\max} + 1.11 \log_{10} R + 0.00189R - 2.09 \qquad (3)$$

with R is distance from the station to the hypocenter in kilometers and A_{max} is maximum trace amplitude in nanometers (instead of μm in a WA record). Eq. 2 was adopted by the International Association of Seismology and Physics of the Earth's Interior (IASPEI) in 2004 as the standard procedure for determining local magnitudes in the distance range up to typically less than 1000 km. For earthquakes in the Earth's crust of regions with attenuation properties that differ from those of coastal California, and for measuring ML with vertical component seismographs, the standard equation takes the form

$$M_L = \log_{10}(A_{\max}) + F(R) + G \qquad (4)$$

where F(R) is an R-dependent calibration function and G a constant which have to compensate for different regional attenuation and/or for any systematic biases of amplitudes measured on vertical instead on horizontal seismographs. Although ML is still widely used and is the best-known magnitude scale, it has several important limitations:

- Regional Dependence:
  - The original ML scale was calibrated specifically for southern California's attenuation properties.
  - When used in regions with different geologic and crustal conditions, ML values may not accurately reflect true earthquake size unless recalibrated.
- Instrumental Sensitivity:
  - ML was based on the Wood-Anderson seismograph, which has a limited frequency range (~1–10 Hz). Modern instruments measure a broader spectrum.
  - Seismological networks using other instruments must correct for differences in response and sensitivity.
- Magnitude Saturation:
  - ML saturates for large earthquakes (typically >M6.5–7.0), meaning it underestimates the energy released in major events. This happens because the amplitude-based measurement doesn't scale linearly with the total energy for large ruptures.
- Wave Type Insensitivity:
  - ML does not distinguish between different wave types (P, S, surface), and is thus less useful for teleseismic events (distant quakes).
- Not Ideal for Deep or Large Earthquakes:
  - ML is most accurate for shallow, local earthquakes (within ~600–1000 km). It is unreliable for deeper or distant events.

Ten years after the introduction of M_L, Beno Gutenberg extended the concept of magnitude determination to teleseismic distances larger than about 1000–2000 km. He used both records of seismic waves that propagate along the Earth's surface (or near to it with a period-dependent penetration depth) and waves which travel through the Earth. Accordingly, the former are termed surface waves (M_s) and the latter body waves (m_b). This normalization ensures that magnitude calculations are independent of the specific type of seismograph used.

1.7.2.2 Surface Wave Magnitude Scale, M_s

At significant distances from the epicenter, body waves typically diminish and scatter to the point where surface waves become the primary contributors to the observed motion. The surface wave magnitude (Gutenberg & Richter, 1936) is a worldwide magnitude scale (Eq. 5) based on the amplitude of Rayleigh waves with a period of about 20 sec. The surface wave magnitude is obtained from

$$M_s = \log A + 1.66 \log \Delta + 2.00 \qquad (5)$$

Where A is the maximum ground displacement in micrometers and Δ is the epicentral distance of the seismometer measured in degrees. Since the M_s is based on the actual ground displacement rather than the seismograph's response, it can be determined using data from any type of seismograph, regardless of its design or sensitivity. The surface wave magnitude is most commonly used to describe the size of shallow (less than about 70 km focal depth), distant (farther than about 1000 km) moderate to large earthquakes. Another, so-called Prague–Moscow formula for M_s (Eq. 6) was proposed in 1962 by Vanek (1962). It is based on the measurement of the maximum ratio of ground displacement amplitude A (in μm) divided by the related period T (in s) $(A/T)_{max}$ in records of shallow earthquakes (h < 60 km) in wide period and distance ranges (3 s < T < 30 s; 2°≤ D° ≤ 160°):

$$M_s = \log_{10}(A/T)_{\max} + 1.66\log_{10} D^\circ + 3.3 \quad (6)$$

This relationship was adopted by the IASPEI in 1967 as international standard.

The Ms scale also suffers from several limitations:

- Magnitude Saturation:
  - Like ML, the Ms scale saturates for large earthquakes—typically above magnitude M7.5–8.0. This means it underestimates the true size of very large events, because surface wave amplitudes do not continue to scale linearly with seismic moment.
  - For example, both the 2004 Sumatra earthquake (Mw 9.1) and much smaller earthquakes can produce similar Ms values (~8.0), leading to underestimation of energy release.
- Inapplicability to Deep Earthquakes:
  - Ms is based on surface wave amplitudes, which are poorly developed or absent in deep-focus earthquakes (depth > 70 km). Therefore, the Ms scale is not suitable for estimating the magnitude of deep seismic events.
- Period Dependency:
  - Ms is calculated using Rayleigh wave amplitudes with a 20-second period. This narrow period band can limit its sensitivity to rupture characteristics, especially for very fast or complex ruptures.
- Regional Bias:
  - The scale assumes average crustal and attenuation properties, but surface wave propagation is strongly influenced by the Earth's structure. Hence, Ms values can vary by region, depending on how efficiently surface waves are transmitted and amplified.
- Instrument and Filtering Requirements:
  - Accurate Ms determination requires specific long-period instrumentation and careful band-pass filtering to isolate the 20-second Rayleigh wave signal. Inconsistent instrumentation or signal processing can introduce biases.
- Less Accurate for Near-Field Events:
  - Ms is optimized for teleseismic events (>2000 km away). It becomes less reliable at regional or local distances, where surface waves may not be fully developed or may interfere with other phases.

1.7.2.3 Body Wave Magnitude Scale, m_B

For deep-focus earthquakes, surface waves are often too weak to provide a reliable evaluation of surface wave magnitude. In such cases, the body wave magnitude scale, introduced by Gutenberg (1945), is used. This worldwide magnitude scale (Eq.7) is based on the amplitude of the first few cycles of P-waves, which are less affected by the earthquake's focal depth. The body wave magnitude can be calculated using the formula

$$m_B = \log_{10}(A/T)_{\max} + Q(D^\circ, h) \quad (7)$$

Where A represents the P-wave amplitude in micrometers, and T is the P-wave period, usually about one second. Revised empirical distance-depth corrections for the calibration of body-wave magnitudes, so-called Q-functions, were published Gutenberg and Richter (1955). Additionally, body wave magnitude can be estimated using the amplitude of one-second-period, higher-mode Rayleigh waves, as described by Nuttli (1972). The resulting magnitude, known as m_{bLg}', is often used to describe intraplate earthquakes. Recently, the IASPEI adopted a measurement procedure for m_{bLg} as international standard, which had been developed for eastern North America with the aim to improve yield estimates of Nevada Test Site explosions. However, as for all other local or regional magnitude scales, the calibration term is strongly influenced

by the local/regional geologic-tectonic conditions in the Earth's crust and requires a proper scaling to this standard, when applied to other areas than eastern North America. The Key Limitations of the Body Wave Magnitude (mb) Scale are:

- Magnitude Saturation (M > 6.0–6.5):
  The mb scale saturates for moderate to large earthquakes, meaning it underestimates the true size of large seismic events. This occurs because short-period P-waves do not fully capture the energy released during large or slow ruptures.
- Insensitive to Long-Period or Slow Earthquakes:
  mb is calculated from short-period (~1 s) P-waves and is therefore ineffective at detecting slow or long-duration earthquakes, which radiate energy in longer periods.
- Not Suitable for Local or Shallow Earthquakes:
  mb is designed for teleseismic distances (>1000 km). It is less accurate for shallow or nearby events, where other magnitude scales like ML or Mw are more appropriate.

The m_B and M_S magnitudes have been widely used for decades, even though there are some issues with how they are measured. They are well-established and useful in their own right, so they will continue to be important reference points. However, the introduction of new standards (m_b, m_{BB}, $M_{s(20)}$ and M_{sBB}) will help improve the accuracy of these measurements by accounting for a broader range of frequencies. The IASPEI (2005) outlines key features of different teleseismic magnitudes (Bormann et al., 2009):

1. m_b: This short-period body-wave magnitude measures the maximum amplitude of P-waves (including related phases) within periods less than 3 seconds. The measurement uses a vertical-component seismograph filtered to mimic a standard short-period seismograph and is applicable for earthquakes at specific distances and depths.
2. m_{BB}: An intermediate-period or broadband body-wave magnitude that measures the maximum ground velocity within a period range of 0.2 to 30 seconds. It uses a similar method to m_b but focuses on broader frequency coverage.
3. M_{S20}: A surface-wave magnitude measuring ground displacement amplitude at periods between 18 and 22 seconds. It is used only for shallow earthquakes (depths ≤ 60 km) recorded at specific distances, using a filter that replicates a long-period seismograph.
4. M_{SBB}: A broadband surface-wave magnitude similar to M_{S20} but measuring maximum ground velocity over a broader period range (3 to 60 seconds). It applies to shallow earthquakes at a wider range of distances. The period at which the maximum velocity occurs should also be recorded, though it's not essential for determining the magnitude.

1.7.2.4 Other Instrumental Magnitude Scale

Various magnitude scales have been developed using different parts of seismic recordings. The coda, which consists of backscattered waves that follow the initial body and surface waves, was identified by Aki (1969) as having certain characteristics independent of the travel path. From these characteristics, Aki developed the coda magnitude (M_C). The duration magnitude (M_D) is another scale, based on the total length of the earthquake's shaking, and is particularly useful for analyzing small earthquakes, which are often of greater interest to seismologists than to engineers (Real & Teng, 1973). In Japan, Tsuboi developed for the Japan Meteorological Agency (JMA) in 1954 a magnitude formula (Eq. 8) for shallow earthquakes (depth h < 60 km) that have been recorded at epicentral distances D up to 200 km

$$M_{JMA} = \log_{10} A_{\max} + 1.73 \log_{10} D - 0.83 \quad (8)$$

A_{max} is the largest ground motion amplitude (in μm) in the total event record of a seismograph with an eigen period of 5 s.

1.7.2.5 Moment Magnitude, M_w

Magnitude scales, like m_b, M_L, m_B, and M_S, used in measuring earthquake sizes often experience "saturation," meaning they can't accurately measure very large earthquakes. This saturation happens because of two main reasons: spectral saturation and insufficient time-window length for measuring amplitudes. Spectral saturation occurs when the earthquake's energy falls outside the range that seismographs can detect. Time-window saturation happens when the time frame used to measure the seismic waves is too short to capture the entire event, especially for large earthquakes. This can lead to underestimations of earthquake magnitudes(Borman, 2021; Hanks & Kanamori, 1979). Therefore, Kanamori (1977)and Hanks and Kanamori (1979) proposed a non-saturating magnitude scale for very large earthquakes, based on seismic moment M_0 data. Kanamori termed it M_w. It is reads in the IASPEI (2005) recommended standard form with M_0 in units of Newton meter Nm (Eq. 9):

$$M_w = \frac{2}{3}\left(\log_{10} M_o - 9.1\right) \tag{9}$$

Hanks and Kanamori (1979) derived M_w scale by substituting the ratio of energy (E_s) and the seismic moment (M_0) (i.e., $E_s/M_0 = (\Delta\sigma/2\mu) = 5 \times 10{-}5$, in which σ is the earthquake stress drop and μ is the shear modulus) into the Gutenberg–Richter energy magnitude equation (Eq.10):

$$\log E_s = 1.5M_s + 4.8 \tag{10}$$

Kanamori substituted M_S in Eq. 10 with the symbol M_w for the envisaged non-saturating moment magnitude and arrives via Eq. (11) at

$$\log E_s = \log M_o - 4.3 = 1.5M_w + 4.8 \tag{11}$$

and when resolving it for M_w it gives Eq. 9 above. The M_w scale is widely considered as the authoritative magnitude scale for determining the size of earthquakes. It is more directly related to an earthquake's energy than other scales and does not saturate; that is, it does not underestimate magnitudes in specific conditions as other scales do (Bormann et al., 2013). It has replaced other magnitude scales as the standard scale used by seismological agencies such as the US Geological Survey for reporting strong earthquakes (usually M > 4).

A group of later introduced complementary or modified versions of the M_w scale are described below:

1. **M_{wp}**: The M_{wp} scale, developed by Tsuboi et al. (1995), utilizes broadband P-waveforms to estimate the M_w quickly and assess tsunami potential for large earthquakes near Japan's coast. It was later adapted for use with teleseismic earthquakes by Tsuboi et al. (1999) and has become the primary method at the Pacific Tsunami Warning Center (PTWC) for rapid M_w estimation. The M_{wp} method involves double integration of broadband P-wave velocity records and scaling the peak of the resulting source-time function to compute M_w. Despite its utility, M_{wp} has faced challenges, particularly in the case of complex or slow ruptures, where it tends to underestimate M_w. Although corrections have been implemented, such as those after the 2004 Sumatra earthquake, M_{wp} has not proven to be more efficient or faster than the traditional Gutenberg magnitude (m_B) measurement.
2. **M_m**: The mantle magnitude (M_m) scale, introduced by Brune and Engen (1969)and further developed by Okal and Talandier (1989); (Okal & Talandier, 1990), uses surface waves with periods between 60 and 410 seconds that penetrate into the Earth's mantle. Mm is closely related to the seismic moment (M_0) and avoids saturation,

enabling rapid, automated measurements without detailed earthquake parameters. It is calculated using the spectral amplitude of Rayleigh waves and includes correction factors. M_m is most accurate for earthquakes with $M_w > 6$ and distances greater than 15-20°. The method has been automated at tsunami warning centers and is reliable within about ±0.2 magnitude units.

3. **m_{Bc}**: Gutenberg and Richter (1955) initially established a relationship between earthquake magnitude (m_B) and seismic energy ($\log E_s$) based on limited data, which could be unreliable for larger, complex earthquakes. Bormann and Khalturin (1975) suggested using multiple P-wave onsets to better estimate energy release, leading to the cumulative magnitude measure (m_{Bc}). This method, automated for rapid M_w estimation, is useful for tsunami warnings but tends to overestimate magnitudes for smaller earthquakes, where the original Gutenberg-Richter assumptions still apply.
4. **M_{ED} and M_{wpd}**: Traditional magnitude scales such as M_{wp} and m_B tend to underestimate the magnitude and tsunamigenic potential of large, complex earthquakes because they do not account for rupture duration and significant sub-events. To address this, new magnitude scales such as M_{ED} and M_{wpd} were developed to include rupture duration in their calculations. These newer scales offer more accurate and timely estimates of an earthquake's size and tsunamigenic potential, especially for slow tsunami earthquakes. They have been implemented operationally in Rome, enhancing early tsunami warning systems.

1.7.2.6 Energy Magnitude, M_e

Choy and Boatwright (1995) scaled the energy magnitude M_e similarly to how Kanamori (1977) scaled M_w using the Gutenberg-Richter relationship (Eq.10). They directly calculated the seismic energy E_s by integrating squared broadband velocity amplitudes over the P-wave duration and correcting for propagation and radiation effects. Then they plotted for hundreds of earthquakes $\log E_S$ over the respective M_S values between 5.5 and 8.3 and determined from a standard least-square regression the best fitting straight line with the prescribed slope of 1.5 Initially, they retained the historical constant 4.8 in their equation, but later reverted to a better-fitting constant of 4.4. This led to the revised formula (Eq. 12):

$$M_e = \left(\frac{\log E_s - 4.4}{1.5}\right) \tag{12}$$

2 Relationships among Different Magnitude Scales and Regression Approaches

2.1 Introduction

The M_w scale, introduced by Kanamori (1977) and further refined by Hanks and Kanamori (1979), is widely considered the most physically reliable and non-saturating method for quantifying earthquake size. Since 1976, the methods for calculating M_w have been well-established and standardized, largely based on the Harvard method for Centroid-Moment-Tensor solutions (Dziewonski et al., 1981). In contrast, traditional magnitude scales, including M_L, m_B, and M_S, along with their various versions, utilize different period and bandwidth ranges and inconsistent methodologies that have occasionally been revised over time (Bormann et al., 2007; Bormann et al., 2009). These inconsistencies create challenges for conducting probabilistic seismic hazard assessments over both intermediate and long-term periods. Consequently, it has become a common practice to convert traditional local or teleseismic magnitudes into equivalent M_w values through empirical regression techniques. This practice aims to generate uniform earthquake catalogs with consistent magnitude representation, making them suitable for seismic hazard assessments, with M_w serving as the standardized metric for earthquake size. Until approximately two decades ago, regression analyses for converting between different magnitude types primarily relied on the least squares method (SLR), which assumes the independent variable has no errors, or the simple orthogonal regression method (SOR), which assumes equal uncertainties for both variables. Recent studies have recognized the limitations of these approaches, advocating for the use of general orthogonal regression methods (GOR)

that account for varying uncertainties between the two regression variables. This chapter examines the most commonly used regression methods for magnitude conversion, assessing their reliability and potential limitations.

2.2 Explanation of notation

In this chapter, the following notation is used in the equations:

- x: represents the independent variable.
- y: denotes the dependent variable.
- X and Y: stand for the true values of the variables.
- x and y (in lowercase): refer to the observed values that are affected by uncertainties.
- δ, ϵ: indicates the errors associated with the independent and dependent variables.
- n: denotes the number of data pairs.

2.3 The Simple Linear Regression Method (SLR)

Simple Linear Regression (SLR) is a straightforward and widely utilized technique for modeling the relationship between two variables. However, its mathematical and statistical validity hinges on certain conditions. A critical requirement is that the independent variable x must be measured with significantly higher accuracy than the dependent variable y. The general framework of the SLR method can be outlined as follows:

Assume the regression line relating the dependent variable Y to the independent variable X is expressed in the form:

$$Y = \beta_0 + \beta_1 x + \varepsilon \tag{13}$$

Where β_0 and β_1 are the parameters to be estimated. The estimator of β_0 and β_1 ,denoted as b_0 and b_1, are derived using information from n observations. Consequently, Eq. (13) becomes:

$$Y = b_0 + b_1 x + \varepsilon \tag{14}$$

here $\hat{Y}$ represents the predicted value of Y for a given value of x. With the availability of n data pairs (x_1, y_1),(x_2,y_2)…..,(x_n,y_n) , Eq. (13) can be written for each observation as:

$$Y_i = \beta_0 + \beta_1 x_i + \varepsilon_i \tag{15}$$

For i=1,2, 3…n

The SLR method aims to minimize the sum of squared vertical deviations (s) (Fig. I. 6) of the observed data points (y_i,x_i) from the predicted line defined by Eq. (13)

$$s = \sum_{i=1}^{n} \varepsilon_i^2 = \sum_{i=1}^{n} (y_i - \beta_0 - \beta_1 x_i)^2 \tag{16}$$

Therefore, the given values of the estimators b_0 and b_1 must produce the least possible value of s. The details of determining b_0 and b_1 are given in the previous literatures (e.g, Draper (1998)). Here we will give only the final formula of both:

$$b_1 = \frac{S_{xy}}{S_{xx}} \tag{17}$$

$$b_0 = \bar{y} - b_1 * \bar{x} \tag{18}$$

Where:

$$S_{xy} = \sum x_i y_i - n\bar{x}\bar{y}$$
$$S_{xx} = \sum x_i^2 - n\bar{x}^2$$
$$\bar{x} = \sum x_i / n; \bar{y} = \sum y_i / n$$

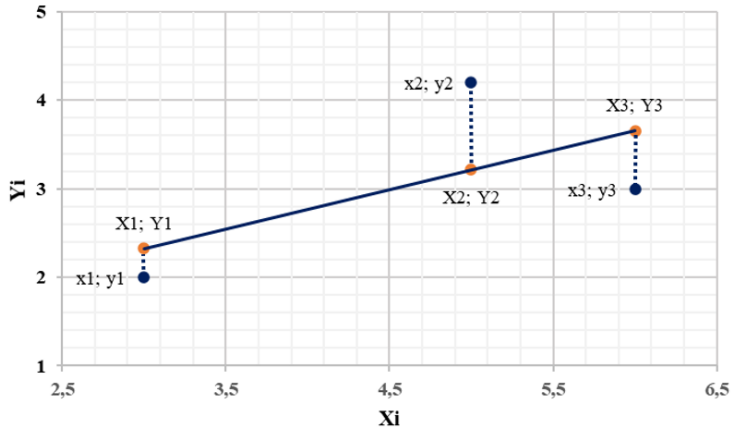

Fig. I. 8: Schematic diagram showing theoretical true points (i.e., (x_i, y_i), i=1, 2, 3) and estimated points (i.e., (X_i, Y_i), i=1, 2, 3) on the fitted SLR regression line (solid black line) for a set of three observed points.

It is essential to note that if x has significant measurement errors, the assumptions of the SLR model are violated, potentially leading to erroneous conclusions. Generally, all measured or calculated magnitude values are subject to initial errors, making standard regression relationships suboptimal. These relationships should only be used as derived: for converting a given magnitude, assumed to be error-free, into another magnitude by estimating its mean value and associated uncertainty (e.g., standard deviation). Standard regression tends to project errors in the independent variable into increased error in the estimated dependent variable. Therefore, inverting an SLR relationship (i.e., solving y over x) to estimate the independent variable X, as sometimes practiced in magnitude conversions, is incorrect (Castellaro et al., 2006). Such misuse of standard regression can easily lead to conversion errors ranging from 0.2 to 0.3 magnitude units (Gutdeutsch et al., 2002).

2.4 The Simple Orthogonal Regression Method (SOR)

Simple Orthogonal regression is a key technique used to correct prediction errors in linear regression. It accounts for measurement errors in both the dependent and independent variables, unlike simple linear regression, which only considers errors in the independent variable. SOR is used to examine the linear relationship between two continuous variables under the assumption of equal uncertainties for both variables (with an error ratio 1). This has been practiced, e.g., by (Ambraseys, 1990; Bormann & Khalturin, 1975; Bormann et al., 2007; Das et al., 2011; Grünthal & Wahlström, 2003; Gusev, 1991; Gutdeutsch et al., 2002; Ristau, 2009).

As illustrated in Fig. I. 7, because the abscissa values and the ordinate values are both subject to measurement error, orthogonal regression equation, is attained by minimizing the sum of the squares of perpendicular (or orthogonal) distances between the data and line. Conversely, in simple linear regression, the objective is to minimize the sum of squared vertical distances between observed y values and predicted Y values on the SLR line. The residual is defined as

$$d_i = \frac{|y_i - \beta_o - \beta_1 xi|}{\sqrt{\beta_1^2 + 1}} \quad (19)$$

Where d_i d is deviation measured perpendicularly from the point to the line (Glaister, 2005; Li, 1984; Scariano & Barnett II, 2003; Vicente de Julián-Ortiz et al., 2010). The sum of the squares of errors between the data points and regression line is to be minimized as:

$$E = \sum_{i=1}^{n} d_i^2 = \sum_{i=1}^{n} \frac{(y_i - \beta_o - \beta_1 x_i)^2}{\beta_1^2 + 1} \tag{20}$$

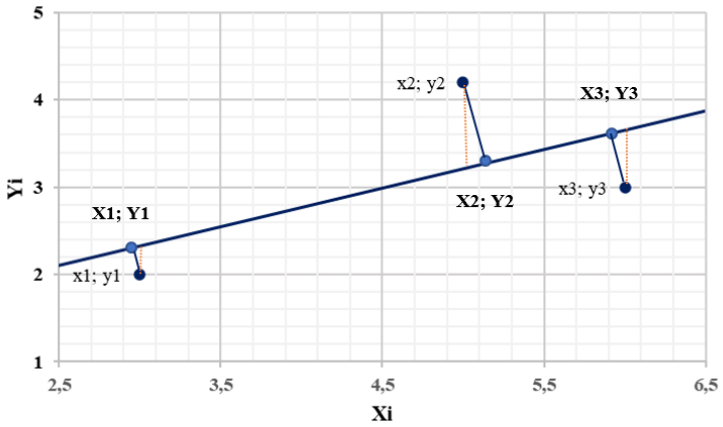

Fig. I. 9: Schematic diagram showing theoretical true points (i.e., (xi, yi), i=1, 2, 3) and estimated points (i.e., (Xi, Yi), i=1, 2, 3) on the fitted SOR regression line (solid black line) for a set of three observed points.

In the two papers by (Bormann et al., 2007; Bormann et al., 2009), Orthogonal Standard Regression (OSR) and Simple Linear Regression (SLR) results are deliberately presented together to highlight their differences and their dependence on the correlation coefficient. In another study, Castellaro and Bormann (2007) demonstrated that OSR, assuming an error ratio (η) of 1, remains superior to SLR as long as the true error ratio (or the square root of the true variance ratio, η_{true}) of the two variables falls within the range of 0.7 to 1.8. This condition is commonly met when comparing magnitudes measured at similar periods. However, outside of this error ratio range, SLR tends to better represent the data relationship. In practice, however, the square root of η can be as small as approximately 0.3. For example, this occurs when comparing short-period m_b values, which typically have initial errors ranging from 0.2 to 0.3, with M_w values from the Global Centroid Moment Tensor (GCMT) catalog, where initial errors are assumed to be no larger, and often even less than 0.1 m.u. (Gasperini et al., 2013a, 2013b; Gasperini et al., 2012; Helffrich, 1997; Kagan, 2003). For instance, Gasperini et al. (2013a) assumed an average initial error of 0.25 m.u. for m_b determinations and 0.1 m.u. for M_w, which corresponds to $\sqrt{\eta}$ =0.4 and η=0.16. Thus, if $\sqrt{\eta}$ differs from 1 and one knows sufficiently well this average error ratio, then a general orthogonal regression (GOR) would be closer to optimal than OSR.

2.5 The General Orthogonal Regression Methods

Recent literature, recognizing the inadequacies of SLR and SOR, has proposed the use of General Orthogonal Regression (GOR) methods that account for different uncertainties in the two regression variables. To our knowledge, the first GOR method applied to magnitude conversions was the chi-square regression (CSQ) introduced by Stromeyer et al. (2004). The authors highlighted that CSQ preserves the symmetry of the derived relationships, allowing them to be inverted. However, they did not definitively demonstrate CSQ's superiority over SLR and SOR for magnitude conversions.

It was only after the study by Castellaro et al. (2006) that the limitations of SLR in this context became clear, specifically its potential to produce systematic magnitude errors and significant bias in estimates of the slope of frequency-magnitude distributions (Gutenberg & Richter, 1944). Castellaro et al. (2006) recommended using GOR methods (Fuller, 2009a) to compute unbiased regression estimates when the ratio η between the variances of the dependent and independent variables

is known. If this ratio cannot be reliably determined, Castello et al. (2007) showed that SOR (equivalent to GOR with η=1) still performs better than SLR under reasonable assumptions.

More recently, (Bethmann et al., 2011) proposed the use of Weighted Total Least Squares (WLS) (Krystek & Anton, 2008), which employs a different geometric approach based on the slope angle α of the regression line and the distance p of the line from the origin.

Lolli and Gasperini (2012) concluded that all considered GO regression methods are suitable for magnitude conversions, provided their underlying assumptions are reasonably met. When only the variance ratio between the dependent and independent variables is known, which is the case most frequently occurring in the practice of magnitude conversions, GOR is the simplest and most widely used method. However, CSQ and WLS are preferable when the uncertainties of individual observations are known, particularly useful when the independent variable comes from a merged catalog with varying variance ratios between the dependent and independent variables.

2.5.1 Chi- Square Regression Method (CSQ)

The Chi-Square Regression technique, introduced by Stromeyer et al. (2004), has been widely used in recent seismological literature for both linear and non-linear equations. In this context, we focus solely on its application to cases where the two variables, Y and X, are linearly correlated.

$$Y = \alpha_o + \alpha_1 X \tag{21}$$

where α_o and α_1 are the regression coefficients. The CSQ is based on the minimization of the chi-square statistics that Stromeyer et al. (2004) defined as the sum of squared regression residuals, normalized to their variance.

$$\chi^2 = \sum_{i=1}^{n} \frac{(y_i - \alpha_1 x_i - \alpha_o)}{\sigma^2(x)(\alpha_1^2 + \eta)} \tag{22}$$

Here σ(x) is the uncertainties of the independent variable and $\eta = \sigma^2(y)/\sigma^2(x)$.

In the more general case when the uncertainty of each single observation is known, the best fitting regression coefficients α_o and α_1 can only be computed by numerical minimization of χ^2. In the case of constant uncertainties for each of the two variables, the problem can be solved analytically by considering that the necessary condition for the minimum is that the derivatives of χ^2 with respect to the coefficients α_o and α_1 vanish. For coefficient α_o , we have

$$\alpha_o = \bar{y} - \alpha_1 \bar{x} \tag{23}$$

The parameters $\bar{x}$ and $\bar{y}$ are the average values of the variables.

For coefficient α_1 , we have

$$\alpha_1 = \frac{\upsilon_{yy} - \eta\upsilon_{xx} \pm \sqrt{(\upsilon_{yy} - \eta\upsilon_{xx})^2 + 4\eta\upsilon_{xy}^2}}{2\upsilon_{xy}}$$

where

$$\upsilon_{xx} = \sum_{i=1}^{n} (x_i - \bar{x})^2 \tag{24}$$

$$\upsilon_{yy} = \sum_{i=1}^{n} (y_i - \bar{y})^2$$

$$\upsilon_{xy} = \sum_{i=1}^{n} [(x_i - \bar{x})(y_i - \bar{y})]$$

Since the square root in Eq. 24 is always greater than the absolute value of the terms outside the square root, it results in two solutions: one positive and one negative. We can disregard the negative solution (which actually represents a maximum of χ2 because the coefficient of the straight line must have the same sign as υ_{xy} .

2.5.2 General Orthogonal Regression Method (GOR)

The GOR method has been a subject of interest for researchers across various fields since its introduction by Adcock (1878). Over the years, GOR has been discovered and redefined multiple times by various researchers, including Anderson (1984), Carroll and Ruppert (1996), (Das et al., 2012, 2014), and Wason et al. (2012). The primary aim of GOR is to address the effects of measurement errors in both variables involved. It is typically applied in scenarios where (1) two methods are used to measure the same quantity, or (2) two variables are inherently related, following the same physical laws (Carroll & Ruppert, 1996). GOR works by minimizing the statistical Euclidean distance between observed data points and their corresponding theoretical points along the GOR line. The fundamental principles of the GOR method have been thoroughly discussed in the literature, including works by Madansky (1959), Fuller (2009a), Carroll and Ruppert (1996), and (Das et al., 2011, 2013). The GOR estimator is obtained by minimizing the sum of squared Euclidian distances (Eq. 24) from the true values

$$\sum_{i-1}^{n}[\frac{(y_i-\alpha_0-\alpha_1 X_i)^2}{\eta}+(x_i-X_i)^2] \tag{25}$$

Fuller (2009a) demonstrated that if the variance ratio η is known from independent information, the best estimators of the coefficients are

Where:

$$\alpha_1=\frac{\upsilon_{yy}-\eta\upsilon_{xx}+\sqrt{(\upsilon_{yy}-\eta\upsilon_{xx})^2+4\eta\upsilon_{xy}^2}}{2\upsilon_{xy}}$$

$$\alpha_0=\bar{y}-\alpha_1*\bar{x}$$

$$\upsilon_{xx}=\frac{1}{n}\sum_{i=1}^{n}(x_i-\bar{x})^2 \tag{26}$$

$$\upsilon_{yy}=\frac{1}{n}\sum_{i=1}^{n}(y_i-\bar{y})^2$$

$$\upsilon_{xy}=\frac{1}{n}\sum_{i=1}^{n}[(x_i-\bar{x})(y_i-\bar{y})]$$

The parameters $\bar{x}$ and $\bar{y}$ are the average values of the variables.

The errors on the regression parameters are given by Fuller (2009b) (Eq. 5 to Eq. 10):

$$\sigma_{\alpha_1}^2=\frac{\sigma_x S_\upsilon+\sigma_y S_\upsilon-\sigma_{\mu\upsilon}^2}{(n+1)\sigma_x^2} \tag{27}$$

$$\sigma_{\alpha_0}^2=\frac{S_\upsilon}{n}+\bar{X}\sigma_a^2 \tag{28}$$

Where;

$$\sigma_x=\frac{\sqrt{(\upsilon_y^2-\eta\upsilon_x^2)^2+4\eta\upsilon_{xy}^2}-(\upsilon_y^2-\eta\upsilon_x^2)}{2\eta} \tag{29}$$

$$\sigma_\mu=\frac{(\upsilon_y^2-\eta\upsilon_x^2)-\sqrt{(\upsilon_y^2-\eta\upsilon_x^2)^2+4\eta\upsilon_{xy}^2}}{2\eta} \tag{30}$$

$$S_{\upsilon} = \frac{(n-1)(\eta + \alpha_1^2)\sigma_{\mu}}{(n-2)} \tag{31}$$

$$\sigma_{\mu\upsilon} = -\alpha_1 \sigma_u \tag{32}$$

In conclusion, SLR, despite its widespread use, assumes that the independent variable is measured without error—an assumption that is not valid for most seismological datasets, where both magnitude estimates and ground motion parameters can carry significant uncertainties. This limitation can lead to biased parameter estimates, particularly in magnitude conversions across different scales. GOR addresses this issue by considering errors in both variables and minimizing the orthogonal distances to the regression line, thus providing a more statistically robust solution. In this study, GOR is adopted to perform magnitude conversions between different scales and to create a unified and consistent seismic dataset. This homogenized dataset is a critical input for the seismic source characterization and the subsequent probabilistic seismic hazard assessment (PSHA), ensuring greater reliability and consistency in the modeling framework.

CHAPTER 2: EARTHQUAKE DATA COMPILATION AND DEVELOPMENT OF A UNIFIED SEISMIC CATALOG

1 Introduction

Earthquake catalogs are crucial for providing comprehensive databases that support seismological investigations. They are essential not only for conducting hazard assessment studies but also for understanding the geodynamic processes driving seismic activity. Typically, seismic catalogs include various magnitude scales, each determined by the characteristics of recorded seismic waves. However, heterogeneity in magnitude types across different catalogs must be corrected to ensure the reliability of seismicity analysis. Therefore, seismologists and earthquake engineers often use magnitude homogenization relationships to standardize magnitude data to a specific type. Among the many magnitude scales, the M_w is widely recognized and commonly used in modern earthquake risk and recurrence analysis. To accurately assess seismic hazards in the study region, it is crucial to develop a unified seismic catalog in terms of M_w, with minimal uncertainties, utilizing the GOR method for superior magnitude conversion. This catalog serves as the primary and essential information source for delineating seismic source zones and comprehensively characterizing them. Additionally, the raw catalog may contain dependent events, such as aftershocks and foreshocks, associated with main shocks. These dependent events must be removed using a declustering algorithm to ensure a Poisson distribution of earthquake events. This chapter outlines the methodologies employed to process the earthquake catalog to achieve these objectives.

2 Plan to Develop a Unified Earthquake Catalog for Northeastern Algeria

Creating a unified earthquake catalog requires converting various types of earthquake magnitudes into a homogeneous magnitude scale. M_w is widely accepted as the most reliable measure of earthquake size because it avoids saturation effects associated with other scales like M_s and body wave magnitude m_b. Typically, correlations are established between M_w values from a reputable source and other magnitude types listed in the earthquake catalog.

While the Global Centroid Moment Tensor (GCMT) catalog is often the primary source for M_w data globally (Lolli et al., 2020), a consistent and comprehensive set of GCMT data is not readily available for Northeastern Algeria (Khemis & Athmani, 2023). This lack of data poses challenges in accurately converting traditional magnitudes to Mw using GCMT data. To address this challenge, the following steps will be undertaken (Fig. II. 1):

2.1 Expand the Study Area and Compile an Expanded M_w Catalog

The first step is to create an expanded M_w catalog covering all of Northern Algeria, not just the northeast, to obtain a broader data set for accurate regression relationships. This expanded catalog will integrate M_w data from various authoritative moment tensor solutions, including:

- Global Centroid Moment Tensor (GCMT) catalog
- European-Mediterranean Regional Centroid Moment Tensors (RCMT) catalog
- MT catalog of the Eidgenössische Technische Hochschule Zurich (ETHZ)

In addition to these direct sources of M_w, proxy M_w values will be calculated through regression analysis using M_s and m_b data. This data will be gathered from well-established international seismic agencies, including:

- European-Mediterranean Seismological Centre (EMSC)
- International Seismological Centre (ISC)
- United States Geological Survey National Earthquake Information Center (USGS NEIC)
- National Geographic Institute (IGN) Spanish Seismic Catalog

2.2 Homogenization of Magnitude Data for Northeastern Algeria

The expanded M_w dataset developed in the previous step will serve as a robust reference for homogenizing other magnitude types specific to Northeastern Algeria. This includes converting M_L reported by the Algerian Center for Research in Astronomy, Astrophysics, and Geophysics (CRAAG) and intensity values (I_0) into a unified M_w scale. This comprehensive approach ensures that all magnitude data for the region can be reliably compared and analyzed.

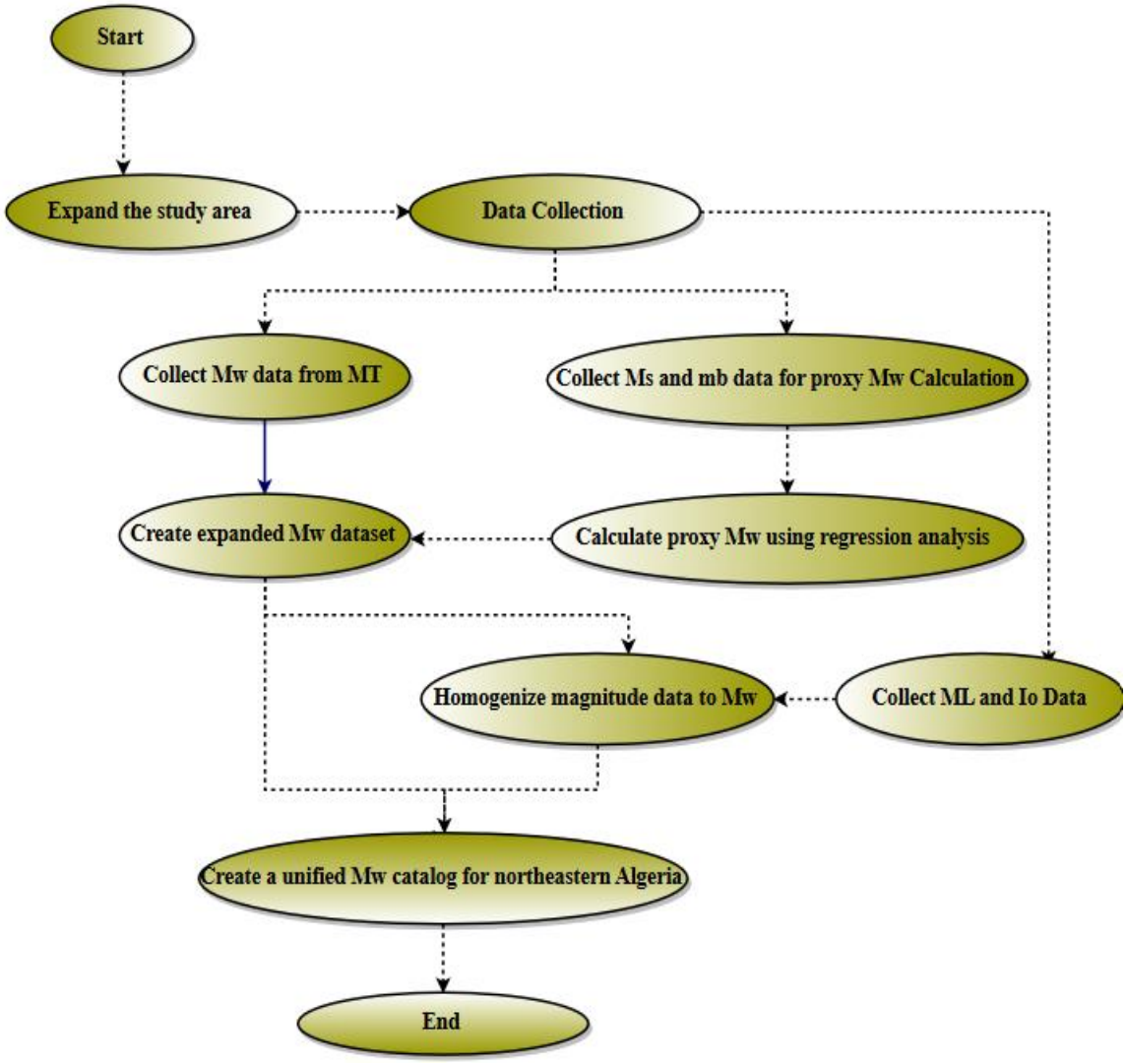

Fig. II. 1: Process for Developing a Unified Earthquake Catalog for Northeastern Algeria

3 Compilation of Earthquake data for the expanded M_w dataset

A variety of international databases were consulted to compile earthquake data for the expanded M_w dataset, covering the geographical area between 32°–38°N latitude and −3°–10°E longitude. The following databases were utilized, considering only magnitudes of $M_w \geq 2.5$, $2.5 \leq M_s \leq 6.5$, and $2.5 \leq m_b \leq 5.5$ for data collection:

- *Global Centroid Moment Tensor (GCMT)*: This widely used seismological and geophysical database, available at https://www.globalcmt.org/CMTsearch.html, offers detailed information on the locations and source parameters of earthquakes with magnitudes greater than 5.0 worldwide. GCMT's main goal is to calculate moment tensors for significant global earthquakes and disseminate the results promptly. Data in this catalog

date back to 1976, with the project known as the Harvard CMT Project before 2006. The GCMT database is highly regarded in the geophysical community for its reliability (Gasperini et al., 2012)

- *European-Mediterranean Seismological Center (EMSC)*: Accessible at https://www.seismicportal.eu/#/eventsListSection, this agency collects and integrates data, both automatically and manually reviewed, since 1998 from various national seismological networks in the Euro-Mediterranean region.
- *International Seismological Center (ISC*): This center's global earthquake catalog, available at http://www.isc.ac.uk/iscbulletin/search/catalogue/, compiles data from over 130 seismological agencies and projects dating back to 1900. The ISC catalog is considered the most comprehensive and authoritative global repository of earthquake parameters.
- *United States Geological Survey National Earthquake Information Center (USGS NEIC)*: Available at https://earthquake.usgs.gov/earthquakes/search/, the NEIC has been contributing earthquake data to the ISC Bulletin since its establishment in 1980, including historical data from its earlier designation as the National Earthquake Information Service (NEIS). The NEIC's primary mission is to accurately determine the magnitude and location of significant earthquakes globally and to disseminate this information quickly to relevant stakeholders.
- *National Geographic Institute (IGN) Spanish Seismic Catalog*: Accessible at https://www.ign.es/web/ign/portal/sis-catalogo-terremotos, the IGN is the main authority for earthquake monitoring and warnings in Spain, covering mainland Spain, Portugal, Morocco, Andorra, parts of France and Algeria, and several Spanish and Portuguese archipelagos.
- *European-Mediterranean Regional Centroid Moment Tensors catalog (RCMT)*: Available at http://www.bo.ingv.it/RCMT/searchRCMT.html, this catalog provides crucial data on seismic events in the European-Mediterranean area. It offers definitive solutions from 1997 onwards and quick, manually-reviewed solutions from 2009 to the present. The catalog is nearly complete for earthquakes with Mw greater than approximately 4.5 to 4.7 (Pondrelli et al., 2011).
- *Eidgenössische Technische Hochschule Zurich (ETHZ) MT catalog*: This catalog, accessible at http://www.seismo.ethz.ch/prod/tensors/mt_oldcat/index_EN, focuses primarily on moment tensors in the broader European-Mediterranean region, though it was discontinued after 2006. ETHZ still provides automatic moment tensor determinations for significant regional earthquakes (Bernardi et al., 2004)

Fig. II. 2 and 3 offer a comprehensive view of the magnitude types (M_s and m_b) and the number of events cataloged, along with their respective timeframes.

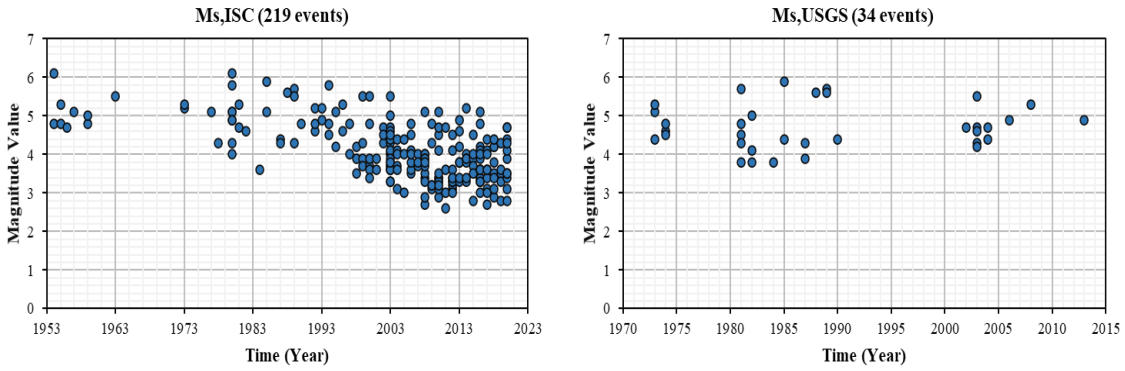

Fig. II. 2: Distribution of Surface Wave Magnitudes (Ms) and Event Counts Over Time in Northern Algeria.

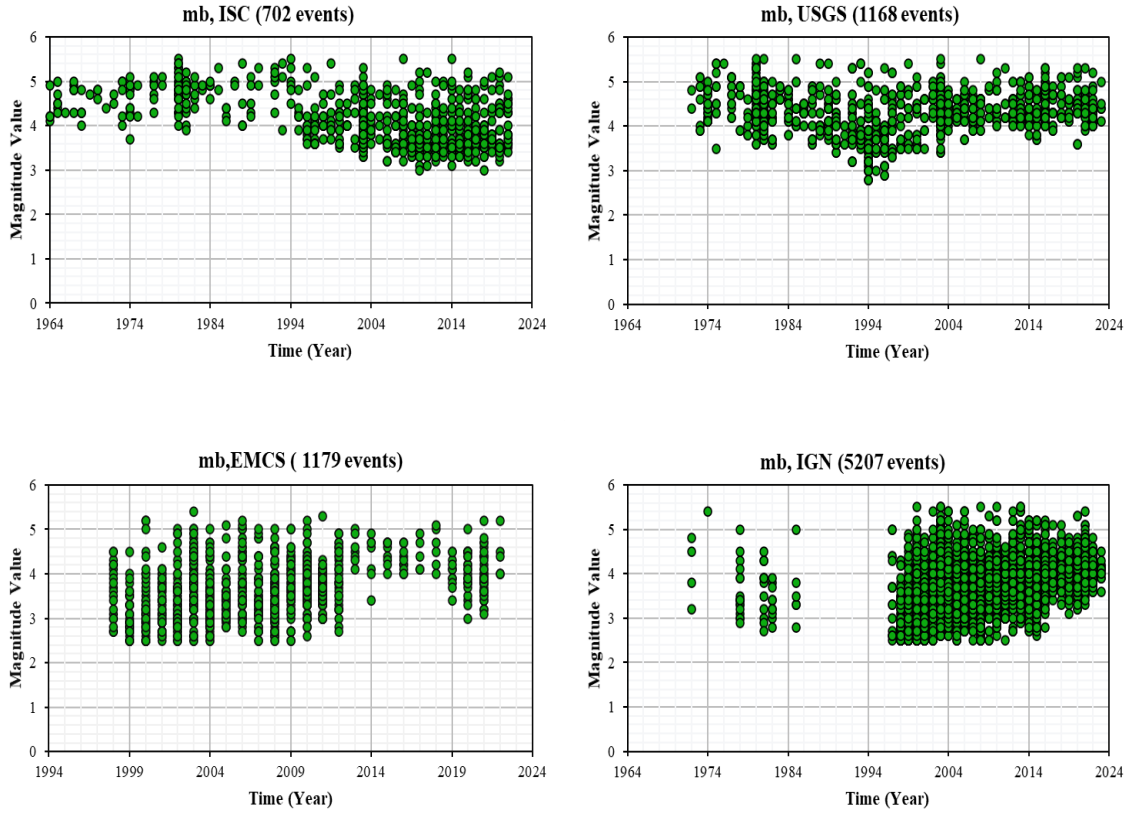

Fig. II. 3: Distribution of Body Wave Magnitudes (mb) and Event Counts Over Time in Northern Algeria.

Table II. 1 and Fig. II. 4 display the M_w values, the corresponding time period, and the number of events collected from each Moment Tensor (MT) catalog.

Table II. 1: Total Number of Mw Events for Northern Algeria

Magnitude **M_w**	**Centroid Moment Tensor**		
	GCMT	ZUR-CMT	RCMT
Total events	68	52	124

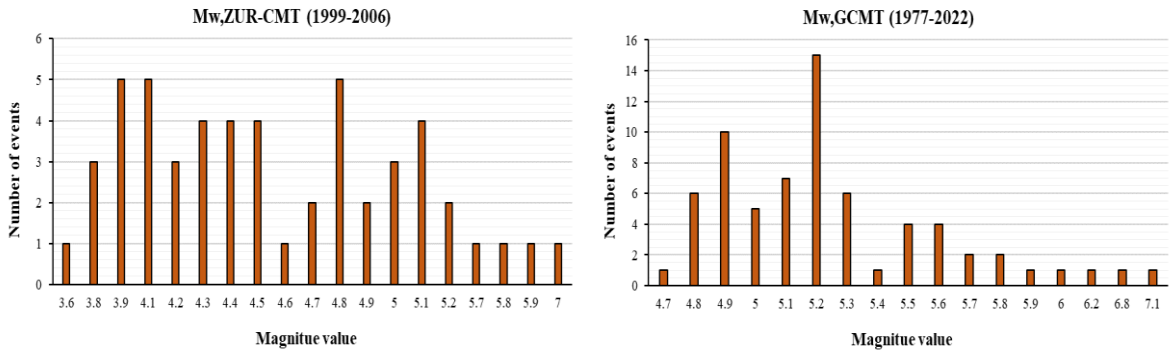

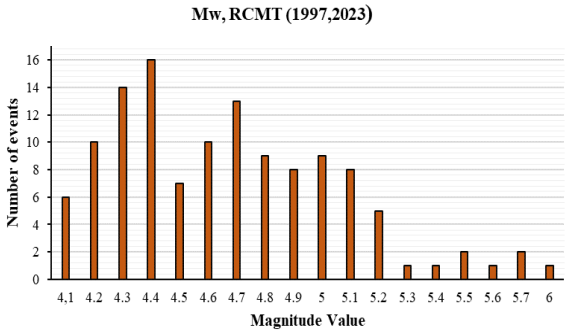

Fig. II. 4: Histograms of each Mw value sourced from the three MT catalogs

The M_w estimates from GCMT were adopted as the reference, and all other moment tensor are calibrated accordingly as in (Gasperini et al., 2012). For the Euro-Mediterranean areas, Gasperini et al. (2012) suggested applying ofset corrections of −0.05 to ETHZ data, while no corrections were needed for RCMT data, as it demonstrated equivalence to GCMT data. To avoid duplication, earthquakes were identified based on their geographic location and date. Data from lower-priority sources were excluded to ensure unique entries in the Mw dataset. GCMT data were prioritized due to their extensive validation and reliability, followed by RCMT data for their consistency with GCMT. Data from ZUR-CMT were then included using the same criteria as Harbi et al. (2010), identifying duplicates by matching origin times (ΔT) within one minute and locations (ΔLat/ΔLon) within one-hundredth degree of latitude/longitude (Eq. 33).

$$\begin{aligned} &\Delta T = 1\,\text{min} \\ &\Delta Lat = 0.01°, \Delta Lon = 0.01° \end{aligned} \tag{33}$$

After diligent application of these criteria, a total of 234 M_w data points were retained in the compilation. The dispersion of all these M_w events is visually represented in Fig. II. 5.

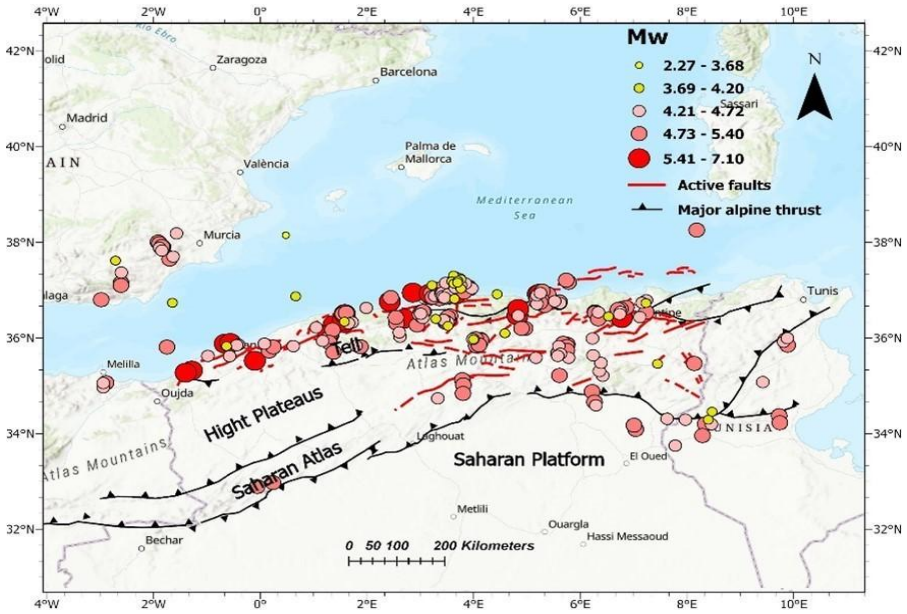

Fig. II. 5: Distribution of the M_w data in Northern Algeria from the three MT catalogs (GCMT, RCMT, and ZUR-CMT)

4 Problems and Proposed Solutions for Proxy M_w Estimation via Regression Analysis

To derive a proxy for M_w from other magnitude scales, it is crucial to use accurate magnitude conversion functions. In Algeria, researchers have often utilized the standard least squares regression (SLR) method to develop these conversion relationships (Bellalem, 2007; Hamlaoui et al., 2017; Harbi et al., 2010; Mouloud & Badreddine, 2017). However, some researchers have preferred using empirical relationships tailored to specific regions or on a global level, which limits their general applicability, especially in northern Algeria. For example, Mazari et al. (2023) applied empirical formulas by Tang et al. (2016) for Chinese earthquakes and by KADİRİOĞLU and Kartal (2016) for Turkish seismic events to convert M_s and m_b magnitudes to M_w. It is important to note that these empirical conversions (KADİRİOĞLU & Kartal, 2016; Tang et al., 2016) assume an η value of 1 within the GOR relationship. As highlighted in the previous chapter, the SLR approach has limitations for magnitude conversion because it assumes that the independent variable has no errors (Das et al., 2018; Wason et al., 2018). This assumption can lead to inaccurate or biased results, making it unsuitable for developing homogenization relationships. To address these biases, the general orthogonal regression (GOR) method has been suggested as an alternative (Fuller, 2009a). However, using the GOR method requires knowledge of the variances of both variables or their ratio (η), information that is typically not available in earthquake catalogs and bulletins. This lack of information about magnitude uncertainties has hindered the reliable use of the GOR method for magnitude conversion. Several studies have suggested that assuming equal uncertainties when applying GOR is not accurate, particularly for conversions between M_w and teleseismic magnitudes like M_s and m_b.

More recently, Bellalem et al. (2022) established new empirical relationships using the GOR method to connect M_L and duration magnitude M_d with M_w in Algeria. However, their work did not thoroughly explain certain methodological details, particularly those related to estimating the error variance ratio (η). The same authors also used empirical relationships from Scordilis (2006)to convert M_s and m_b magnitudes from ISC and USGS catalogs into M_w on a global scale. Additionally, they employed relationships from Cabañas et al. (2015)specific to Spain to convert m_b magnitudes recorded by the IGN. In these instances, Scordilis (2006)used the SLR method, whereas Cabañas et al. (2015)applied the GOR method, assuming η equals 1.

On the other hand, Khemis and Athmani (2023) developed new region-specific empirical relationships based on the GOR method to convert M_s and m_b magnitudes from ISC and USGS catalogs into M_w. They chose to use predefined standard deviation values for m_b and M_s as reported by different agencies.

Table II. 2 below summarizes the empirical relationships used by various researchers in Algeria for converting M_s and m_b into M_w.

Table II. 2: Algeria Summary of Magnitude Conversion Models Applied in Algerian Seismological Studies to Convert M_s and m_b into M_w.

AUT	MAG	METH	σ_{Mi}	σ_{Mw}	n	Conversion Equation	Reference	Context
Mazari et al. (2023)	$M_{s,ISC}$	GOR	/	/	1	$M_w = 0.8126(\pm0.034602)M_s + 1.1723\ (\pm0.208173)$ $M_s \geq 5.5$ $M_w = 0.5716(\pm0.024927)\ M_s + 2.4980\ (\pm0.117197)$ $3.4 \leq M_s \leq 5.4$	(Kadirioglu ˇ and Kartal, 2016)	Turkey (32°N 45°N and 23°E 48°E)

	$M_{s,USGS}$	GOR	/	/	1	$M_w = 0.8126(\pm0.034602)M_s + 1.1723 (\pm0.208173)$ $M_s \geq 5.5$ $M_w = 0.5716(\pm0.024927)M_s + 2.4980 (\pm0.117197)$ $3.4 \leq M_s \leq 5.4$	(Kadirioglu ˇ and Kartal, 2016)	Turkey(32°N 45°N and 23°E 48°E)
	$m_{b,ISC}$	GOR	/	/	1	$M_w = 1.16m_b - 0.55$	Tang et al.2016	China (29°N 46°N and 74°E 107°E)
	$m_{b,USGS}$	GOR	/	/	1	$M_w = 1.16m_b - 0.55$	Tang et al.2016	China (29°N 46°N and 74°E 107°E)
	$m_{b,IGN}$	GOR	/	/	1	$M_w = 1.16m_b - 0.55$	Tang et al.2016	China (29°N 46°N and 74°E 107°E)
	$m_{b,EMCS}$	GOR	/	/	1	$M_w = 1.16m_b - 0.55$	Tang et al.2016	China (29°N 46°N and 74°E 107°E)
Khemis and Athmani (2023)	$M_{s,ISC}$	GOR	0.2	0.07	0.125	$M_w = 0.716(\pm0.022)M_{s,ISC} + 1.807(\pm0.103)$	Khemis and Athmani (2023)	Northern Algeria (32° to 38° N and -3° to 10° E)
	$M_{s,USGS}$	GOR	0.2	0.07	0.125	$M_w = 0.772(\pm0.074)M_{s,USGS} + 1.475(\pm0.376)$	/	Northern Algeria (32° to 38° N and -3° to 10° E)
	$m_{b,ISC}$	GOR	0.25	0.07	0.08	$M_w = 1.076 (\pm0.037) - 0.228(\pm0.177)m_{b,ISC}$	/	Northern Algeria (32° to 38° N and -3° to 10° E)
	$m_{b,USGS}$	GOR	0.25	0.07	0.08	$M_w = 1.293 (\pm0.054) - 1.371(\pm0.267)m_{b,USGS}$	/	Northern Algeria (32° to 38° N and -3° to 10° E)
	$m_{b,IGN}$	/	/	/	/	/	/	/
	$m_{b,EMCS}$	/	/	/	/	/	/	/
Bellalem et al. (2022)	$M_{s,ISC}$	SLR	/	/	/	$M_w = 0.67(\pm0.005)M_s + 2.07(\pm0.03)$ $3.0 \leq M_s \leq 6.1$ $MW = 0.99(\pm0.002)M_s + 0.08(\pm0.13)$ $6.2 \leq M_s \leq 8.2$	Scordilis et al. 2006	Global
	$M_{s,USGS}$	SLR	/	/	/	$M_w = 0.67(\pm0.005)M_s + 2.07(\pm0.03)$ $3.0 \leq M_s \leq 6.1,$	Scordilis et al. 2006	Global

						$M_w = 0.99(\pm0.002)M_s + 0.08(\pm0.13)$ $6.2 \leq M_s \leq 8.2$		
	$m_{b,ISC}$	SLR	/	/	/	$M_w = 0.85(\pm0.04)m_b + 1.03(\pm0.23)$ $3.5 \leq m_b \leq 6.2$	Scordilis et al. 2006	Global
	$m_{b,USGS}$	SLR	/	/	/	$M_w = 0.85(\pm0.04)m_b + 1.03(\pm0.23)$ $3.5 \leq m_b \leq 6.2$	Scordilis et al. 2006	Global
	$m_{b,IGN}$	GOR	/	/	1	$M_w = -1.528\ (\pm0.385) + 1.213(\pm0.077)m_b$ (VC)	Cabañas et al. (2015)	Spain (34° N 45°N and 13° W 6°E)
	$m_{b,EMCS}$	/	/	/	/	/	/	/

To overcome these limitations, our research aims to develop new empirical correlations between M_s and m_b magnitudes and M_w, using data from the GCMT, RCMT, and ETHZ catalogs. These correlations will help expand the M_w dataset for northern Algeria and its surrounding regions. We use the GOR approach to derive these homogenization relationships, incorporating suitable values for the error variance ratio (η). Our methodology builds on the foundational work of Gasperini et al. (2013a) and (Lolli & Gasperini, 2012; Lolli et al., 2020), which established specific standard deviation values for different magnitude types. Gasperini et al. (2012) estimated the average uncertainties associated with individual M_w measurements, finding deviations of 0.07 units for the GCMT, RCMT, and ETHZ catalogs. These estimates were based on comparisons of standard deviations between catalog pairs, following the application of offset corrections. Previous studies, such as those by Helffrich (1997) and Kagan (2003), have explored uncertainties ranging from 0.05 to 0.15 units, considering factors like depth, magnitude, and time.

To approximate the uncertainty of various magnitude types, we follow the procedure outlined by Gasperini et al. (2013a) and Lolli et al. (2020). For the dependent variable M_w, an assumption is made that the uncertainty (σ_{M_w}) equals 0.07. Subsequently, the uncertainty of the independent variable M_i (σ_{M_i}) is adjusted in order to coincide the a priori variance of the regression (Eq.34) with the empirical variance estimated from regression residuals (Eq.35).

$$\sigma^2_{a\,priori} = \sigma^2_{Mw} + \beta^2\sigma^2_{Mi} \tag{34}$$

$$\sigma^2_{empirical} = \frac{1}{N-2}\sum_{j=0}^{N}(M_{wj} - \alpha - \beta\, M_{ij})^2 \tag{35}$$

In which α and β are the linear regression intercept and coefficient (slope), respectively, and N is the number of $(M_w - M_i)$ data pairs used for the regression. By equating these two variances, an approximate estimation of the uncertainty of M_i can be inferred (Eq.36).

$$\sigma_{M_i} = \frac{1}{\beta}\sqrt{\frac{1}{N-2}\left(\sum_{j=0}^{N}(M_{wj} - \alpha - \beta\, M_{ij})^2\right) - \sigma^2_{Mw}} \tag{36}$$

Importantly, since varying σ_{M_i} may vary the regression parameters, as well as the a priori and empirical standard deviations, a series of iterations is required to ensure that $\sigma^2_{a\,priori}$ and $\sigma^2_{empirical}$ coincide with one another. Flowchart below (Fig. II. 6) summarize all the necessary steps discussed above to develop an expanded M_w dataset.

Seismic data for Ms and mb in relation to Mw generally do not follow a consistent linear trend across all magnitude ranges. Key clarifications include:

- **Scaling Coefficients** Kanamori and Anderson (1975) postulated a scaling coefficient between M_s and M_w of 2/3 for low magnitudes, 1 for intermediate magnitudes, and 2 for high magnitudes, based on theoretical considerations of surface wave excitation with a period of around 20s.
- **Transition Points for Ms:** A transition point between slopes of intermediate and low magnitudes is suggested to occur at M_s < 6.2-6.5 (Ekström & Dziewonski, 1988; Scordilis, 2006), while the transition at high magnitudes, often characterized by saturation, remains imprecise, likely occurring for M_s > 8 (Lolli et al., 2023).
- **Patterns for mb:** A parallel scenario is anticipated for m_b, with transition points adjusted to lower magnitudes due to the shorter period of seismic waves sampled (within the range of 1 to 5 seconds). Gasperini et al. (2013a) demonstrated that m_b from ISC aligns with M_w at lower values (m_b < 4–4.5) before reaching saturation for m_b > 5–5.5. Accordingly, it can be inferred that transitions between slopes 1 and 2 occur around mb = 5–5.5. The precise transition point between slope 1 and 2/3 remains uncertain, with Gasperini et al. (2013a) and Lolli et al. (2014) suggesting its absence beyond m_b = 3.5, approximating the minimum m_b computed by ISC and other seismic agencies.

To address the non-linear nature of the data at higher magnitudes, the ranges of Ms and mb magnitudes in this study for Northern Algeria are limited to 6.5 and 5.5, respectively, allowing for a focus on the ranges where linear relationships are applicable. The standard deviation values for Ms and mb magnitudes, along with the corresponding error variance ratios for their conversions, were computed using a MATLAB program and are presented in

Table II. 3 below.

Table II. 3: Standard Deviation σ_{M_i} and Error Variance Ratios η for M_s and m_b Conversions

Magnitudes	$\mathbf{M_{s,ISC}}$	$\mathbf{M_{s,USGS}}$	$\mathbf{m_{b,ISC}}$	$\mathbf{m_{b,USGS}}$	$\mathbf{m_{b,IGN}}$	$\mathbf{m_{b,EMCS}}$
σ_{M_i}	0.182	0.228	0.159	0.179	0.198	0.143
Conversions	$M_{s,ISC}\rightarrow M_w$	$M_{s,USGS}\rightarrow M_w$	$m_{b,ISC}\rightarrow M_w$	$m_{b,USGS}\rightarrow M_w$	$m_{b,IGN}\rightarrow M_w$	$m_{b,EMCS}\rightarrow M_w$
η	0.147	0.094	0.194	0.152	0.125	0.236

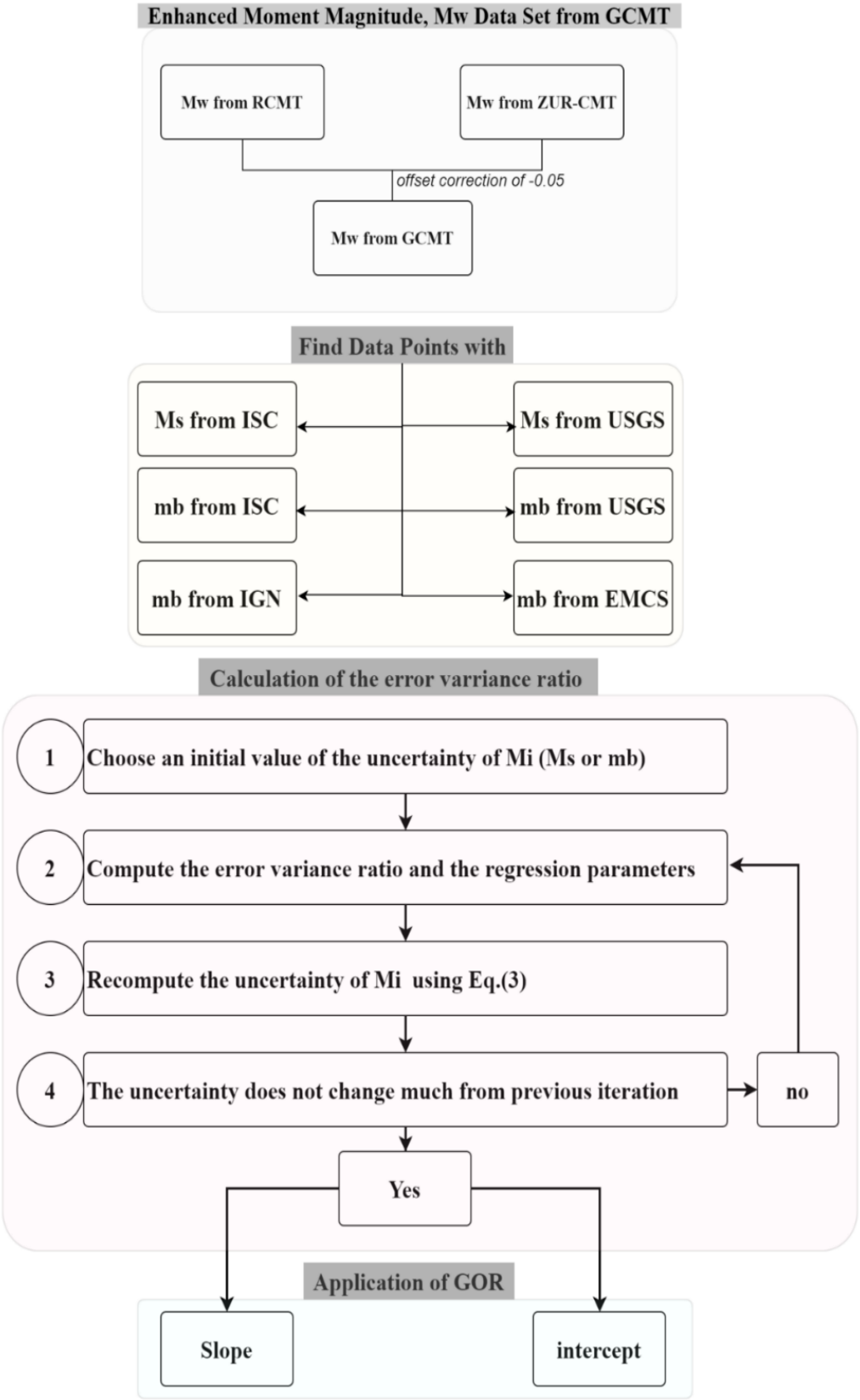

Fig. II. 6: Methodology followed to obtain an expanded M_w data Set.

5 Magnitude Conversion

5.1 Correlation of M_s to M_w

Although both NEIC and ISC use the same formula to estimate M_s (Eq. 6, Chapter 1), their methodologies differ slightly. NEIC emphasizes the vertical component of Rayleigh waves within a narrower period range (18-22 seconds) and an epicentral distance between 20° and 160°, while ISC incorporates both vertical and horizontal components over a wider range of periods (10-60 seconds) and distances (5° to 160°) (Petrova & Gabsatarova, 2020). Despite these methodological differences, studies (e.g., Scordilis (2006) and Das et al. (2011)) have shown that the magnitudes reported by both organizations are generally consistent on a global scale, allowing for the creation of unified datasets. However, in some regions, such as northern Algeria, a minor but significant discrepancy of approximately 0.05 magnitude units has been detected between the two datasets (Khemis & Athmani, 2023). This regional variation has led to the development of distinct relationships for NEIC and ISC data to address local differences. Following a similar approach, Khemis and Athmani (2023) used general orthogonal GOR to establish relationships between M_s from ISC and NEIC and M_w from GCMT, RCMT, and ETHZ. They assumed a standard deviation of 0.20 for M_s, while in our study, the calculated standard deviations were approximately 0.20 (0.182 for $M_{s,ISC}$ and 0.228 for $M_{s,NEIC}$). Consequently, we observed a slight discrepancy between the GOR lines proposed by Khemis and Athmani (2023) and those derived from our analysis (see Figs. II. 7 and 8). The conversion equations for $M_{s,ISC}$ and $M_{s,USGS}$, based on datasets of 77 and 18 entries, with coefficients η of 0.147 and 0.094, respectively, are given in Eqs. 37 and 38. The regression plots are given in Fig II.7 and 8 alongside other best fit line to allow for visual comparaison.

$$M_w = 0.656(\pm 0.024) M_{S,ISC} + 2.069(\pm 0.110)$$
$$R^2 = 0.894 \qquad (37)$$

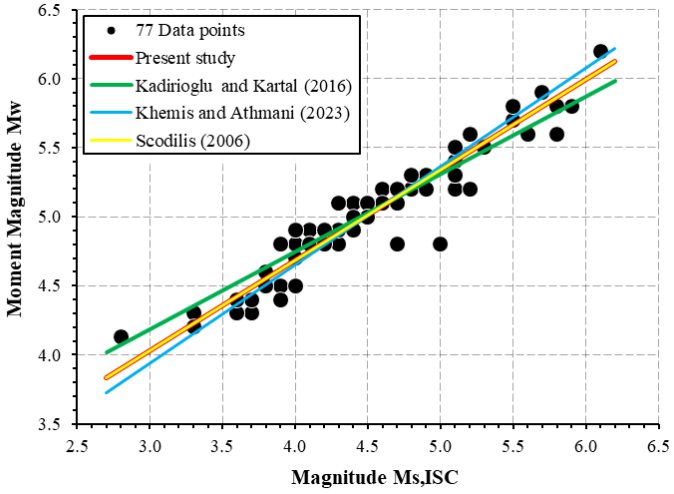

Fig. II. 7: Linear regression relationships for M_W against $M_{S,ISC}$

$$M_w = 0.657(\pm 0.073) M_{S,USGS} + 2.037(\pm 0.371)$$
$$R^2 = 0.755 \qquad (38)$$

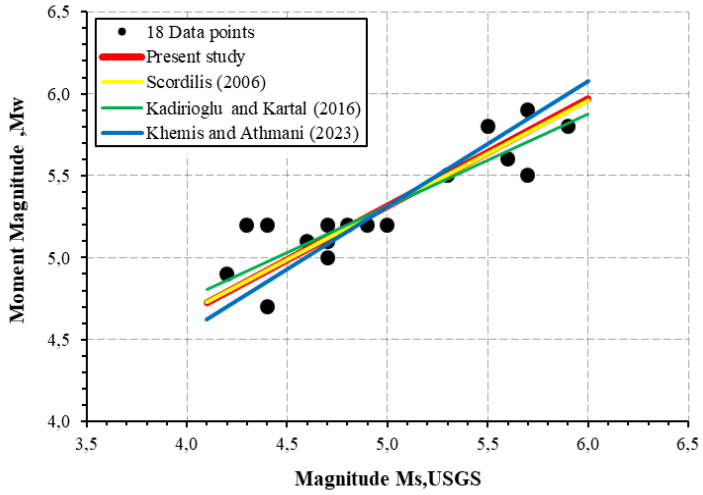

Fig. II. 8: Linear regression relationships for M_W against $M_{S,USGS}$

5.2 Correlation of m_b to M_w

Several studies, such as those by Scordilis (2006) and Das et al. (2011), have consistently demonstrated that $m_{b,ISC}$ and $m_{b,USGS}$ are not globally equivalent. This discrepancy is evident even in focused regional studies like northern Algeria (Khemis & Athmani, 2023), making it clear that these datasets cannot be merged into a single, unified set.

When converting mb to M_w, Khemis and Athmani (2023) relied on a fixed standard deviation of 0.25 for m_b. In contrast, our study computed the standard deviations for m_b reported by various agencies, and our results revealed notable differences from the assumed value. Specifically, we found standard deviations of 0.159 for $m_{b,ISC}$, 0.179 for $m_{b,USGS}$, 0.198 for $m_{b,IGN}$, and 0.143 for $m_{b,EMCS}$. Based on these findings, we opted to establish new conversion relationships that account for the appropriate error variance ratios, better reflecting the true variability in the data.

5.2.1 Correlation of m_b from ISC to M_w

Eq. (39) outlines the GOR relationship used to convert m_b values from ISC to M_w, based on a dataset consisting of 82 entries and a coefficient η of 0.194. The corresponding regression relationship is illustrated in Fig. II. 9.

$$M_w = 1.061(\pm 0.043) m_{b,ISC} - 0.162(\pm 0.204) \qquad (39)$$
$$R^2 = 0.855$$

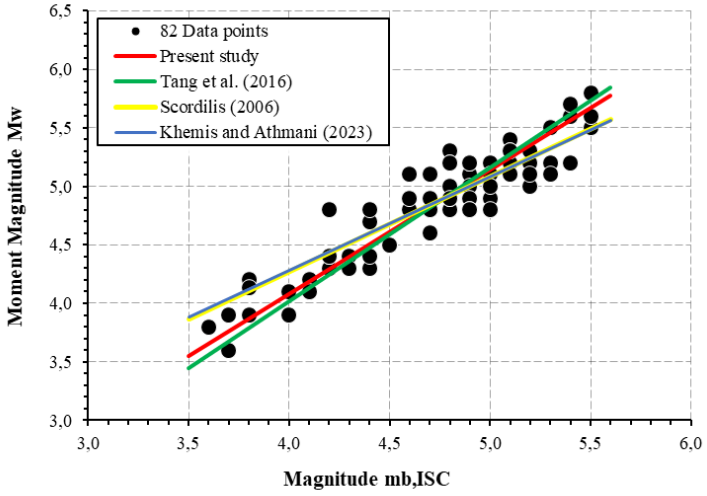

Fig. II. 9: Linear regression relationships for M_W against $m_{b,ISC}$

5.2.2 Correlation of m_b from USGS to M_w

The GOR relationship for converting m_b values from the USGS to M_w is expressed in Eq. (40), which is based on a dataset of 112 entries and a coefficient η of 0.152. The regression relationship between these two magnitudes is visually represented in Fig. II. 10

$$M_w = 1.489(\pm 0.077) m_{b,USGS} - 2.316(\pm 0.369) \qquad R^2 = 0.605 \tag{40}$$

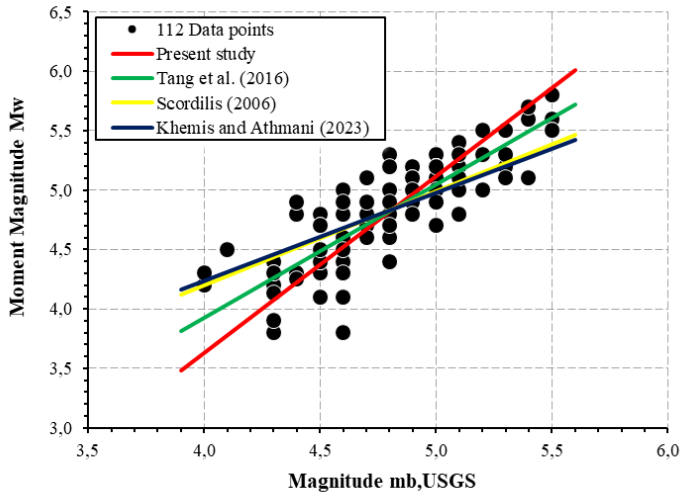

Fig. II. 10: Linear regression relationships for M_W against $m_{b,USGS}$

5.2.3 Correlation of m_b from IGN to M_w

Eq. (41) presents the empirical relationship used to convert m_b values from the IGN into M_w, based on a dataset of 53 entries and a coefficient η of 0.125. The regression relationship obtained through the GOR technique is illustrated in Fig. II. 11.

$$M_w = 1.517(\pm 0.129) m_{b,IGN} - 2.850(\pm 0.645) \qquad R^2 = 0.447 \tag{41}$$

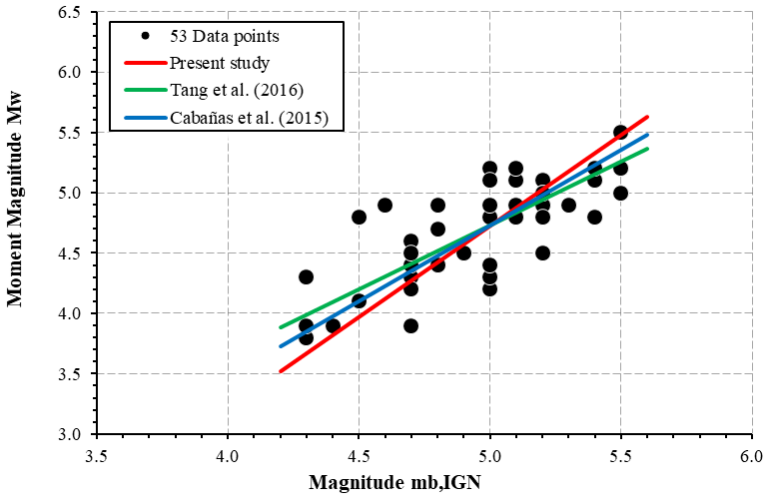

Fig. II. 11: Linear regression relationships for M_W against $m_{b,IGN}$

5.2.4 Correlation of m_b from EMCS to M_w

Eq. (42) presents the empirical correlation for converting mb from the EMCS to M_w, derived from a dataset of 53 events with a coefficient η of 0.236. The regression relationship, established using the GOR technique, is shown in Fig. II. 12.

$$M_w = 1.340(\pm 0.099) m_{b,EMCS} - 1.653(\pm 0.465) \qquad R^2 = 0.645 \tag{42}$$

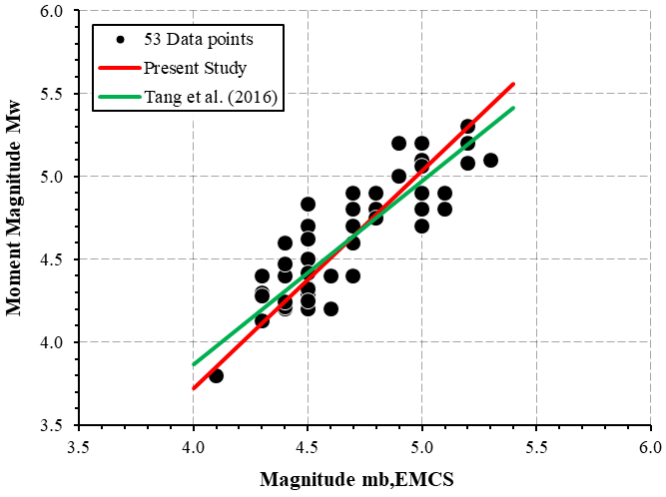

Fig. II. 12: Linear regression relationships for M_W against $m_{b,EMCS}$

The Root Mean Square Error (RMSE) is a commonly used metric to evaluate the accuracy of estimation models. It calculates the square root of the average of the squared differences between predicted and observed values, providing an effective measure of model performance. RMSE is particularly valuable for assessing the quality of predictions by quantifying the extent to which the predicted values deviate from the true values. A smaller RMSE indicates better alignment between the predicted and actual values, signifying higher accuracy and reliability of the model.

$$RMSE = \sqrt{\frac{\sum_{i=1}^{N} (y_{obs,i} - Y_{\text{model,i}})^2}{N}} \tag{43}$$

To assess the accuracy of our newly developed empirical relationships for the northern Algeria region and compare them with existing models (Cabañas et al., 2015; Khemis & Athmani, 2023; Scordilis, 2006; Tang et al., 2016), we calculated the RMSE between the moment magnitude (Mw) values derived from the Centroid Moment Tensor (CMT) method and those predicted by various empirical equations. The results of this comparison are summarized in Table II.4. A lower RMSE value indicates that the predicted Mw values are closer to those obtained from the CMT method, reflecting the accuracy and reliability of each empirical model.

Table II. 4 displays the RMSE values for each of the empirical relationships evaluated. Analyzing these values reveals that our newly developed empirical relationships consistently outperform the others in nearly all cases, making them the most suitable choice for researchers conducting seismic analyses in the region.

Table II. 4: Comparison of M_w Estimates from Different Empirical Relationships.

	RMSE Values					
Conversions	Kadirioglu ˇ and Kartal (2016)	Tang et al (2016)	Scordilis et al (2006)	Khemis and Athmani, (2023)	Cabañas et al. (2015)	Our Study
$M_{s,ISC}$ →Mw	0.143	/	0.155	0.152	/	0.139
$M_{s,USGS}$→M_w	0.150	/	0.187	0.187	/	0.165
$m_{b,USGS}$→M_w	/	0.305	0.261	0.183	/	0.276
$m_{b,ISC}$ →M_w	/	0.215	0.380	0.247	/	0.183
$m_{b,IGN}$ →Mw	/	0.578	/	/	0.324	0.309
$m_{b,EMCS}$→M_w	/	0.331	/	/	/	0.205

The expanded M_w dataset includes 5,668 seismic events (see Fig. II. 13) with Mw ≥ 2.5, covering the period from 1954 to 2023. In merging the data, we established a priority order (outlined in Table II. 5) that favored datasets derived from regression relationships with the highest correlation coefficients. This strategy allowed us to incorporate the most reliable and well-correlated data, thereby improving the overall quality of our Mw dataset.

Table II. 5:Priority order for magnitude scales during data merging process.

Priority Order	**Magnitude scales**	R^2
(1)	M_w from CMTs	1
(2)	M_w from $M_{s,\ ISC}$	0.894
(3)	M_w from $m_{b,ISC}$	0.855
(4)	M_w from $M_{s,USGS}$	0.755
(5)	M_w from $m_{b,\ EMCS}$	0.645
(6)	M_w from $m_{b,USGS}$	0.605
(7)	M_w from $m_{b,IGN}$	0.447

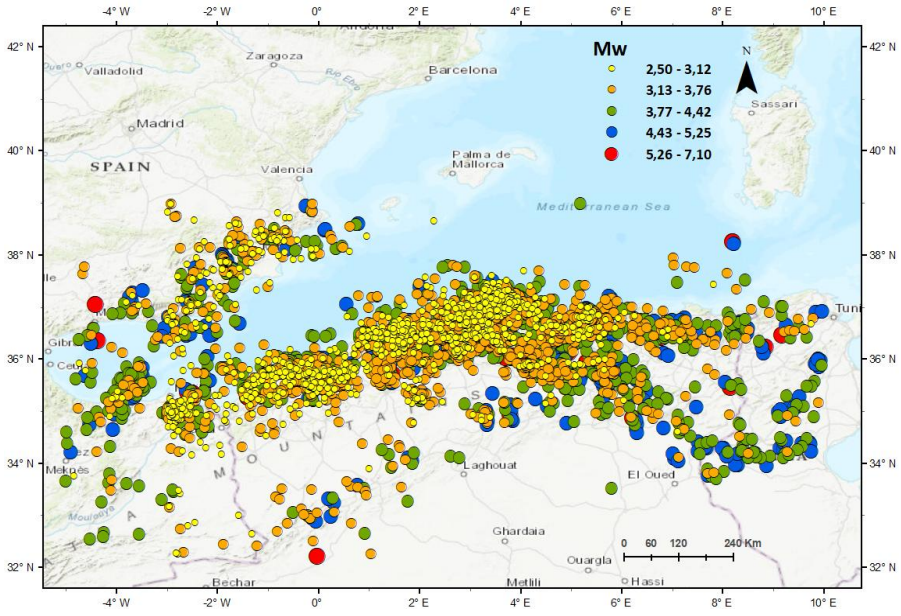

Fig. II. 13: The spatial distribution of the expanded Mw dataset.

For the Northeast region of Algeria, the catalog compiled encompasses a total of 1345 seismic events with $M_w \geq 2{,}5$ (Fig. II. 14 on the right side), covering a period from 1957 to 2023.

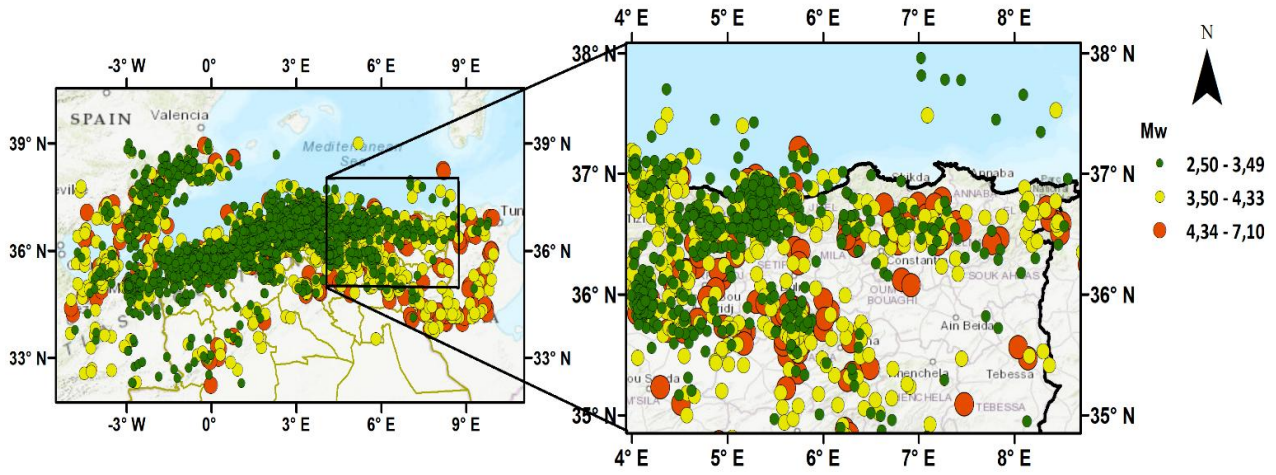

Fig. II. 14: M_w data for the northeast of Algeria from the Expanded M_w catalog.

6 Compilation of Historical and Local Magnitude Data

6.1 The historical Data

In regions where significant earthquakes occur infrequently, the likelihood of experiencing a major seismic event during the instrumental observation period is quite low. This scarcity can lead to imprecise estimates of large, rare rupture scenarios when relying solely on instrumental catalogs (Baker et al., 2021). To overcome this challenge, recent instrumentally recorded events are integrated with historical data from before the instrumental era. In Algeria, the scientific community has made substantial efforts over the last few decades to improve the quality and scope of earthquake catalog databases. A variety of national and regional catalogs, alongside scholarly works such as those by (Benouar et al., 1994) and (Harbi et al., 2010), have emerged. Harbi, in particular, has played a pivotal role in deepening our understanding of seismic activity in Northeast Algeria since her first publication on the subject in 1999(Harbi et al., 1999). Her extensive research has led to the identification and inclusion of numerous historical earthquakes in the catalog. Notably, her investigation into the seismic effects during the Roman period revealed impacts on archaeological structures (Ferdi & Harbi, 2014). However, her most significant achievement lies in her meticulous review of French archives, which resulted in the discovery of many new seismic events and a reassessment of previously recorded ones. The work of Harbi et al. (2010) aimed to consolidate reliable catalog data from both historical and instrumental sources, irrespective of their geographic origin—local, regional, or global. Their compilation, which focuses on Northeast Algeria, serves as the foundation for our CRAAG catalog. (Harbi et al., 2010), we have gathered a total of 663 historical events with $I_0 \geq 3$, spanning the years 1357 to 2010. Fig. II. 15 illustrates the distribution of these historical events.

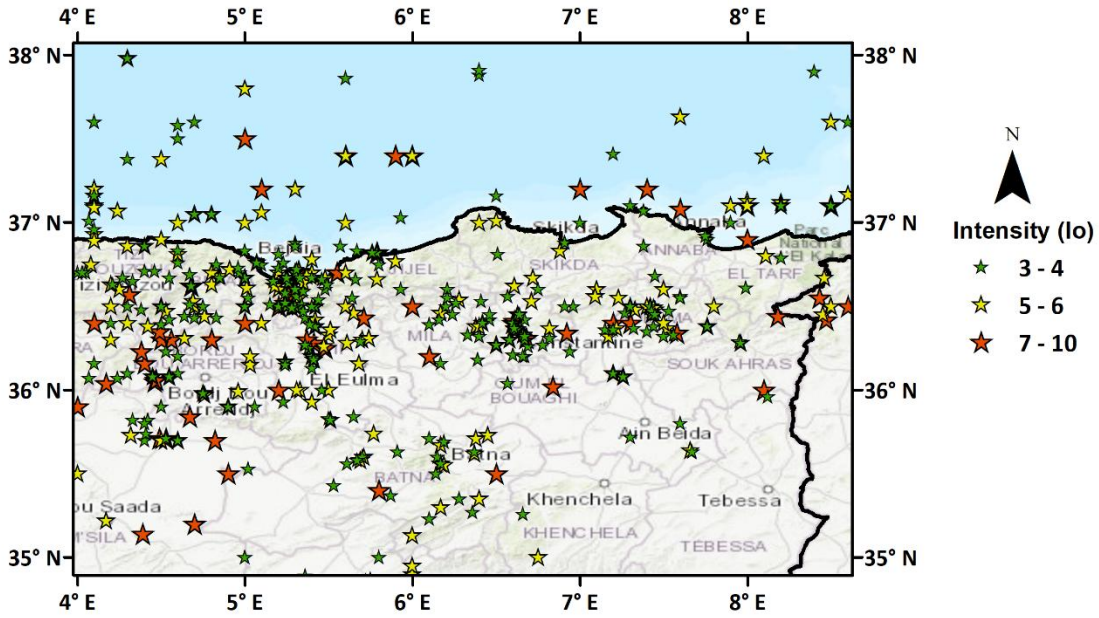

Fig. II. 15: Distribution of Historical Data I_0 in Northeastern Algeria (Harbi et al., 2010)

6.2 The M_L data from the Centre of Research on Astronomy, Astrophysics, and Geophysics (CRAAG)

We have enhanced the existing CRAAG instrumental data from Harbi et al. (2010) by incorporating additional information from the ISC and EMSC databases. The CRAAG earthquake data are regularly updated each year and are made publicly available through the ISC and EMSC online platforms (Bellalem et al., 2022).

A distinctive aspect of this catalog is its strong focus on ML as the primary measure for reporting magnitude values. Notably, it includes around 3,616 seismic events (illustrated in Fig. II. 16) with M_L values of 2.5 or higher, covering the timeframe from 1992 to 2022.

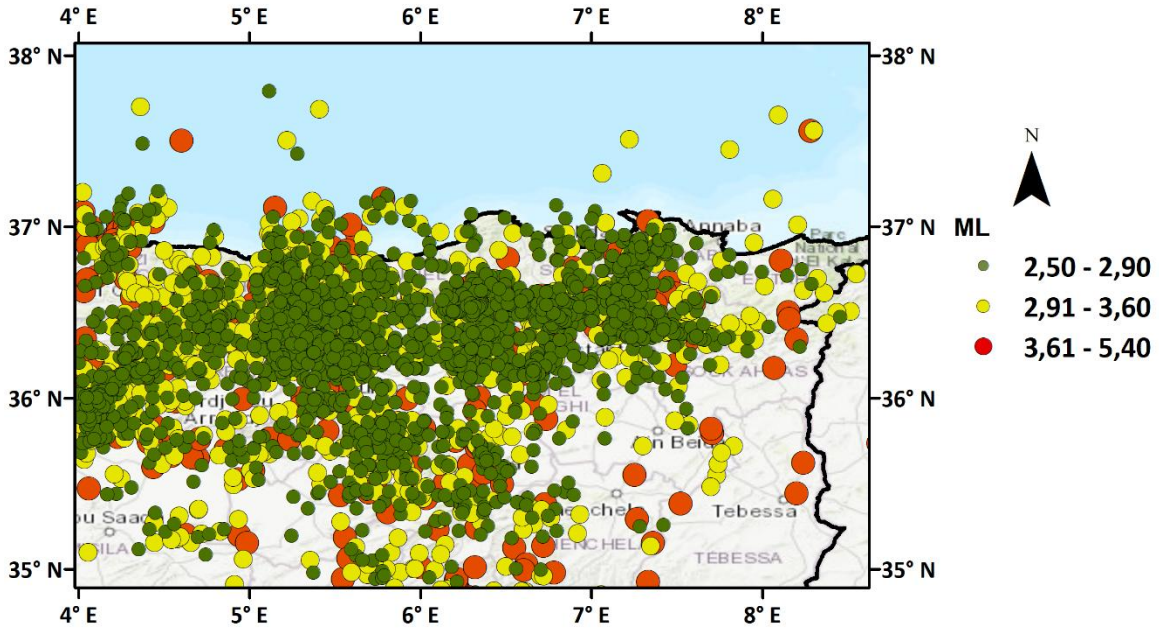

Fig. II. 16: Distribution of M_L Data Sourced from CRAAG in Northeastern Algeria

6.3 Conversion of M_L magnitudes and Intensity I_o to M_w

Theoretical and empirical studies (Bakun, 1984; Deichmann, 2006; Hanks & Kanamori, 1979; Heaton et al., 1986) indicate that, in principle, M_L and M_w should be equivalent. Heaton et al. (1986) noted that while M_L and M_w align closely up to a magnitude of 6, M_L begins to increase at a slower rate than M_w beyond this point. Over the past two decades, global research ((Bindi et al., 2005; Castello et al., 2007; Gasperini & Ferrari, 2000; Johnston, 1996) has resulted in empirical linear conversion equations of the form (Eq. 44)

$$M_w = \beta \times M_L + \alpha \tag{44}$$

where the estimated slope typically falls between 0.6 and 0.8, significantly lower than the theoretical expectation of 1. These studies utilized OLS regression; however, this method is rigorously applicable only when the uncertainty of the predictor (independent) variable is minimal compared to that of the dependent variable, a condition that often does not hold true for magnitude measurements, especially when comparing M_L to M_w. To address this limitation, a GOR approach, which takes into account the uncertainties of both predictor and response variables, is necessary. Recently, Bellalem et al. (2022) established new empirical relationships in Algeria using GOR to connect M_L scales from CRAAG with M_w. However, some critical methodological aspects, particularly regarding the estimation of the error variance ratio (η), were not thoroughly explained.

(Gasperini et al., 2013b) explored the M_L-M_w relationship in Italy using GOR with a carefully chosen error variance ratio. Their findings suggested that the M_L scale, derived from real or synthesized Wood–Anderson waveforms, generally correlates well with M_w, although it tends to underestimate M_w by approximately 0.1 to 0.2 magnitude units. As of now, CRAAG has not developed a relationship between its reported M_L values and other magnitude scales used by regional agencies. In our analysis, we consider the equivalent Mw simply as the value of M_L, in line with theoretical principles.

This study produced a magnitude-intensity relationship based on 24 earthquakes with Intensity (I_0) and M_w, represented by Eq. (45). The regression relationship derived from the GOR method, utilizing an error variance ratio η of 1, is illustrated in Fig. II. 17, alongside other relationships published by Algerian researchers (Benbelkacem et al., 2022; Cabañas et al., 2015; Mezcua, 2002). Historical earthquakes cataloged by Harbi et al. (2010), for which only intensity values are available, have been converted to M_w using this empirical relationship.

$$\begin{aligned} M_w &= 0.747(\pm 0.089) \times I_o + 0.727(\pm 0.414) \\ R^2 &= 0.576 \end{aligned} \tag{45}$$

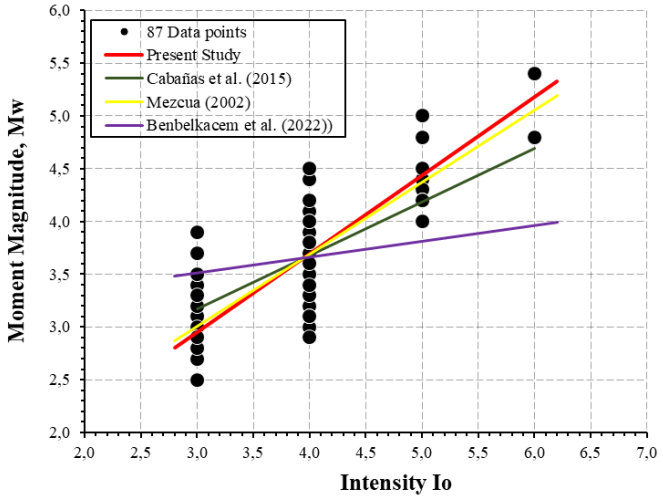

Fig. II. 17: Linear regression relationships for M_w against I_o

7 The Final Unified Earthquake Catalog for the northeastern of Algeria

The final Homogenized Earthquake Catalog (HEC) compiled in this study includes 5,111 events with $M_w \geq 2$ (Fig. II. 18). A portion of this catalog, specifically for events with magnitudes $M_w \geq 5.5$, is displayed in Table II. 9 in Appendix. The merging process followed the criteria established Harbi et al. (2010). Specifically:

1. Duplicate events were identified if their origin times (ΔT) differed by less than one minute.
2. Their locations ($\Delta Lat/\Delta Lon$) were within one hundredth of a degree of latitude/longitude.

Additionally, we implemented a priority order for the data:

1. Priority was given to the computation of M_w proxies from M_L of the national seismic network.
2. Followed by the data obtained from the developed expended catalog and the computation of M_w proxies from I_{max} .

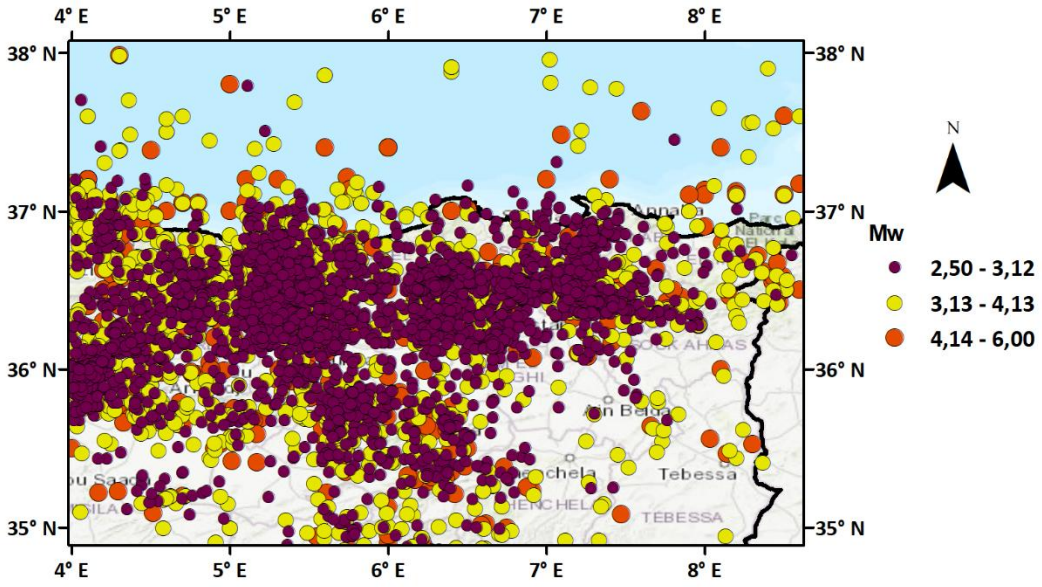

Fig. II. 18: Spatial distribution of all events of the prepared HEC for the northeastern Algeria.

8 Identification of Main-Shocks (Declustring)

Seismicity can be categorized into two main types: independent and dependent earthquakes. Independent earthquakes, often referred to as background or parent earthquakes, are caused by long-term tectonic forces unrelated to earlier seismic events, while dependent earthquakes—like aftershocks, foreshocks, and seismic clusters—are triggered by earlier seismic activity. Separating these two types is crucial for understanding seismic behavior, a process called seismicity declustering. Declustering is essential for many applications in seismology, such as seismic hazard assessment, earthquake prediction research, and the development of models for clustered seismicity. The objective of declustering is to identify and isolate independent events from dependent ones, allowing researchers to focus on background seismicity for better understanding of earthquake hazards and patterns (van Stiphout et al., 2012).

However, declustering is not a simple task and lacks a unique solution. In large tectonic regions, the subset of independent earthquakes typically follows a stationary Poisson process, where events occur randomly in time but at a constant rate. Seismic swarms, often caused by magma or fluid intrusions, are exceptions. Though swarms consist of independent events, they are best modeled using a non-homogeneous Poisson process due to their time-varying occurrence rates.

Historically, declustering methods evolved as researchers sought to differentiate between independent and dependent earthquakes. Early efforts by Aki (1963) and Knopoff (1964) identified that earthquake catalogs deviate from a Poisson distribution due to the presence of aftershocks. Knopoff introduced an early declustering method, excluding aftershocks

manually, and used a ten-day binning technique to study earthquake frequencies. This was a basic attempt to remove dependent events from seismic catalogs.

A significant advance came with Gardner and Knopoff (1974) introduction of a more formal method for identifying aftershocks using inter-event time and space distances. Their approach, known as the "window method," uses a threshold distance—determined by the mainshock's magnitude—to classify aftershocks. This simple approach has been widely used for its ease of application, but it has limitations, such as ignoring aftershocks of aftershocks and assuming circular spatial windows for larger earthquakes. Uhrhammer (1986) modified the length of the space time windows. This modified version is also used by many researchers for declustering purpose.

Reasenberg (1985) improved upon this by developing a method that links aftershocks in a seismic cluster, allowing earthquakes to be classified as part of a sequence. This method employed Omori's law, which models the decreasing rate of aftershocks over time. Reasenberg's algorithm considers spatial and temporal factors to classify dependent earthquakes more accurately.

Another notable contribution came from Molchan and Dmitrieva (1992), who applied game theory to declustering, creating an optimal method for aftershock identification. This method introduced flexibility, allowing for different approaches to declustering based on varying conceptual models.

Moving into the 21st century, Zhuang et al. (2002) introduced a stochastic approach based on the ETAS model (Epidemic-Type Aftershock Sequence). Unlike deterministic methods, which label earthquakes as either mainshocks or aftershocks, the ETAS model assigns probabilities that an event is triggered by a previous earthquake. This model optimizes the space-time distances between events and removes the need for arbitrary thresholds, though the optimization process can be computationally demanding. Additionally, the model allows for multiple mainshocks to be linked to the same aftershock, reflecting the uncertainty in pinpointing the exact cause of subsequent seismic events.

Marsan and Lengline (2008) advanced this concept further by generalizing the triggering mechanism without assuming a fixed form for the space-time relationship. They used an Expectation-Maximization algorithm to improve the robustness and ease of computation of their model. Unlike earlier models, their approach was less sensitive to initial parameter choices, making it a more flexible tool for declustering.

Other methods, like those by Zaliapin et al. (2008) and Hainzl et al. (2006), offered alternative approaches for identifying background earthquakes. Zaliapin's method explored graphical representations of space-time distances, while Hainzl focused on using inter-event times to reconstruct background seismicity rates.

In this study, three distinct methods were employed to decluster the earthquake catalog of the Northeastern region of Algeria. The first two methods are based on the Window method: the Gardner and Knopoff (1974) approach, and a modified version by Uhrhammer (1986). The third method used is the Linked Window method, introduced by Reasenberg (1985).

The Window methods aim to identify dependent seismic events (such as aftershocks) within a defined space-time window surrounding a larger earthquake. These large events, known as mainshocks, are considered independent, while all other events within the window are treated as dependent and removed. The size of the window is proportional to the magnitude of the main event, meaning a larger event results in a bigger space-time window. The window dimensions for Gardner and Knopoff's method are outlined in Eq. 46, which calculates the spatial and temporal window sizes based on the magnitude of the earthquake.

$$d = 10^{0.1238M+0.983} \ \ and \ t = \begin{cases} 10^{0.032M+2.7389}, if \ \ M \geq 6.5 \\ 10^{0.5409M-0.547}, else \end{cases} \tag{46}$$

Where, d= Spatial window size in kms, t=time window size in days, and M=Magnitude of the earthquake.

Uhrhammer's (1986) modification further refines this process, proposing updated formulas for spatial and temporal window sizes (d(km) and t (days)). Governing correlations for this method are given in eq. (47), where M is the magnitude of earthquakes.

$$d = e^{-1.024+0.804M} \quad and \quad t = e^{-2.87+1.235M} \tag{47}$$

On the other hand, Reasenberg's Linked Window method takes a different approach by focusing on the spatial and temporal relationships between seismic events. Events that occur within the interaction zone of a previous earthquake are considered aftershocks, forming a cluster of related events. If a new event falls within the interaction zone of a cluster, it is added to that cluster. Moreover, if two clusters overlap spatially, they merge into a single cluster. This method employs spherical spatial windows, determined by the hypocenter of the earthquake, and the size of the window is based on the source dimension, a function of the earthquake's magnitude. Eq. 48 describes how the temporal window (τ) depends on the maximum and minimum magnitudes in the catalog, as well as the probability of a dependent event occurring within a given timeframe, which typically ranges between 1 and 10 days.

$$\tau = \frac{-\ln(1-P)}{10^{\frac{2(\Delta M-1)}{3}}} \tag{48}$$

Where, $\Delta M = Mmax - Mmin$ and P is the probability of occurrence of a dependent event. τ value is in between 1 and 10 days.

The declustering methods described above were applied to the prepared HEC using MatLab. When using the Gardner and Knopoff (1974) approach, the number of remaining events in the catalogue is 3175. In contrast, applying the modified window size by Uhrhammer (1976) yields 4113 independent main events. This indicates that the original Gardner and Knopoff (1974) window results in fewer events compared to the Uhrhammer (1976) method. Using the Reasenberg (1985) method, 4250 main events were identified. Due to its shorter windows and event-by-event approach, this method detects more events than the previous two. Additionally, Reasenberg (1985) considers hypocentral distances, which are generally greater than epicentral distances between events, further contributing to the higher number of main events identified. Table II. 7 and Fig. II. 19 show a summury of the remained events using Gardner and Knopoff (1974), Reasenberg (1985) and Uhrhammer (1986) methods.

Table II. 6: Comparison of Declustering Algorithems for the Final HEC.

Declustring algorithms	**Gardnerand Knopoff (1974)**	**Urhammer (1986)**	**Reasenberg (1985)**
Declustered catalogs	3175	4113	4250

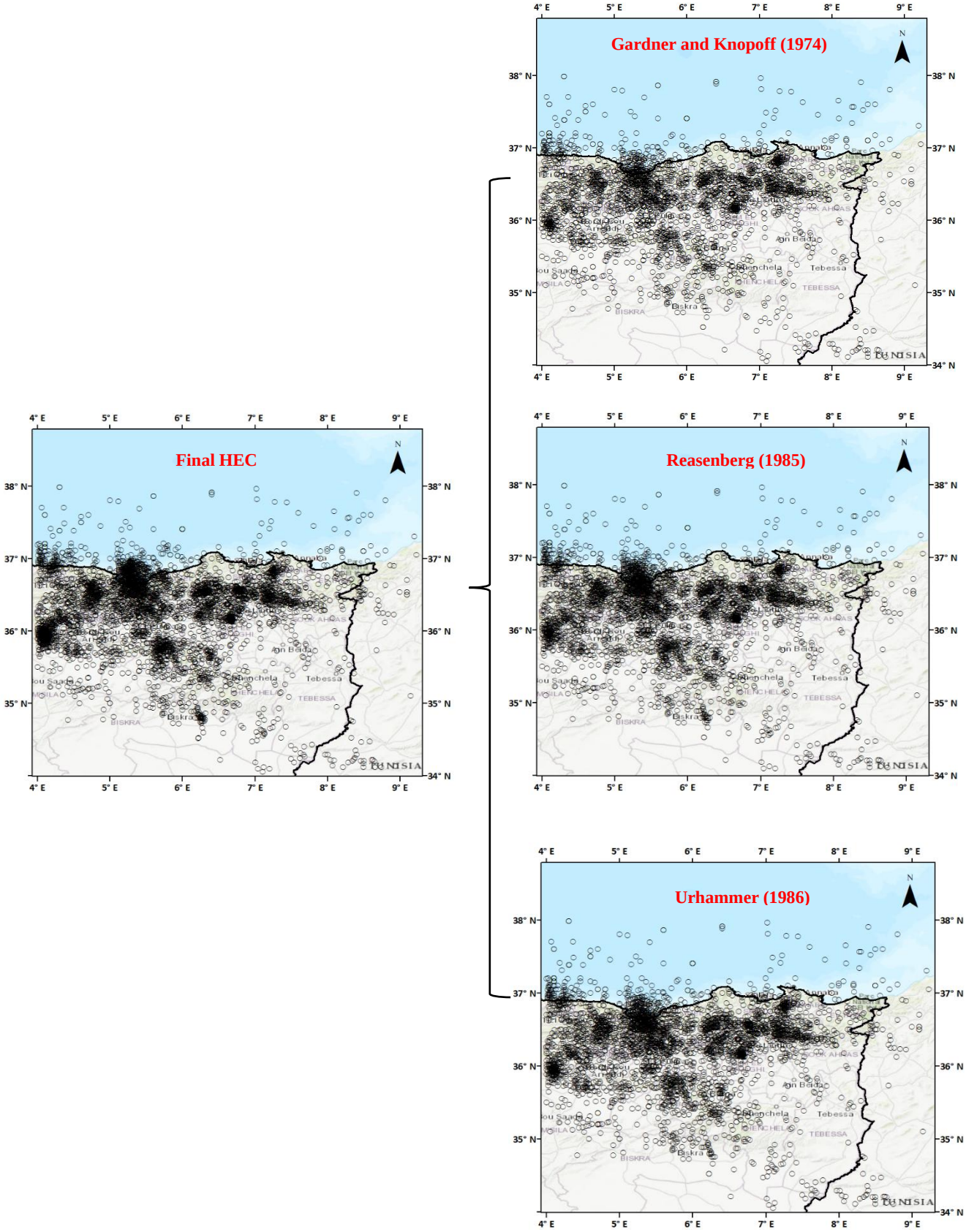

Fig. II. 19: Spatial Representation of Earthquakes Before and After Applying the Tree Declustring Methods.

9 Completeness Analysis of the Declusterd Catalogs

Since the data collection relies on both instrumental and historical sources, it is possible that not all past seismic events are represented in the catalog. Using the entire catalog directly for hazard analysis may lead to underestimation of results. Therefore, to ensure accuracy, only the complete portion of the catalog should be utilized. It is important to note that the catalog might not contain all events for every magnitude range or for every year. Thus, it is essential to determine which magnitude ranges are fully captured in the catalog and over what time periods, ensuring that only this verified section is employed in further analyses.

In this study, a completeness test is applied to all catalogs generated using various declustering methods. The completeness in terms of magnitude and time is compared among the three declustered catalogs produced by each method. To assess magnitude completeness, the minimum magnitude threshold of the catalog is estimated, and only earthquakes with magnitudes above this threshold are considered complete. This threshold is known as the magnitude of completeness (M_c) (Rydelek & Sacks, 1989)

Here, the maximum curvature (MAXC) method proposed by Wiemer and Wyss (2000)is used to evaluate the catalog's completeness with respect to magnitude. In this approach, the cumulative number of earthquake events is plotted against magnitude, generating a curve. According to Wiemer and Wyss (2000), the point of maximum curvature on the curve corresponds to the M_c. Fig. II. 20 illustrates the M_c values for all three declustered catalogs.

Fig. II. 20(a) shows that the maximum curvature for the declustered catalog, obtained using the Gardner and Knopoff (1974) window method, occurs at a magnitude of 2.5, which represents the magnitude of completeness. Similarly, Figs. II. 20(b) and 20(c) indicate that the magnitude of completeness (Mc) is also 2.5 for the catalogs declustered using the Uhrhammer (1976) window method and the Reasenberg (1985) method, respectively. In all three cases, the M_c is consistently identified as 2.5.

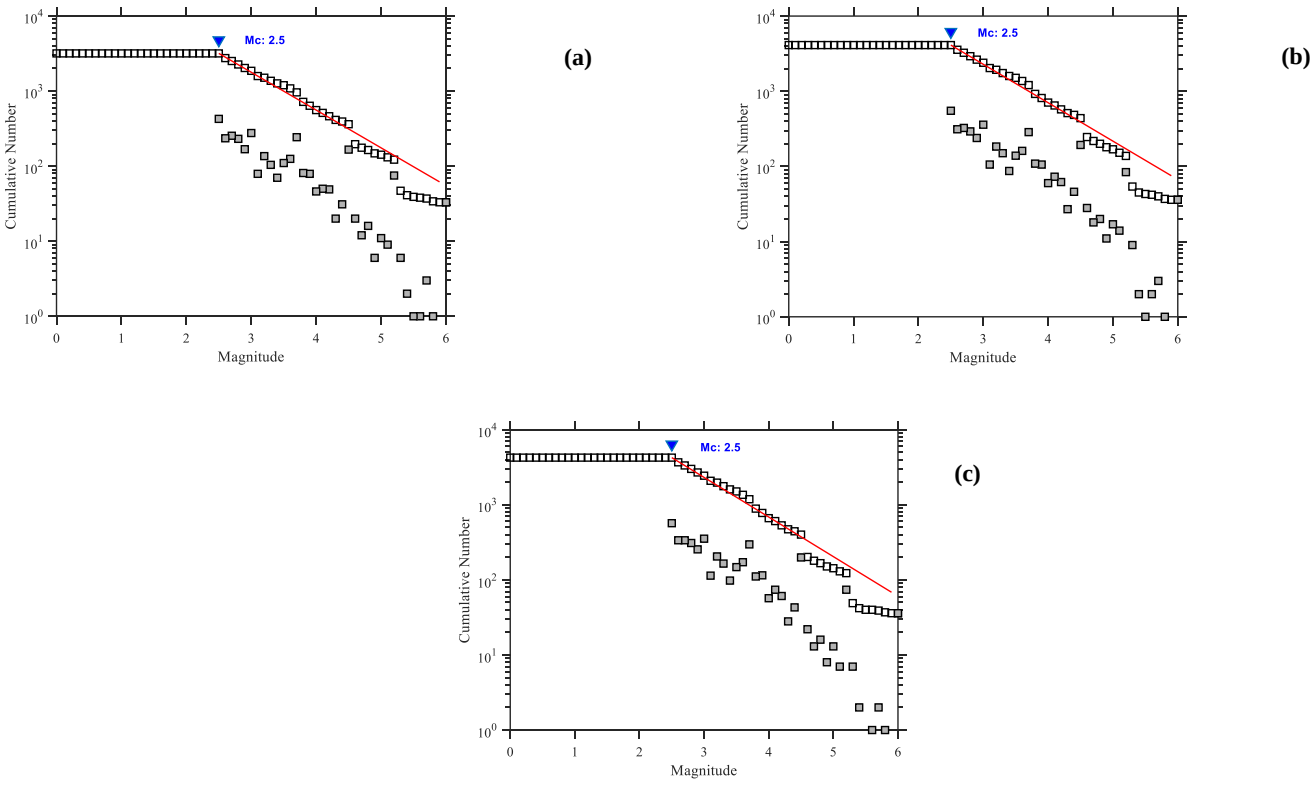

Fig. II. 20: Cumulative frequency distribution plots and M_c value for (a) Catalog obtained by Gardner and Knopoff (1974) window method, b. Catalog obtained by Uhrhammer (1976) window method and (c) Catalog obtained by Reasenberg (1985) method.

Stepp (1972) introduced a method to determine the completeness of earthquake data over time, assessing the completeness of specific magnitudes over fixed time periods. To implement this, magnitudes are first categorized into specific ranges, and tests are applied to each group. According to Stepp (1972), within each group, the earthquake catalog is segmented into time intervals, or bins, which contain the earthquakes occurring within a given time span, starting from the latest year in the catalog. This method assumes that earthquake occurrences follow a Poisson distribution. Based on this, if x1, x2, x3, ..., xn represent the number of earthquakes occurring within a fixed time interval, the unbiased mean rate (λ) for each time period can be calculated using a specified formula (Eq. 49).

$$\lambda = \frac{1}{n}\sum_{i=1}^{n} x_i \tag{49}$$

And for this dataset the variance will be

$$\sigma_{\lambda}^{2} = \frac{\lambda}{n} \tag{50}$$

Where, n is the unit time interval. If one year is taken as the time interval, then n will be equal to T, where T is the sample length. Then the standard deviation ($\sigma\lambda$) will become:

$$\sigma_{\lambda} = \sqrt{\frac{\lambda}{T}} \tag{51}$$

In his study, Stepp (1972) discovered that for a constant mean rate (λ) in each magnitude class, the standard deviation (σ_{λ}) follows the relation $1/\sqrt{T}$. To test for completeness, σ_{λ} was plotted against the time interval for all magnitude groups, and the points were compared to the $1/\sqrt{T}$ line on the same graph. It was concluded that the data was complete for a given time interval (T) if the plotted points formed a straight line parallel to the $1/\sqrt{T}$ slope.
The number of earthquakes per decade for each declustred catalog were grouped into tree magnitude ranges, i.e., $2.5 \leq Mw \leq 3.50$, $3.51 \leq Mw \leq 4{,}5$ and $4.5 \leq Mw \leq 6$, 4.5 and are presented in Table II. 10 in Appendix.

For the tree declustred catalogs, the rate of earthquake occurrence as a function of the time interval given in Table II. 11 in Appendix for different magnitude ranges. The rate is given as N/T, where 'N' is the cumulative number of earthquakes in the time interval 'T'. Standard deviation is calculated using Eq. (51). The plotted points of each magnitude range follow a straight line path as long as the data set is complete in that magnitude interval. For a particular region, the lines of all the magnitude ranges should have the same slope as $1/\sqrt{T}$.
Fig. II. 21 illustrates the relationship between σ_{λ} and T for various magnitude classes across different declustered catalogs. The plotted data points are compared against the $1/\sqrt{T}$ line; when the slope of the points remains parallel to this line, it indicates that the data is complete. The three panels of Fig. II. 21 demonstrate the catalog's completeness over time, evaluated using the Gardner and Knopoff (1974) window method (first panel), the Uhrhammer (1976) window method (second panel), and the Reasenberg (1985) method (third panel), respectively

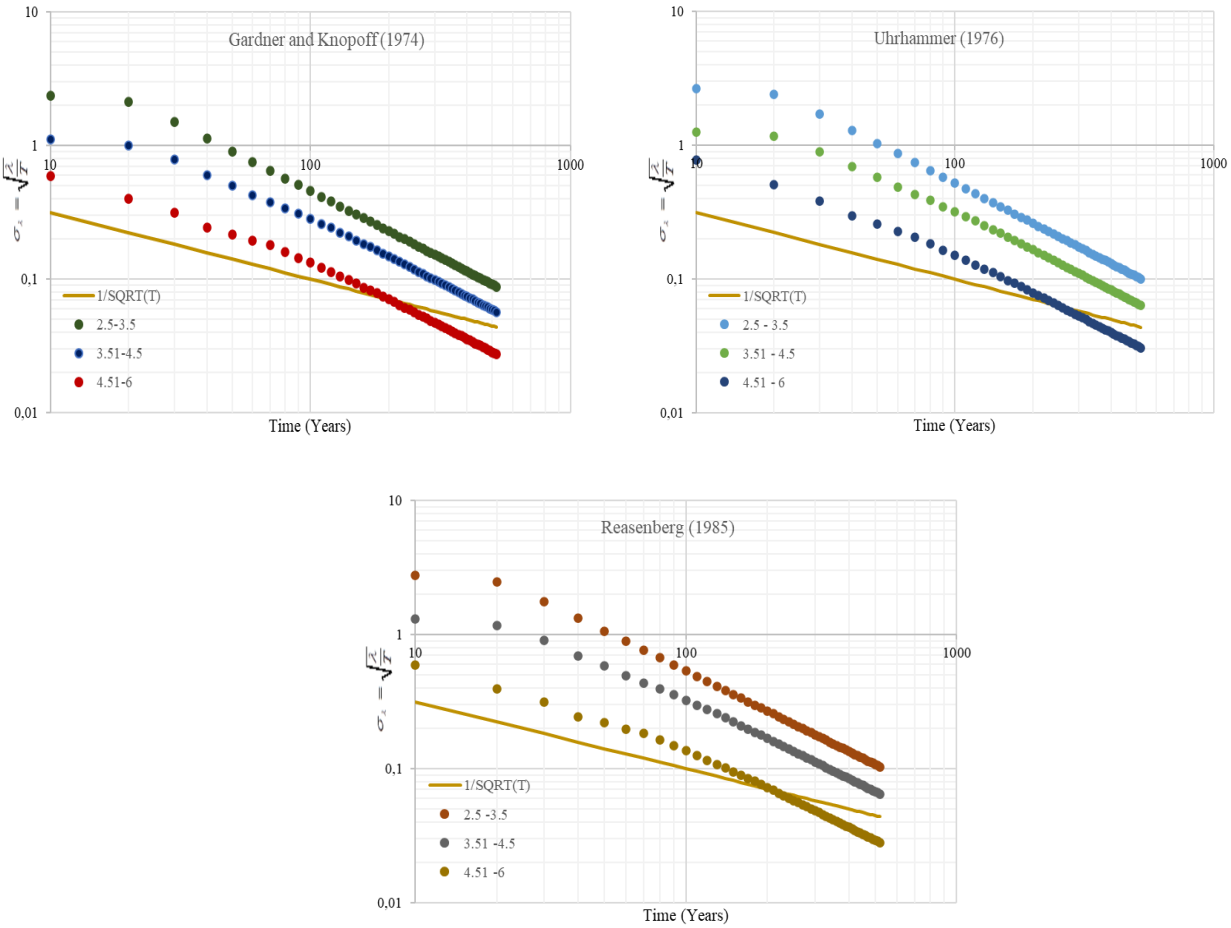

Fig. II. 21: Completeness analysis of earthquake data

Table II. 10 summarizes the year of completeness for different magnitude classes for each of the three catalogs. It is seen from Table 10 that for almost all the cases the year of completeness is same for the three catalogs.

Table II. 7: Year of completeness for different magnitude classes for all the catalogue

Methods	Magnitude classes	Year of completeness
Gardner and Knopoff (1974)	2.50 – 3.50	30
	3.51 – 4.50	75
	4.51 – 6.00	150
Uhrhammer (1976)	2.50 – 3.50	30
	3.51 – 4.50	75
	4.51 – 6.00	173
Reasenberg (1985)	2.50 – 3.50	30
	3.51 – 4.50	75
	4.51 – 6.00	173

A recent study by van Stiphout et al. (2012) indicates that using the methods developed by Reasenberg (1985) with standard parameters or with most of the varying parameters does not yield a Poisson distribution for the seismicity background. Also, from the comparative analysis above, the original Gardner and Knopoff (1974) window results in fewer events compared to the Uhrhammer (1976) method. Accordingly, the HEC was declustered to remove aftershocks and foreshocks, following Uhrhammer (1986) method for the present study.

The completeness of the HEC was analyzed using Stepp (1972) method (the result are shown in Fig. II. 22 and Table II. 10) and using the Visual Cumulative Method proposed by Tinti and Mulargia (1985) (Fig. II. 22).

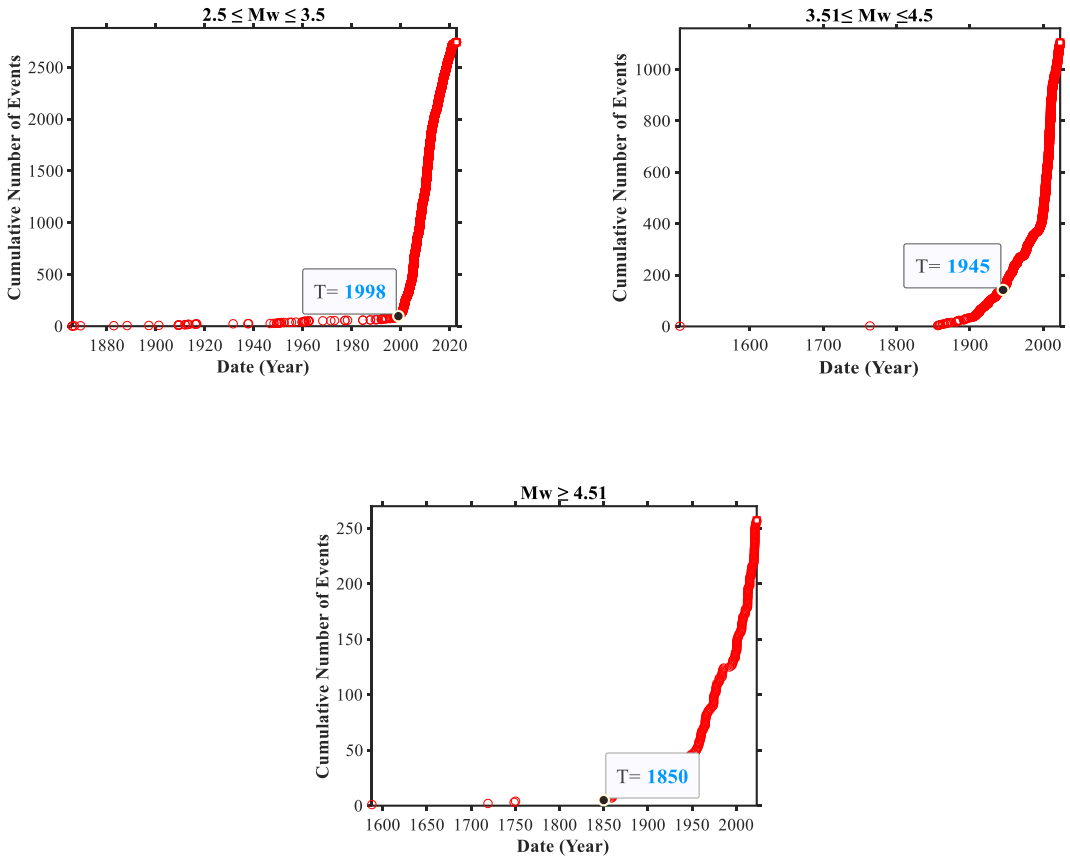

Fig. II. 22: All magnitude classes within the completeness periods

The results are summarized in Table II. 11 and compared with findings from Bellalem (2007), Hamlaoui et al. (2017), and Mouloud and Badreddine (2017).

Table II. 8: Completeness Periods for Different Magnitude Classes

Magnitude Class	Bellalem (2007)	Hamlaoui et al. (2017)	Mouloud and Badreddine (2017)	Present Study
2.5 ≤ M ≤3.5	/	2000	/	1998
3.5 ≤ M ≤4.5	1930	1991	1993	1945
M ≥ 4.5	1865	1830	1870	1850

Our completeness analysis indicates the following periods for different magnitude classes:

- For magnitudes 2.5 ≤ M ≤ 3.5, the completeness period in our study is identified as 1998, which is slightly earlier than Hamlaoui et al. (2017), who reported a completeness period starting from 2000.
- For magnitudes 3.5 ≤ M ≤ 4.5, our results show a completeness period starting from 1945. This is later than Bellalem's finding of 1930 and earlier than Hamidatou et al. (2017)'s period starting from 1993. Hamlaoui et al. (2017) reported an earlier period starting from 1991. The discrepancies in these periods can be attributed to differences in data sources and methodologies used in each study.
- For magnitudes 4.5 and greater, our completeness period begins in 1850, which is close to Hamidatou et al. (2017)'s period starting from 1870 but earlier than Bellalem's 1865. Hamlaoui et al. (2017) reported the earliest

period, beginning in 1830. The slight variations in these periods may result from the different catalog compilation techniques and the historical data availability in each study.

Overall, our completeness periods are reasonably consistent with those reported in the previous studies, with some variations due to methodological differences and the inherent uncertainties in historical earthquake data. These comparisons highlight the robustness of our analysis and the reliability of our earthquake catalog for seismic hazard assessment in the study area.

CHAPTER 3: SEISMICITY ANALYSIS AND CHARACTERIZATION OF SEISMIC SOURCE ZONES

1 Introduction

This chapter begins by outlining the geographic context of the study area, followed by a detailed examination of its geomorphological and geological characteristics, based on foundational studies such as those by (e.g., (Harbi et al., 2003; Meghraoui, 1988). The seismotectonic framework is then presented, emphasizing the key active fault structures that define the seismic landscape of northeastern Algeria. Accurately identifying and characterizing seismic sources is a key step for reliable seismic hazard assessments. By analyzing the spatial distribution of earthquakes, geological formations, and fault orientations, regions of consistent seismic behavior can be delineated. For each identified seismic zone, it is essential to compile distinct earthquake catalogs and estimate seismicity parameters using the maximum likelihood method, with a defined threshold magnitude.

2 Characterization of the Study Area

2.1 Geographical, Geomorphological, and Geological Context of the Study Area

Our study focuses on the northeastern region of Algeria, which lies between longitudes 4°E and 8.5°E and latitudes 35°N and 38°N (Fig. III. 1, left side). This area is bounded by the Mediterranean Sea to the north, Tunisia to the east, Lesser Kabylia and the Titteri Mountains to the northwest, the High Plateaus to the southwest, and the Saharan platform to the south.

Administratively, this region encompasses the wilayas of Bouira, Bourdj Bou Arreridj, M'sila, Béjaia, Jijel, Skikda, Annaba, Guelma, Constantine, Souk Ahras, Oum El Bouaghi, Khenchela, Tébessa, Batna, Biskra, and Sétif. Sétif is the largest of these wilayas in terms of population.

Sétif is also historically significant as the site of the 419 CE earthquake that destroyed the Byzantine city of "Sitifis" (now modern-day Sétif). Other major cities in the study area include Constantine, known as the capital of eastern Algeria, where the most significant earthquake of the 20th century struck on October 27, 1985, and Jijel, the location of the most extensively documented historical earthquake, which occurred on August 22, 1856.

These cities are undergoing rapid urbanization, although, regrettably, much of this development occurs without adherence to seismic safety standards.

From a geomorphological perspective, the study area exhibits diverse features, comprising significant basins and mountain ranges.

- The intra-mountain basins of Constantine and Mila are marked by high altitudes and steep, narrow valleys, while the Neogene and Quaternary basin of Annaba is characterized by its recent geological formations. The Guelma Basin represents a "pull-apart" structure between dextral east-west strike-slip faults, and the Soummam Basin is a narrow depression that stretches from east to west before shifting to a southwest-northeast orientation. Additionally, the Neogene Basin of Hodna, defined by its salt lakes (chotts), and the Chott Melrhir Basin, filled with Cretaceous deposits and structured during the Tertiary, complete the basin formations.
- The mountain ranges include the Babors Range, a limestone fold belt running WSW-ENE with deep valleys and towering peaks, and the Bibans Range, oriented east to west and composed of Tellian nappes. The Djurdjura Range, also known as the Kabyle Dorsal, is another limestone range, with its orientation shifting from east-west to northwest-southeast. The Hodna Mountains are distinguished by their relief aligned along the N110 axis, while the Aurès Mountains, Nemencha Mountains, and Ouled Naïl Mountains all share a dominant northeast-southwest orientation, featuring rugged landscapes and steep slopes.

From a geological standpoint, the study area is located in the eastern part of the Tellian and Atlassic zones. The terrain, from north to south, spans the following domains (Fig. III. 1, right side):

- The Algerian submarine margin, heavily influenced by the deposits from the Messinian Salinity Crisis (Lofi et al., 2011).
- The internal domain (northern Tell), which includes the Kabyle nuclei, consisting of the Kabyle basement (Precambrian and Paleozoic) that originated from the breakup of ALKAPECA. This area also includes the Kabyle Dorsal, a Meso-Cenozoic limestone chain, which is subdivided into three main units: internal, median, and external (Durand, 1969).
- The external domain (southern Tell), represented by the parautochthonous Tellian units (Babors and Bibans), where the Mesozoic and Tertiary sedimentation (ranging from the Triassic to the Eocene) is of African origin. This domain is further divided into three major units (Vila, 1980): (1) ultra-Tellian units, (2) Tellian units in the strict sense, and (3) Peni-Tellian units.
- Between the internal and external domains lie the Flysch nappes, which are primarily composed of conglomerates. These nappes can be classified into three categories: (1) northern Kabyle flyschs (internal), (2) southern Kabyle flyschs (relatively external), and (3) flyschs that have been thrust over the external Tell.
- The intra-continental Atlas, situated to the south of the Tell, is separated from the Saharan platform by the South Atlas Front. This domain consists of autochthonous units and is divided into the Saharan Atlas in the center and the Aurès Mountains in the eastern region of Algeria.

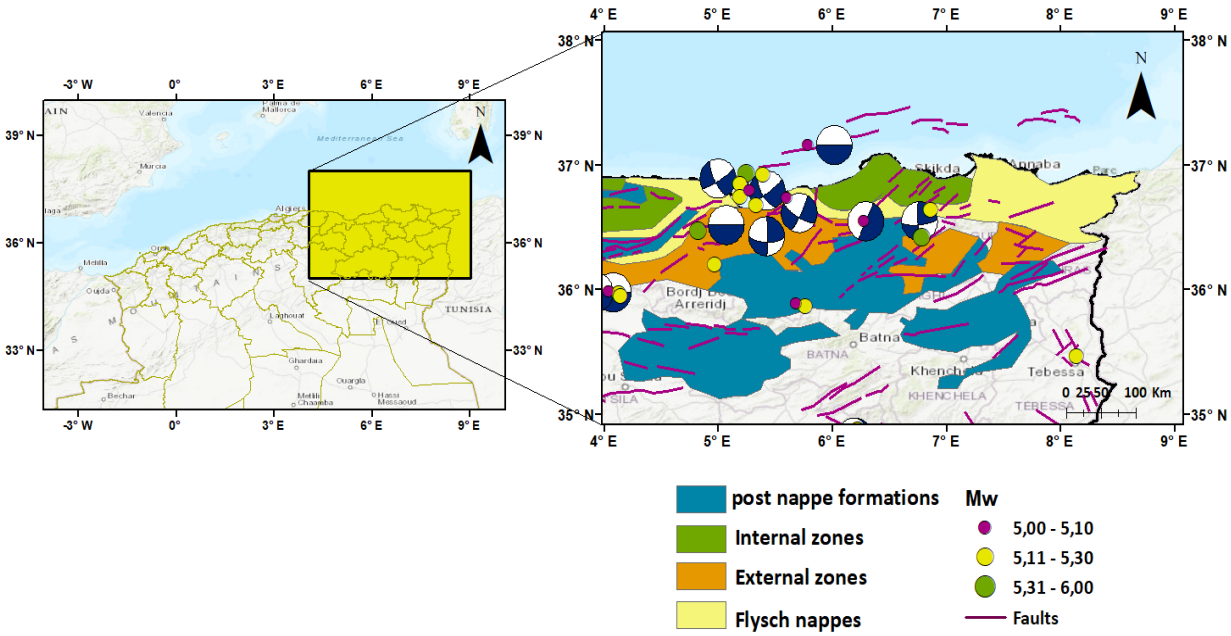

Fig. III. 1: Geographical Location, Geological Map, Major events, some of focal mechanisms, and active Faults of the Study Area.

2.2 Seismotectonic Context of the Study Area

From a seismotectonic perspective, we present the main earthquakes and the major active sources that exist in our study area**.**

2.2.1 The major earthquakes in the Eastern Algerian region:

We present some earthquakes that have occurred in our study area (Table III. 1). These earthquakes are categorized into two main groups: historical seismicity, which includes events recorded before 1900, and instrumental seismicity, which covers those recorded from 1900 onwards.

Table III. 1: Some of the major earthquakes occurred in the study Area.

Historical Seismicity				Instrumental Seismicity		
N°	Date	site	Io	N°	Date	M
1	419	Setif	/	1	10/02/1937	5,7
2	22/08/1856	Jijel	VIII	2	12/02/1946	5,5
3	27/09/1860	Akbou	VII	3	21/02/1960	5,5
4	25/02/1865	Bejaia	VIII	4	02/12/1961	5,5
5	16/11/1869	Biskra	IX	5	04/09/1963	5,7
6	03/12/1885	Msila	IX	6	27/10/1985	6,0
7	22/09/1886	S.El Gozlane	VII	7	21/05/2003	6,8
8	08/01/1887	Mansourah	VIII	8	19/05/2013	5,5

2.2.2 Active Faults

The data from the seismic history, the photo-geological analysis, field investigations and new data published on Neogene and Quaternary deposits of the northeast part of Algeria have helped to highlight a number of active and probably active faults (Fig. III. 1). The geometrical characteristics of these faults are summarized in Table III. 2 by the Algerian National Earthquake Engineering Center (CGS, 2011).

Table III. 2: Seismic sources lines in the northeastern of Algeria and their characteristics (CGS 2011)

Name of the fault	Type	Length	Direction	Pendage	Depth	M_w
Fault of Ain Smara	Sinistral strike-slip	65km	NE-SW	Vertical	15km	7
Front Constantine tablecloths	Reverse	55km	E-W	50°N	15km	7
Fault of Temlouka	Sinistral strike-slip	25km	NE-SW	Vertical	10km	6
Fault of Sigus	Reverse	60km	E-S	60°N	15km	7
Fault of north of Guelma	Dextral strike-slip	33km	E-S	Vertical	15km	6.7
Fault of south of Guelma	Sinistral strike-slip	30km	NE-SW to E-W	Vertical	15km	6.7
Fault of Hammam N'Bails	Reverse	13km	NE-SW	45°NW	10km	6.5
Fault of Bouchougouf	Strike-slip	18km	NE-SW	Vertical	10km	6.3
Fault of Sebhket Djendli	Reverse	12km	NE-SW	40°N	10km	6.4
Fault of Djebel Youcef	Reverse	26km	NE-SW to ENE-WSW	60-70°S	10km	6.5
Fault of north Djemila	Reverse	45km	NE-SW	50°NW	15km	7
Fault of Jijel Sea	Reverse	100km	NE-SW	40°NW	18km	7.4
Fault of Annaba Sea	Reverse	80km	E-W	40°S	18km	7.3

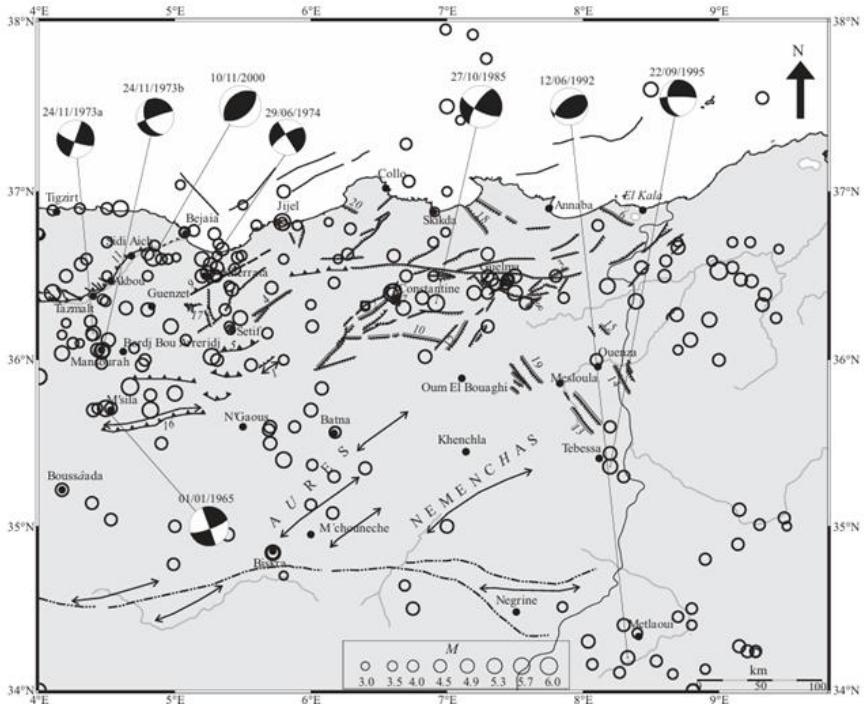

Fig. III. 2 seismotectonic setting of the northeastern of Algeria showing potential active faults (Harbi et al., 2003)

3 Characterization of Seismic Source Zones

The initial phase of seismic hazard analysis involves identifying and characterizing the seismic sources that could potentially impact the specified site. These sources are classified into three categories: area sources, fault sources, and point sources (Fig. III. 2). To validate the presence of these sources, the seismic characteristics within the sources must differ from those of the broader region.

3.1 Faults Sources

Faults are the most recognizable seismic sources. A fault can be defined as a three-dimensional surface that indicates a weakness in the Earth's subsurface rocks, where earthquakes are likely to occur. However, accurately determining the rates of occurrence for all event sizes on a particular fault can be challenging. Even when past seismic events have been recorded on a fault, predicting its future rupture behavior remains uncertain. A seismic source model should account for the probabilities of various rupture scenarios. In seismic hazard analysis, a fault source is typically represented by a simple polygon in three-dimensional space, often a quadrilateral or rectangle aligned with the fault's strike and dip.

3.2 Area Sources

In certain regions, although active faults are recognized, it may not be feasible to characterize them as individual sources. In cases where only minor seismic events have occurred, which did not reach the surface, the precise locations of the responsible faults may remain undetermined. In such instances, it is common to define an area source that encompasses the seismic activity across a specified region. For hazard calculations, individual earthquake ruptures may be simulated, assuming a uniform distribution of their spatial locations throughout the area source. The general orientation of these ruptures can be inferred from focal mechanism analyses or in-situ measurements. However, these ruptures are generated along hypothetical faults that reflect the aggregate seismic activity within the area source. Typically, area sources are represented as polygons or polyhedra. The seismic characteristics within an area source should be relatively uniform but

distinct from those in surrounding regions. Variations may exist in activity levels, the distribution of magnitudes, the geological structure of the area, or the inferred rupture geometries and faulting styles.

3.3 Points Sources

Point source models depict seismic activity as occurring at a specific point, without considering the dimensions of the rupture.

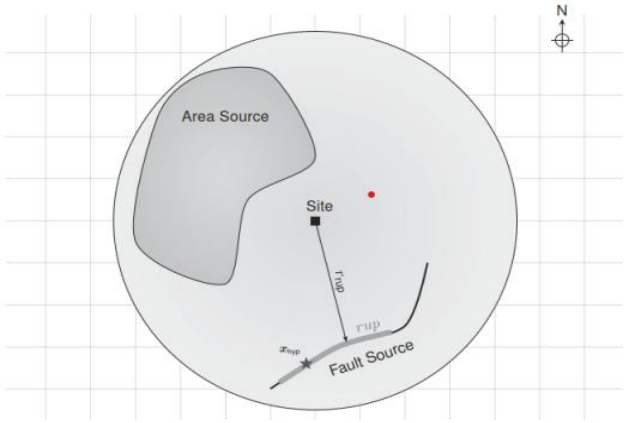

Fig. III. 3: A seismic source model comprise of Area Source and Fault source

4 Previous Initiatives in Seismic Source Characterization within the Study Area

In seismic hazard assessment, identifying seismogenic source zones is a fundamental step. Over the years, several initiatives have sought to delineate these zones across Northern and Northeastern Algeria (Fig. III. 3). These efforts have been instrumental in refining our understanding of the region's seismic potential.

The pioneering work by Hamdache et al. (1998) marked an early effort to classify seismic source zones in Northern Algeria, identifying four distinct areas based on observed fault mechanisms. Shortly after, Harbi et al. (1999) built upon this by correlating seismicity with neotectonics faults, particularly focusing on the Eastern Tellian Atlas and surrounding regions. Their study combined geological and geophysical data, along with insights from earlier research, to provide a clearer picture of the region's active tectonics.

In 2000, Aoudia et al. (2000) expanded the scope significantly by identifying twelve source zones within the Tell Atlas. Their methodology was comprehensive, integrating the distribution of Quaternary and active faults, thrust-related tectonics, local and regional kinematics, and patterns of earthquake epicenters. This study provided a more detailed zoning framework by linking geological structures with seismicity in the region.

Three years later, Montilla et al. (2003) introduced a new zoning model, defining thirteen seismogenic zones across Northern Algeria. Their approach emphasized seismic homogeneity within the zones, relying more on seismic data than on geological context. This represented a shift toward data-driven zoning, reflecting advancements in seismic monitoring and analysis.

The work of Yelles-Chaouche et al. (2006) further refined seismic source characterization by utilizing data from Algeria's seismic monitoring network, as well as field studies conducted after major earthquakes. Their findings highlighted various areas with distinct seismotectonic characteristics and provided valuable insights into seismic activity across the country.

In 2017, Hamlaoui et al. (2017) concentrated on Northeastern Algeria, defining seven seismic source zones. Their approach adjusted previous zonations, slightly altering the boundaries to better capture seismicity, particularly in the region between 33–38N and 4–9E. This work aligned closely with earlier seismic hazard studies but introduced subtle changes to enhance the precision of the source demarcations.

That same year, Mouloud and Badreddine (2017) proposed five source zones specifically for the Constantine region, based on a combination of seismicity, geology, and tectonics. Their research was followed by an extended study in 2021, where Hamidatou et al. (2021) defined ten seismic source zones in Northeastern Algeria, consolidating knowledge from previous studies to refine the regional seismic hazard framework.

Lastly, Abacha (2018) introduced a model with nine seismogenic zones in Northeastern Algeria. Their approach was based on a thorough seismological and tectonic analysis, contributing further to the evolving understanding of seismicity in the region.

Hamdache et al. (1998)

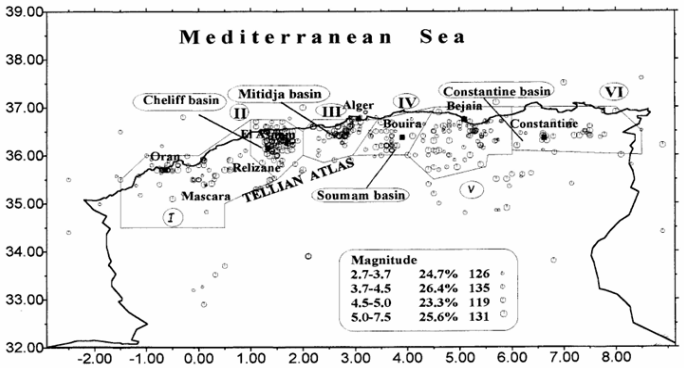

Aoudia et al. (2000)

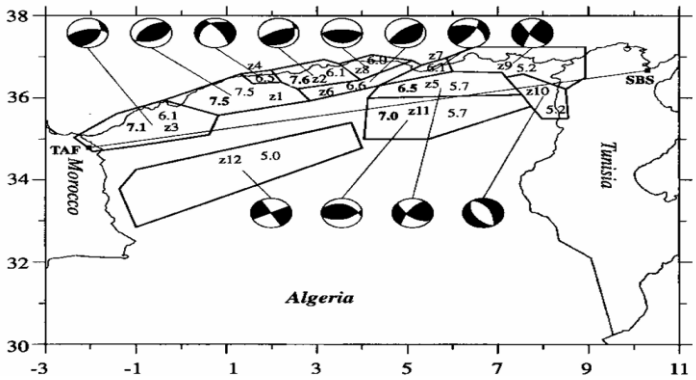

Montilla et al. (2003)

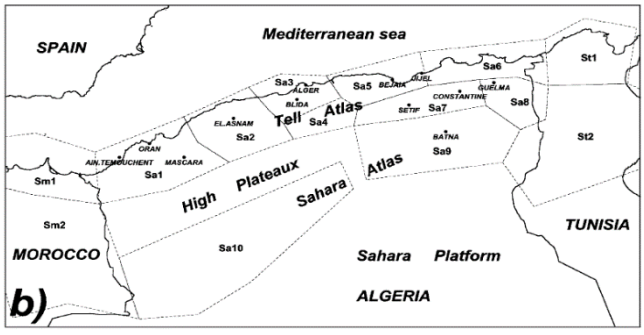

Hamlaoui et al. (2017)

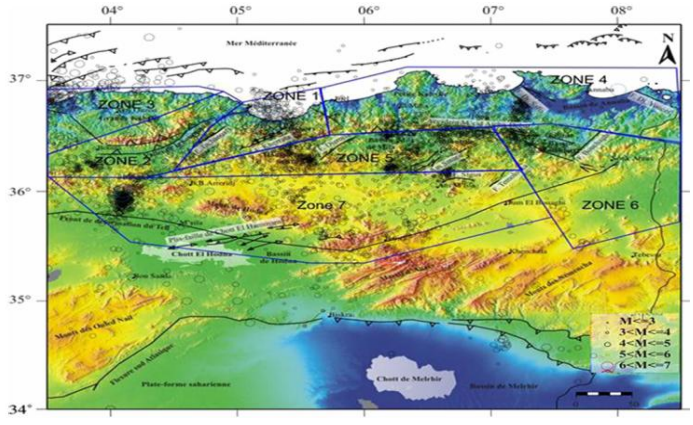

Mouloud and Badreddine (2017)

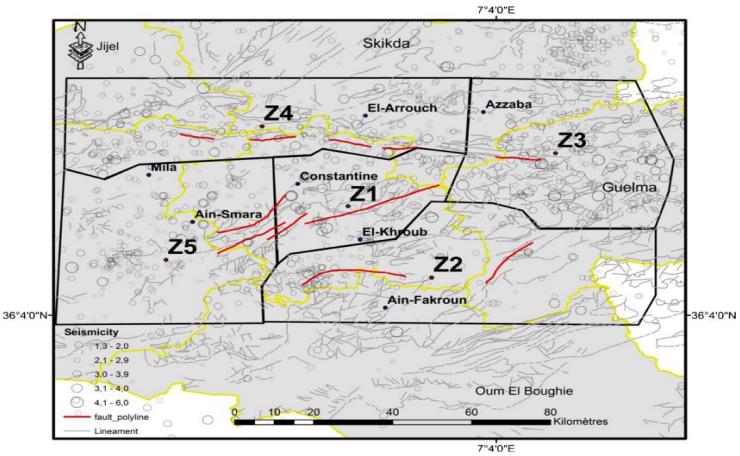

Hamidatou et al. (2021)

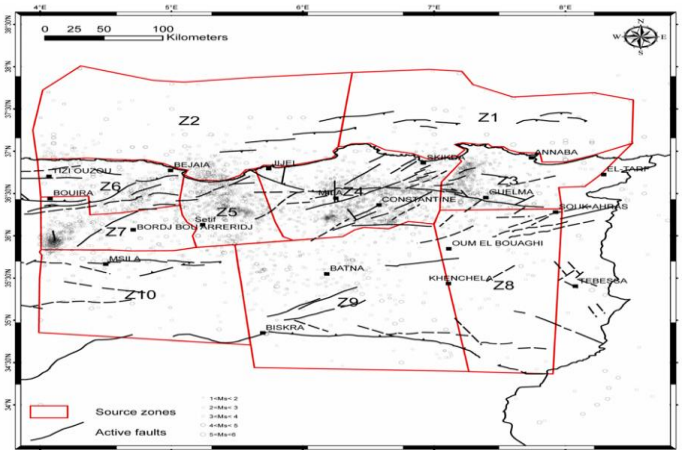

Abacha (2018)

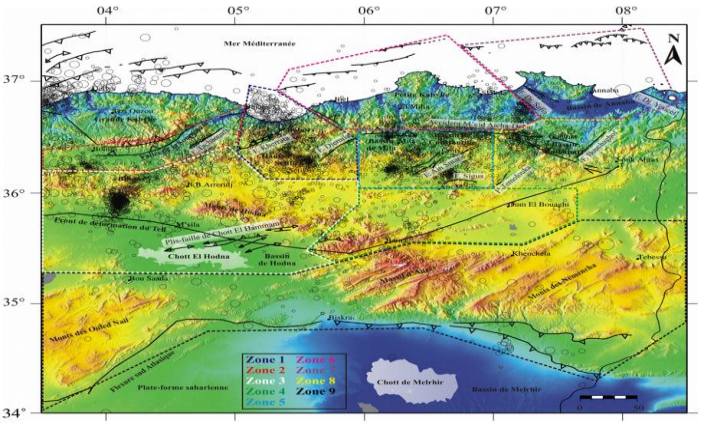

Fig. III. 4: Some of zoning maps provided by Algerian researchers.

5 Delineation of Seismic Source Zones According to the Present Study

It should be noted that the area under study can be subdivided into two distinct regions: the area of responsibility and the area of influence.

1. Area of Responsibility: This is the primary area of interest for seismic hazard assessment, which is discretized into grids.
2. Area of Influence: This area encompasses regions where seismic activity could potentially impact the area of responsibility.

In some studies, researchers consider all seismic sources within a radius of 200, 300 km or even 500 km, depending on the hypo-central distance for which the ground motion prediction equations (GMPEs) used in the analysis phase are applicable.

In our paper, we have outlined our philosophy for defining the seismic zone. We focused on the distribution of seismic events within the study area and aligned our zoning with previous maps provided by Algerian researchers. Specifically, we aimed to respect the north-south and east-west limits defined by these researchers, making adjustments to the seismic zone boundaries in accordance with only the distribution of seismic events (Fig. III. 4). The subsequent subsections offer a general overview of each seismic source.

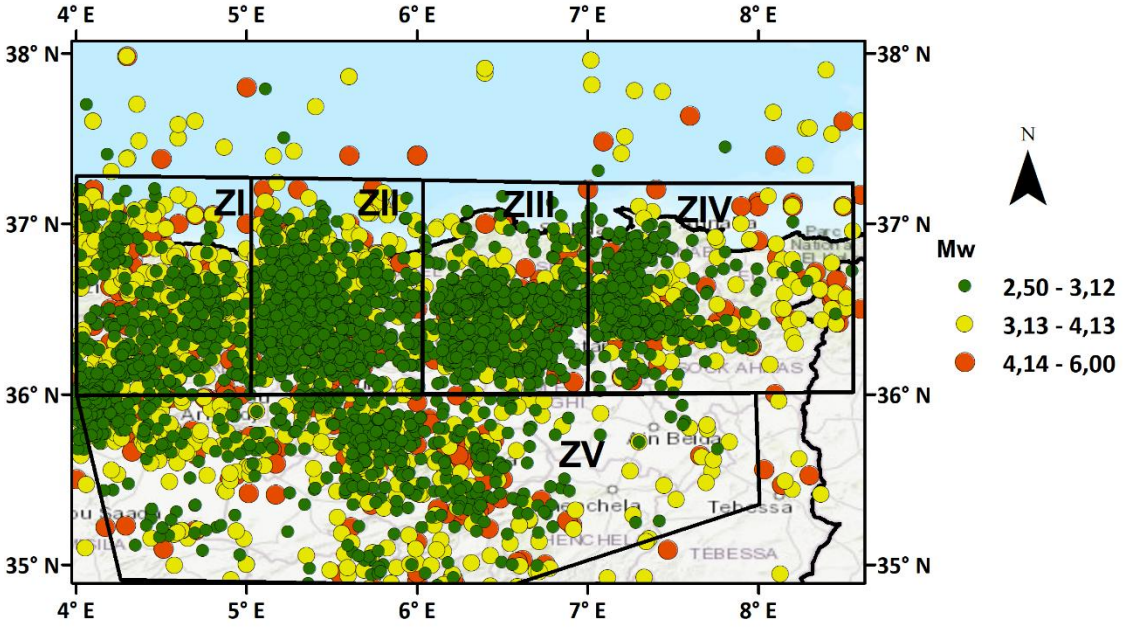

Fig. III. 5: The seismic source zones of the northeast of Algeria

5.1 Seismic Zone I

In this zone, seismic activity is primarily concentrated in two prominent areas: the Bibans zone and the Soummam Basin. Notably, the most significant instrumental earthquake within this cluster occurred on November 10, 2000, in Béni-Ouartilane, triggered by the Tachaouaft fault. This fault demonstrates a reverse faulting mechanism with a northeast-southwest orientation, dipping 38° towards the southeast, spanning a length of 40 km(Abacha, 2018). Historical records reveal a total of 687 seismic events documented in this zone from 1850 to 2023.

5.2 Seismic Zone II

This zone encompasses the Babors Mountains, which extend northeastward as a continuation of the Bibans mountain range. The historic Kherrata earthquake of February 17, 1949, left discernible surface traces that facilitated Rothé's observations and mapping of the N070 fold-fault, famously known as the Kherrata fault. This fault has long been attributed by researchers (Harbi et al., 2003; Harbi et al., 1999; Meghraoui, 1988) as the principal driver of seismic activity in the region. However, recent seismic events have unveiled a more complex tectonic picture. Events like the 2006 Lalaam earthquake (M_w = 5.2) documented by Beldjoudi et al. (2009), the Bejaia-Babors seismic sequences (Boulahia et al., 2021), and the 2020 El Aouana earthquake have revealed the presence of new right-lateral NW–SE en echelon faults. These strike-slip faults form a corridor connecting the offshore thrust fault system to the Mcid Aïcha-Debbagh Fault, as highlighted by Yelles-Chaouche et al. (2022).

In the Djemila Tellian Nappe, located east of Setif, seismic activity primarily revolves around the northern Djemila fault, characterized by its E-SW orientation. This seismicity, typically associated with low-magnitude events, is believed to be influenced significantly by active hydrothermal sources, as suggested by Vila (1980).

Throughout history, a total of 1111 seismic events have been recorded in this zone from 1862 to 2023. The most significant earthquake reported in this area registered a magnitude of 6 on March 18, 2021.

5.3 Seismic Zone III

This zone encompasses the Constantine region and its surrounding areas, presenting unique geological features that distinguish it from other intra-mountain basins in the Tell region. Notably, the Constantine Basin stands out due to its elevated altitude, setting it apart from its counterparts. To the east, it is bounded by the Guelma Basin (Zone IV), delineated by the Temolouka fault, which serves as a significant geological boundary between the two basins(Aoudia et al., 2000). Within the confines of the Constantine Zone, three prominent neotectonic faults exert considerable influence on the Plio-Quaternary deposits:

- The Ain Smara fault, notable for its activity during the 1985 Constantine earthquake, comprises three segments spanning approximately 30 km. Its trajectory follows a NE-SW direction, demonstrating a strike-slip character consistent with the focal mechanism observed during the aforementioned earthquake.
- The Northern Constantine fault (M'cid Aicha-Debar fault), extending over 80 km in an east-west orientation.
- The Sigus fault, with a length of around 30 km, also follows an east-west orientation, contributing to the region's tectonic complexity.

The seismic history of this zone is punctuated by significant events, with the last major earthquake recorded at a magnitude of M_w= 5.95 on March 14, 1963. In total, 739 earthquakes have been documented in this zone.

5.4 Seismic Zone IV

This zone encompasses the Guelma Neogene basin and its surrounding area, which includes the Annaba region. The Guelma Neogene basin stands out for its distinctive formation as a pull-apart basin, resulting from the interaction of two overlapping east-west dextral strike-slip faults. Along the boundaries of this basin, normal fault systems run predominantly in a north-south to NNW-SSE direction, intersecting the sub-parallel shear faults.

The Annaba region, situated at the easternmost part of Algeria's Tell Atlas and extending toward Tunisia, is delineated by the Jebel Safia fault to the west and the Cape Rosa fault to the east.

The most significant earthquake recorded in this seismic zone was a magnitude M_w=5.95 event on December 21, 1980. Throughout its history, the zone has experienced a total of 533 earthquakes.

5.5 Seismic Zone V

This zone encompasses the Chot El Hodna and Batna regions. The Chot El Hodna area, situated southeast of the Bibans, is marked by notable relief features oriented at approximately N110°, notably Djebel Mâadid (1863 m), shaping the Hodna Mountains. South of these mountains lies the Neogene Hodna basin, sharing characteristics with other active Neogene basins in the Tell Atlas region like Cheliff and Metidja. This basin features peneplain surfaces with internal drainage basins known as "chotts" or salt lakes(Abacha, 2018).

Within this area, several anticlines with a NE-SW orientation impact recent deposits, mirroring similar active structures found elsewhere in the Tell region.

The Batna region comprises Neogene formations originating from the Ain Regada Platform and the Belezma Mountains. This region intersects two significant tectonic lineaments (Hamidatou et al., 2021): the Tenes-Negrine lineament, a dextral shear zone extending about 700 km from N110°E to N120°E, and the Sidi Ferdjani-El Kantra lineament, a sinistral strike-slip fault oriented at N055°E and spanning around 400 km. These lineaments are pivotal in the Cenozoic evolution of the area and are associated with seismic activity. Throughout its history, the zone has experienced a total of 857 earthquakes.

6 Seismicity Parameters of Each Seismic Source Zone

6.1 Magnitude Frequency Distribution

A magnitude-frequency distribution is a mathematical model that outlines the probability of various seismic events originating from a given seismic source (Baker et al., 2021). In this research, the earthquake magnitude distribution within a seismic source zone is characterized using a broad range of magnitudes, based on the Gutenberg and Richter (1944) distribution. After analyzing earthquake data at both global and regional levels, Gutenberg and Richter (1944) introduced a linear correlation between earthquake magnitude and the logarithmic frequency of occurrences at that magnitude. This log-linear relationship has been extensively applied in later studies to quantify the annual occurrence of events exceeding a certain magnitude threshold (Eq. 52).

$$\log(\lambda_M) = a - b \times M \tag{52}$$

In this model, λ_M represents the mean annual rate of exceedance of magnitude M. The parameter *a* reflects the overall seismic activity of a region, while *b*, defines the slope of the frequency-magnitude distribution (FMD). The b-value indicates the proportion of larger earthquakes relative to smaller ones and is inversely linked to the stress variations in the surrounding geological formations (Mobarki & Talbi, 2022). Several techniques have been developed to calculate the b-value, with Aki's classic estimator (Aki, 1965) being the most widely accepted. In this study, Aki's estimator is utilized to determine the average b-value for each defined seismic source zone. The formula applied is (Eq. 53):

$$b = \frac{\log_{10}(e)}{\overline{M} - \left(M_c - \frac{\Delta M_{bin}}{2}\right)} \tag{53}$$

Here, the parameters $\overline{M}$, M_c and ΔM_{bin} denote the mean magnitude, the completeness magnitude, and the magnitude bin, respectively. In this analysis, a bin size of 0.1 is used.

6.1.1 The Magnitude of Completeness M_c

The completeness magnitude (M_c) represents the lowest magnitude at which all seismic events within a given space-time volume are consistently detected(Rydelek & Sacks, 1989). Historically, limitations in the coverage of seismic stations and the sensitivity of seismographs in certain areas meant that smaller earthquakes often went unrecorded. This led to incomplete datasets, where events below a specific magnitude threshold were missing, complicating the accurate estimation of seismicity parameters and introducing uncertainties. To mitigate these issues, it is crucial to filter out incomplete data from the seismic catalog and define a completeness magnitude (M_c) (Balouch et al., 2023).

Several approaches are available to calculate Mc, such as the Maximum Curvature Technique (MAXC), the Goodness-of-Fit Test (GFT), the stability of the b-value method, and the Entire Magnitude Range (EMR) approach (Wiemer & Wyss, 2000; Woessner & Wiemer, 2005). In this study, we utilize the Zmap7-Master software package (Wiemer, 2001) to determine Mc by applying the Maximum Curvature Technique (MAXC). Using Zmap Master 2007, we computed key seismicity parameters, including λM, b-value, and Mc, for the declustered sub-catalogs corresponding to each seismic source zone. The findings are presented in Table III. 3 and Fig. III. 5.

Table III. 3: Seismicity Parameters for Each Seismic Zones.

Seismic Zone	Mc	λ_M	B
Z1	2.9	1.925	0.50±0.02
Z2	2.5	2.068	0.51±0.01
Z3	2.5	2.626	0.75±0.03
Z4	2.5	2.159	0.69±0.03
Z5	3	2.183	0.54±0.02

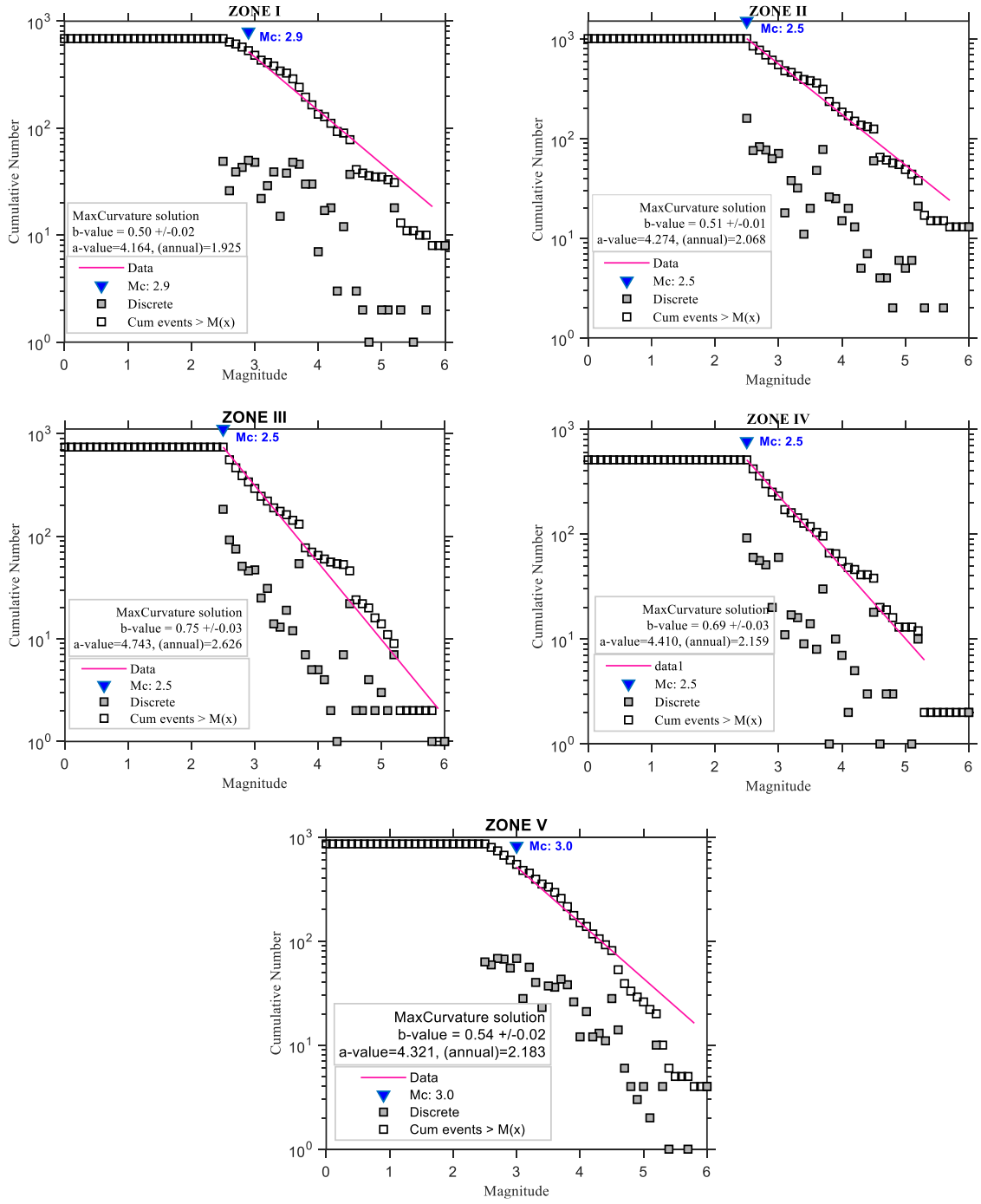

Fig. III. 6: Frequency magnitude distribution for each seismic source zone.

In Table III. 4, we compared our b-values with those from several previously published works in the same region and its surroundings

Table III. 4: Comparison of b-values in Different Seismic Zones from Present Study and Previous Studies

Present Study		**Abacha (2018)**		**Peláez et al. (2005)**		**Hamlaoui et al. (2017)**		**Hamidatou et al. (2021)**	
Zone	**B**	**Zone**	**b**	**Zone**	**b**	**Zone**	**b**	**Zone**	**b**
Z1	0.50	**Z2**	0.68	**Sa5**	0.62	**Z2**	0.77	**Z2**	/
								Z6	1.21
						Z3	1.20		
								Z7	1.01

Z2	0.51	**Z1**	0.62	**Sa5**	0.62	**Z1**	0.79	**Z2**	
								Z4	1.13
						Z5	0.90		
								Z5	1.17
Z3	0.75	**Z5**	0.85	**Sa6**	0.54	**Z4**	0.81	**Z1**	/
		Z6	0.98			**Z5**	0.90	**Z4**	1.13
Z4	0.69	**Z7**	1.64	**Sa6**	0.54	**Z4**	0.81	**Z1**	/
		Z8	0.65	**Sa8**	0.67	**Z6**	0.80	**Z3**	1.2
Z5	0.54	**Z3**	0.56	**Sa7**	0.54	**Z6**	0.80	**Z8**	0.72
		Z4	0.67	**Sa8**	0.67	**Z7**	1.21	**Z9**	0.90
		Z9	0.82	**Sa9**	0.54			**Z10**	0.92

In our study, the b-values obtained are lower than those previously reported for the same region and its neighboring areas, indicating a relatively higher occurrence of large-magnitude earthquakes within our defined zones. For instance, in Zone 1, we observed a b-value of 0.50, whereas Abacha (2018) and Hamlaoui et al. (2017) recorded higher values of 0.68 and 0.77, respectively. Similar patterns are seen in Zones 2, 3, and 5. These discrepancies in b-values can likely be explained by differences in the datasets used for each seismic source, reflecting the influence of data selection on the characterization of seismicity.

6.1.2 The maximum Magnitude M_{max}

The $M_{\max}$, representing the highest potential strain release in an earthquake, is a critical parameter in seismic hazard assessment. Various authors have used deterministic methods to estimate $M_{\max}$ (Mueller, 2010; Wells & Coppersmith, 1994; Wheeler, 2009), with a common conservative approach involving the addition of a predefined increment, Δ, to the observed maximum magnitude $M_{\max}^{obs}$. This increment, typically ranging from 0.25 to 1.0(Kijko & Singh, 2011; Wheeler, 2009), is selected based on expert knowledge about the potential of active faults in the region. For instance, Poggi et al. (2020) used an increment of Δ = 0.5 to estimate $M_{\max}$ in North Africa. In our study, we have also adopted the same increment for the deterministic estimation of $M_{\max}$. This approach is particularly cautious, especially in cases where information about active fault potential is limited. However, this arbitrary method can be avoided by using more rigorous probabilistic procedures. Two main probabilistic approaches are often employed for Mmax estimation: a purely statistical method based on local data (Kijko, 2004) and a Bayesian method that updates a regional model using local data(Cornell, 1994). These methods are especially useful for estimating M_{max} in regional seismic databases that describe areal sources. In the Current investigation two values of $M_{\max}$ for each source zone were computed 1) $M_{\max}^{obs}$ 2) adding an increment of Δ = 0.5 to the observed maximum magnitude. The corresponding results are provided in Table III. 5 below.

Table III. 5: Estimated Values of the Maximum Magnitude for each Zone

Seismic Zone	$M_{\max}^{obs}$	$M_{\max} = M_{\max}^{obs} + 0.5$
Z1	5.95	6.45
Z2	6	6.50
Z3	5.95	6.45
Z4	5.95	6.45
Z5	5.95	6.45

CHAPTER 4: COMPREHENSIVE SEISMIC HAZARD ASSESSMENT FOR NORTHEASTERN ALGERIA: METHODOLOGIES AND REGIONAL APPLICATION

1 Seismic Hazard Analysis Methodologies

1.1 Introduction

Seismic hazard analysis (SHA) involves estimating the likely ground motion caused by a strong earthquake at a specific site (Reiter, 1990). It assesses the potential impact of earthquake-related phenomena, such as ground shaking, liquefaction, and fault rupture, which can lead to significant disasters. By utilizing the complete database on seismicity, tectonics, geology, and attenuation properties, seismic hazard analysis provides a site-specific estimate of design ground motion (Gupta, 2002). This evaluation offers crucial insights into the severity of ground shaking that may be experienced during future earthquakes (Gupta, 2002). Such information is vital for designing earthquake-resistant structures or assessing the safety of existing ones, such as dams, nuclear power plants, long-span bridges, and high-rise buildings. Additionally, SHA plays a key role in the development of seismic zoning maps for broader applications.

SHA comprises two primary components:

- Identifying and characterizing the sources of seismic hazards
- Evaluating the effects these sources may have at a given location

All methods for SHA include these two elements. There are two principal approaches to estimating seismic hazards at a site: deterministic and probabilistic (Bommer, 2002; McGuire, 2001; Reiter, 1990). This chapter outlines the essential principles of SHA, which form the foundation for defining seismic design forces. It introduces both the probabilistic and deterministic methods, highlighting their core components, and provides a step-by-step explanation of each method.

1.2 Seismicity and Earthquake Recurrence Model

All relevant information, alongside additional details, has been comprehensively discussed in the previous chapter. This section provides a concise summary.

The initial stage of Seismic Hazard Analysis (SHA) involves identifying potential seismic sources and evaluating historical seismic events that could impact the study area. These sources—encompassing faults, points sources, and area sources—are delineated through detailed geological and seismotectonic investigations. Seismic activity, characterized by the frequency of earthquake occurrences within the region of interest, is assessed using earthquake catalogs. These catalogs compile the locations and magnitudes of earthquakes that are pertinent from an engineering standpoint, typically those exceeding a defined magnitude threshold. Geological and seismotectonic studies subsequently associate these seismic events with specific sources.

A crucial component of Probabilistic Seismic Hazard Analysis (PSHA) is the earthquake recurrence model, which estimates the mean annual frequency of events surpassing a specified magnitude. The Gutenberg and Richter (1944) remains one of the most fundamental yet effective tools for this purpose, offering a logarithmic formula that links the probability of earthquake occurrences to magnitude, as detailed in Equation (59) in the coming chapter.

To construct an earthquake recurrence model, the dataset is filtered to exclude foreshocks and aftershocks. Seismic events are then sorted by magnitude, and the annual exceedance rate—reflecting the frequency of events above a certain threshold—is computed. This rate decreases with increasing magnitude, highlighting the more frequent occurrence of minor earthquakes compared to larger ones.

However, the standard Gutenberg-Richter model does not account for the physical constraints of seismic sources in generating extremely large events, which manifest as deviations from a linear trend at higher magnitudes. This limitation is addressed by employing the truncated Gutenberg-Richter model, which incorporates a maximum magnitude (M_{max}), beyond which the likelihood of an event becomes negligible.

The determination of M_{max} can be derived from earthquake catalogs or through empirical relationships based on fault dimensions. The catalog-based approach is particularly useful for area sources but can also be adapted for faults. In such cases, the largest observed magnitude may be adjusted upwards (e.g., by 0.5 units) to accommodate uncertainties. Alternatively, empirical models—like those proposed by Wells and Coppersmith (1994), estimate M_{max} based on fault rupture characteristics, accounting for various faulting mechanisms.

Within earthquake recurrence models, the reciprocal of the mean annual exceedance rate signifies the recurrence interval or return period of specific seismic events. For instance, if the recurrence interval for a magnitude 6.0 earthquake ($M \geq 6$) is 50 years, it indicates that such an event is expected to occur, on average, once every 50 years. This metric is a critical indicator of the potential hazard level for a given site or region. In PSHA, earthquake occurrences are commonly modeled using a Poisson process.

A Poisson process presupposes that event occur randomly at a specified average rate, with each event being independent of previous occurrences. This implies that the probability of an earthquake remains constant between successive events, regardless of historical data. In the context of PSHA, seismic events are treated as random processes, and the mean exceedance rate is derived from earthquake recurrence models.

For example, if the mean exceedance rate for events of magnitude 5.0 or greater ($M \geq 5.0$) is approximately 0.225, then an earthquake of at least magnitude 5.0 is anticipated every 4 to 5 years on average within the study area.

It is important to note, however, that seismic events are not entirely independent. The occurrence of an earthquake can influence subsequent seismic activity. When stress is released along one fault segment due to an event, it diminishes the likelihood of a similar magnitude event occurring soon thereafter in the same segment. Thus, the assumption of a Poisson process, which treats seismic events as independent with no temporal memory, does not fully encapsulate the complexities of seismic mechanisms. Nonetheless, assuming independence is generally acceptable if foreshocks and aftershocks are excluded from the earthquake catalog, a common practice in seismic hazard analysis. This aligns with the Poisson model, where the exposure time (t)—often the expected lifespan of structures, such as 50 years—is used as a parameter. Within this Poisson framework, the probability of observing nnn events exceeding a certain magnitude (m*) during the exposure time (t) can be calculated using Eq. (54).

$$P(M > m^*) = \frac{\exp(-t * \lambda_m(M > m^*))(t * \lambda_m(M > m^*))^n}{n} \tag{54}$$

The primary objective in PSHA is not to forecast the precise number of events exceeding a specific magnitude within a given period, but rather to estimate the probability of at least one such event occurring within a set timeframe. This probability, known as the "probability of exceedance," is determined by subtracting the probability of no event occurrence (where n=0 in Eq. (54)) from one. Eq. (55) formalizes this concept, while Eq. (56) refines it to link the exceedance probability for a particular magnitude (m*) with the mean annual exceedance rate over a designated exposure time.

$$P(M > m^*) = 1 - \exp(-t * \lambda_m(M > m^*)) \tag{55}$$

$$\lambda_m(M > m^*) = -\frac{\ln(1 - P(M > m^*))}{t} \tag{56}$$

For instance, assuming an exposure period of 50 years with a 10% probability of exceeding a particular magnitude (m*), the mean annual exceedance rate is approximately 0.0021, as calculated from Eq. (56). By applying this rate to the recurrence model, a magnitude of roughly 6.2 is derived. Consequently, there is a 10% probability of experiencing an earthquake with a magnitude of 6.2 or greater within the next 50 years in the study area.

1.3 Ground-Motion Prediction Equations (Attenuation Relationships)

A key element in any seismic hazard analysis is the selection of appropriate ground-motion prediction equations (GMPEs). GMPEs are employed to estimate ground-motion intensity parameters—such as Peak Ground Acceleration (PGA), Peak Ground Velocity (PGV), and spectral ordinates (e.g., spectral acceleration, Sa, at various vibration periods)—at a specific site by accounting for source, path, and site effects. These factors are primarily characterized by independent variables: magnitude (M), source-to-site distance (R), site classification (SC), and style-of-faulting (SoF). The source effects are captured through magnitude and style-of-faulting, path effects are modeled by the source-to-site distance, and site effects are expressed via site classification, reflecting the impact of local soil conditions on ground-motion amplitudes.

GMPEs are derived through regression analysis applied to empirical ground-motion datasets. The inherent variability in ground-motion parameters, evidenced by extensive datasets, necessitates the use of regression techniques for developing these predictive models. The standard exponential form of GMPEs, originating from earthquake source theory, is represented in Eq. 57.

$$Y = \exp[f(M) * f(R)8f(SC) * f(SoF)] \tag{57}$$

As depicted in Eq. 57, the ground-motion intensity parameter Y is computed through a multiplicative process involving several independent parameters: magnitude (M), distance (R), site classification (SC), and style-of-faulting (SoF). The resulting parameter Y is generally considered to follow a log-normal distribution. This relationship is generalized in Eq. 58

$$\ln(Y) = \theta(M,R,SC,SoF) + \varepsilon * \sigma_{\ln y} \tag{58}$$

In this equation, θ(M, R, SC, SoF) is a composite functional term that represents the combined effects of the functions f(M), f(R), f(SC), and f (SoF). It denotes the predicted logarithmic mean μ of ln(Y). Here, $\sigma_{\ln Y}$ is the standard deviation (also referred to as "sigma") of ln(Y), capturing the dispersion of observations, while ϵ is a standard normal variable representing the number of standard deviations above (for positive values of ϵ) or below (for negative values of ϵ) the predicted mean. Thus, ϵ reflects the observed variability in ln(Y).

1.4 Probabilistic Seismic Hazard Analysis (PSHA)

Probabilistic Seismic Hazard Analysis (PSHA) is a mathematical framework designed to estimate the annual rate (or probability) of exceeding specific levels of ground-motion intensity at a site, across a spectrum of potential intensities. This assessment is crucial for evaluating the seismic risk to a structure, as it allows for a comprehensive understanding of how frequently different levels of ground shaking might occur. The results of such an analysis are typically summarized in a ground-motion hazard curve, also referred to simply as a hazard curve. This curve illustrates that lower intensity levels are exceeded more frequently, while higher intensities are comparatively rare. The hazard curve thus provides a clear visual representation of the relationship between ground-motion intensity and its likelihood of exceedance, serving as a foundational tool for seismic risk assessment.

PSHA offers a rigorous approach by integrating uncertainties inherent in seismic hazard assessments directly into ground-motion intensity calculations. While this inclusion of uncertainty adds complexity to the analysis, it enhances the reliability and defensibility of the results, making them more suitable for engineering decision-making aimed at risk mitigation. The move towards probabilistic, risk-based regulations in various industries has been ongoing for decades (Pate-Cornell, 1994; Bedford and Cooke, 2001; Hartford, 2009). Such regulations enable more effective cost–benefit

analyses and provide clearer design objectives, ensuring uniform safety standards across diverse projects and geographic areas. we introduce terminology to precisely refer to types of uncertainties considered in hazard and risk studies

- Epistemic Uncertainty (derived from the Greek word *episteme*, meaning "knowledge") refers to the limitations in our current understanding of the processes involved. This type of uncertainty arises when the value of a parameter is unknown—such as the maximum magnitude an earthquake from a given seismic source could generate—and is due to insufficient data or gaps in our understanding of the physical processes. Unlike other uncertainties, epistemic uncertainty is potentially reducible; with additional data or advanced research, the uncertainties can be narrowed, leading to more precise estimates. This reducibility is particularly important in seismic hazard analysis, as it allows analysts to target specific areas for further study if a source of epistemic uncertainty significantly influences the analysis.
- Aleatory Variability (from the Latin word *alea*, meaning "game of dice") captures the inherent randomness in natural processes. This variability is evident when a parameter fluctuates across repeated observations, despite having consistent model formulations. For instance, variations in ground-motion amplitudes from similar seismic events with comparable rupture and site characteristics demonstrate aleatory variability. Unlike epistemic uncertainty, aleatory variability is intrinsic to the natural processes and cannot be reduced through additional study or data acquisition.

The aleatory variability of the attenuation relations is taken into account in the PSHA by considering the standard deviation of the model error. The epistemic uncertainty is considered by multiple models for the evaluation of seismic hazard and combining them using a logic tree.

The classic procedure known as the Cornell-McGuire procedure for the PSHA includes the following four steps and a representative illustration is given in Fig. IV. 1:

a) The first step in PSHA involves the identification and characterization of seismic sources that may affect the designated site. These sources can be categorized as area, fault, or point sources.

b) Subsequently, the following stage involves defining the temporal and magnitude distributions of seismicity for each seismic source.

c) while the third attempts to predict the ground motion. GMPE are used to predict ground motion at the site itself.

d) The integration of uncertainties in the earthquake location, earthquake magnitude, and ground motion prediction equation is a crucial step in determining the probability that a specific ground motion parameter will be surpassed at a designated site within a specified time interval. Therefore, the PSHA can be associated with the computation of the exceedance probability given a certain earthquake from a whole set of faults, which is achieved using Eq. 59

$$\lambda\left(IM>x\right)=\sum_{i=1}^{n_s}\lambda\left(M_i>m_{\min}\right)\sum_{j=1}^{n_M}\sum_{k=1}^{n_R}\left[P\left(IM>x\middle|m_j r_k\right).P\left(M_i=m_j\right).P\left(R_i=r_k\right)\right] \tag{59}$$

where $\lambda\left(IM>x\right)$ is the rate of occurrence of an intensity measure IM exceeding an intensity level x; $\lambda\left(M_i>m_{\min}\right)$ is the rate of occurrence of an ith magnitude M_i exceeding the minimum magnitude $m_{\min}$; $P\left(IM>x\middle|m_j r_k\right)$ is the exceedance probability of $IM>x$ given j-th magnitude m_j and k-th distance r_k; $P\left(M_i=m_j\right)$ is the probability that $M_i=m_j$; $R_i=r_k$ is the probability that; n_s is the total number of sources considered; and n_M and n_R are the discretization intervals for magnitude and distance, respectively.

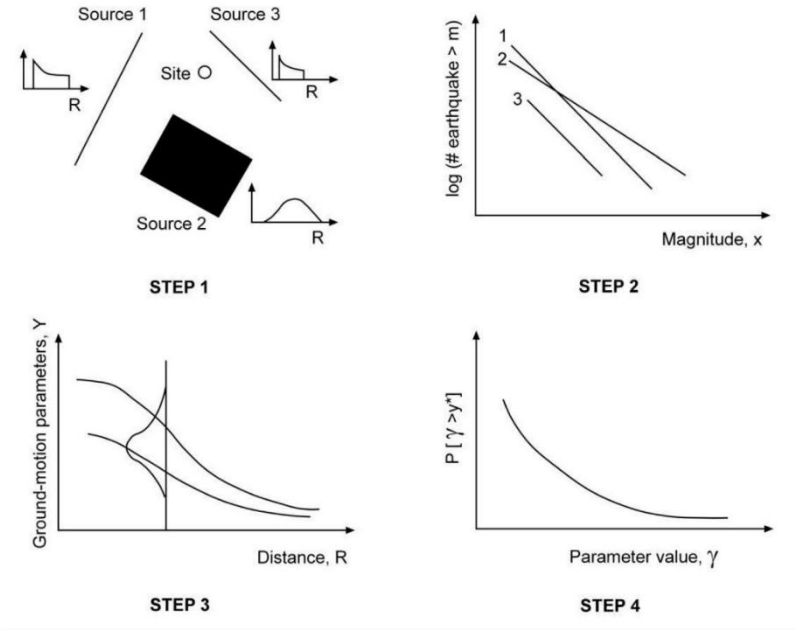

Fig. IV. 1: Diagrams showing four steps of probabilistic seismic hazard analysis (Gürboğa & Sarp, 2013)

The return period of an IM exceedance is defined as the reciprocal of the rate of exceedance:

$$RP = \frac{1}{\lambda} \tag{60}$$

where λ is the exceedance rate and RP is the return period. Typically, λ has units of events per year, so RP has units of years per event. For example, if a given IM has a 0.01 annual rate of exceedance, then the return period is equal to 1/ (0.01 years−1) = 100 years. This does not imply that the ground motion will be exceeded exactly once every 100 years, but rather that the average (or mean) time between exceedances is 100 years. Thus, the reciprocal of the exceedance rate is more precisely termed the mean return period. While the mean return period, or simply return period, is commonly used to refer to the reciprocal of the rate of exceedance, it is often clearer to report rates rather than return periods. For a given rate of exceedance, one can also compute a probability of exceeding a given IM within a given window of time (Eq. 55 and Eq. 56).

1.5 Deterministic Seismic Hazard Analysis (DSHA)

Deterministic Seismic Hazard Assessment (DSHA) can be regarded as a specialized subset of Probabilistic Seismic Hazard Assessment (PSHA), in which a specific earthquake scenario—defined by a combination of magnitude and source-to-site distance—is chosen to represent the dominant or "controlling" earthquake. In essence, DSHA focuses on identifying the maximum potential ground motion that could be produced by seismic sources within the region of interest. The earthquake that generates this maximum ground motion is termed the "controlling earthquake" and serves as a representation of the seismic hazard at the site under study.

In DSHA, the ground-motion intensity measure (such as Peak Ground Acceleration, PGA, or spectral acceleration, SaS_aSa, at a specified period) is calculated based on the scenario of the controlling earthquake. This measure is then used for structural design or seismic performance evaluation. Unlike PSHA, DSHA does not incorporate a concept of return periods; consequently, the methodology does not provide any indication of the likelihood or recurrence interval of the controlling earthquake. Instead, DSHA concentrates exclusively on a worst-case scenario, without quantifying its probability of occurrence over the service life of the structure.

The selection of the worst-case scenario, however, introduces a degree of subjectivity, as the determination of the controlling earthquake and its corresponding ground-motion parameters relies heavily on expert judgment. It is important to acknowledge that the earthquake or ground motion identified through DSHA may not truly represent the "worst-case" scenario, as there is always a possibility of larger, unforeseen events exceeding the chosen parameters.

Below is a summary of the key steps involved in DSHA, and are illustrated in Fig. IV. 2:

a) Identify Seismic Sources: Determine the active seismic sources in the study area, including style-of-faulting information. For instance, S1 S2 and S3 could represent active faults likely to influence the seismic hazard at the project site, as illustrated in Fig. 31. Understanding the faulting style (e.g., strike-slip, normal, or reverse) is crucial for accurate hazard assessment.

b) Estimate Maximum Probable Magnitudes: Calculate the maximum credible magnitudes (denoted as M_{max}) for each identified seismic source. This can be achieved by analyzing the compiled earthquake catalog. Alternatively, empirical relationships between magnitude and fault rupture length can be utilized. This method assumes that a full or substantial segment of the fault may rupture during the controlling earthquake. To account for uncertainties in the largest possible event, hazard experts might increase the estimated magnitude by an additional 0.5 units or incorporate the standard deviation of the magnitude-rupture length relationship.

c) Compute Source-to-Site Distances: Measure the shortest distance from each identified seismic source to the project site.

d) Assess Site Soil Conditions: Conduct in situ geotechnical investigations to determine the soil properties at the site. The identified soil conditions will influence the local ground response and should be factored into hazard calculations.

e) Apply Ground-Motion Prediction Equations (GMPEs): Select an appropriate GMPE to estimate the desired ground-motion parameter using the parameters obtained in previous steps, including magnitude, source-to-site distance, soil classification, and faulting style.

f) Determine the Controlling Earthquake Scenario: Compare the computed ground-motion parameters from each seismic source. The highest value is selected for use in design or seismic performance assessment. This scenario defines the controlling earthquake specific to the project.

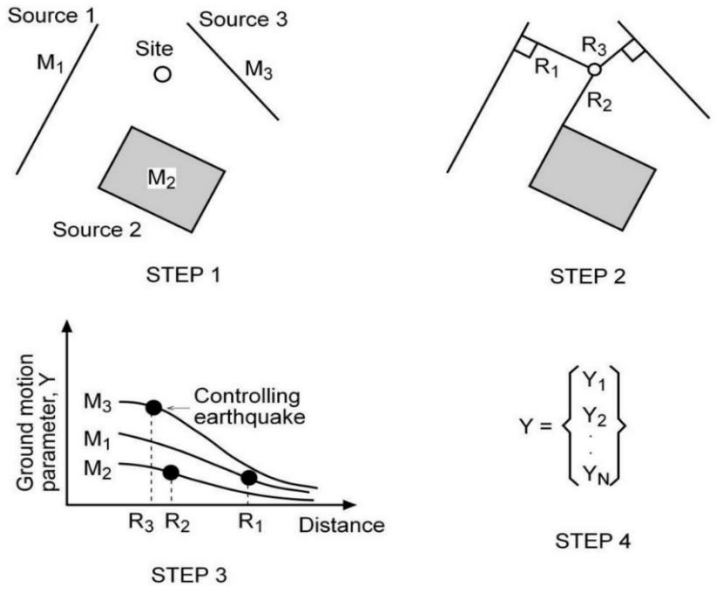

Fig. IV. 2: Diagrams showing four steps of deterministic seismic hazard analysis (Gürboğa & Sarp, 2013)

1.5.1 Limitations

DSHA has inherent limitations, described in details in (Baker et al., 2021), due to its approach of using a single "design earthquake" scenario. First, DSHA does not capture the true "worst-case" earthquake event; it relies on a scenario that is considered large but does not account for the possibility of even larger earthquakes or stronger ground motions. This can give a misleading sense of maximum safety.

Another challenge with DSHA is its sensitivity to specific choices, such as the selected earthquake magnitude and the assumed level of ground shaking. Since these choices rely heavily on expert judgment, the results may vary widely and lack robustness, making them less reliable.

Additionally, DSHA does not incorporate the rate or frequency of earthquake events, which means it cannot account for differences in earthquake occurrence across regions. This results in inconsistent safety levels in different geographic areas and types of structures, as DSHA does not consider factors like how often earthquakes might happen.

2 Probabilistic Seismic Hazard Calculation for the Northeastern Region of Algeria

2.1 Introduction

The seismic hazard assessment for Northeastern Algeria was conducted utilizing a state-of-the-art PSHA following the classical Cornell–McGuire methodology. This analysis incorporated areal seismic source models-defined in previous chapter, and multiple ground motion attenuation relationships. The most up-to-date information on the region's seismicity was integrated. The hazard curves obtained from PSHA show the variation of peak ground acceleration (PGA) or spectral acceleration (Sa) against the mean annual rate of exceedance, as well as uniform hazard spectra for return periods of 100 and 475 years. For calculating the seismic hazard values, the entire study area was divided into grids of required size, and the hazard values at the center of each grid cell have been calculated. To enhance the robustness of the assessment, a logic-tree framework was employed, enabling a systematic consideration of epistemic uncertainties by evaluating alternative hypotheses related to maximum magnitudes and ground motion prediction equations. This approach ensures that the analysis reflects the most reliable scientific interpretation and data currently available. As previously outlined, the core stages in PSHA involve:

1. Identification and characterization of seismic sources,
2. Determination of earthquake recurrence rates,
3. Assessment of ground motion using attenuation relationships,
4. Estimation of the mean annual exceedance rate for the selected ground motion parameters, accounting for uncertainties in earthquake location, magnitude, and attenuation characteristics.

The first two stages—source identification and recurrence rate characterization—were thoroughly addressed in Chapter 3. Therefore, this chapter will proceed with a detailed exploration of the remaining stages.

2.2 Ground Motion Prediction Equation

A thorough PSHA demands reliable models to estimate the probability distribution of ground motion intensities, taking into account all potential earthquake scenarios (Baker et al., 2021). To achieve this, Ground Motion Prediction Equations (GMPEs), often called Ground Motion Models (GMMs) or attenuation relationships, should be tailored to the specific characteristics of the region under study. These models are constructed to reflect the area's geological conditions, tectonic context, faulting styles, and soil types(Sawires et al., 2017). In Algeria, due to the scarcity of strong-motion data, there exists only a single Algeria-specific GMPE, developed by (Laouami et al., 2018) .

Therefore, it was necessary to supplement the analysis with globally recognized GMPEs (Sawires et al., 2016; Sawires et al., 2020). Among the selected models by Algerian researchers were those proposed by (Akkar & Bommer, 2010; Ambraseys et al., 1996; Bindi et al., 2011; Boore & Atkinson, 2008; Boore et al., 2014; Sadigh et al., 1993). For the

current study the selected GMPEs are listed in Table IV. 1. The choice of these GMPEs was guided by several key criteria outlined by Bommer et al. (2010) ensuring that the chosen models provide accurate and reliable predictions for ground motion, essential for the seismic hazard evaluation in Northeastern Algeria. The criteria include

1. Tectonic Relevance: The GMPE should be derived from a tectonic setting similar to the target region. Akkar and Bommer (2010), Ambraseys et al. (1996), and Bindi et al. (2011) all meet this criterion as they are developed for regions comparable to northern Algeria.
2. Data Quality: The GMPE should be based on a robust dataset with well-defined earthquake source parameters, source-to-site distances, and site classifications. The selected GMPEs are based on extensive datasets that cover a wide range of seismic events.
3. Empirical Validation: The GMPE should have been validated through peer-reviewed publications and widely accepted in the scientific community. The chosen GMPEs have undergone rigorous validation and are widely used in seismic hazard assessments.
4. Magnitude and Distance Ranges**:** The GMPE should cover the magnitude and distance ranges relevant to the target region. The selected GMPEs encompass the necessary ranges to provide accurate predictions for our study area.
5. Applicability to Engineering Analyses**:** The GMPE should provide predictions for the required ground-motion parameters, including spectral accelerations at relevant periods. The selected GMPEs provide comprehensive spectral predictions, suitable for engineering analyses in Algeria.

Table IV. 1: List of the Selected GMPEs in the present study

GMPE's Reference	Application Area	Magnitude (M) Range	Distance (R) Range	R Type	Period Range	Style of Faulting
Ambraseys et al. (1996)	Europe and adjacent regions	4.0 - 7.9	0 – 212 km	R_{rup}	0.10 -2.0s	U
Akkar and Bommer (2010)	Southern Europe, North Africa, and Middle East	5.0 - 7.6	0 – 100 km	R_{JB}	0.05 - 3.0s	N, R, SS
Bindi et al. (2011)	Italy	4.1 - 6.9	0 – 200 km	R_{JB}	0.04 - 2.0s	N, R, SS, U

R_{JB}: Joyner-Boore distance; R_{rup}: distance from the rupture plane. N: normal fault; R: reverse fault; SS: strike-slip fault; U: undefined style of faulting.

The selected GMPEs—Akkar and Bommer (2010), Ambraseys et al. (1996), and Bindi et al. (2011)—were chosen due to their strong alignment with the region's tectonic characteristics, the reliability of their underlying datasets, and their robust empirical validation. These models also offer comprehensive coverage across the required ranges of magnitude and distance, making them highly suitable for engineering applications. Detailed justifications for each selection are provided below.

- **Akkar and Bommer (2010):**

1. Tectonic Relevance: Developed specifically for Southern Europe, North Africa, and the Middle East, it aligns well with the tectonic context of Algeria.
2. Data Quality: The model is based on an extensive dataset that includes a wide range of magnitudes and distances (up to 100 km), ensuring robust empirical predictions.
3. Empirical Validation: This GMPE has been extensively validated and is widely used in seismic hazard assessments in regions with similar seismic characteristics.

4. Magnitude and Distance Ranges: Covers a broad range of magnitudes and distances relevant to the study area.
5. Engineering Applicability: Provides spectral acceleration predictions at multiple periods, which are essential for engineering analyses.

- **Ambraseys et al. (1996):**

1. Tectonic Relevance: This GMPE is specifically tailored for Europe and adjacent regions, including North Africa, making it directly applicable to Algeria.
2. Data Quality: Utilizes a comprehensive dataset of European earthquakes, providing a robust empirical basis for predictions.
3. Historical Significance: A foundational model with extensive validation, widely used in seismic hazard assessments.
4. Magnitude and Distance Ranges: Covers the necessary ranges to provide accurate predictions for our study area.
5. Engineering Applicability: Offers spectral acceleration values at relevant periods, useful for engineering applications.

- **Bindi et al. (2011):**

1. Tectonic Relevance: Developed for Italy, a region with seismic characteristics comparable to those of Algeria, making it suitable for our study area.
2. Data Quality: Based on a robust dataset that includes numerous seismic events within a similar tectonic setting, ensuring reliable predictions.
3. Empirical Validation: Extensively validated and widely used in seismic hazard assessments.
4. Magnitude and Distance Ranges: Encompasses the necessary ranges for accurate predictions.
5. Engineering Applicability: Provides comprehensive spectral acceleration predictions, suitable for detailed engineering analyses.

2.3 Logic tree Structure

In PSHA, managing epistemic uncertainty involves using a logic tree with branches that represent different models and parameters, each assigned a subjective weight to indicate its likelihood of being correct. Uncertainty in seismic source models is typically handled by considering alternative configurations, while ground-motion predictions often involve selecting multiple Ground Motion Models (GMMs) or modifying a base model to account for uncertainty. Each branch of the logic tree has an associated weight. In each column, weights are assigned to each branch, and the weights of branches connecting to a common parent node sum to 1. The weight associated with a complete set of branches (i.e., a complete path transversing from left to right through the tree) is the product of weights associated with each branch in the set. Because the sum of weights for each set of branches sharing a parent node sums to 1, the weights associated with all terminal nodes will also sum to 1. Collectively, the terminal branches and weights specify a discrete probability distribution of epistemic uncertainties on the model set (Scherbaum & Kuehn, 2011). The present study considers one type of source models (Areal sources), two different maximum magnitudes, and three different attenuation relations (Fig. IV. 3).

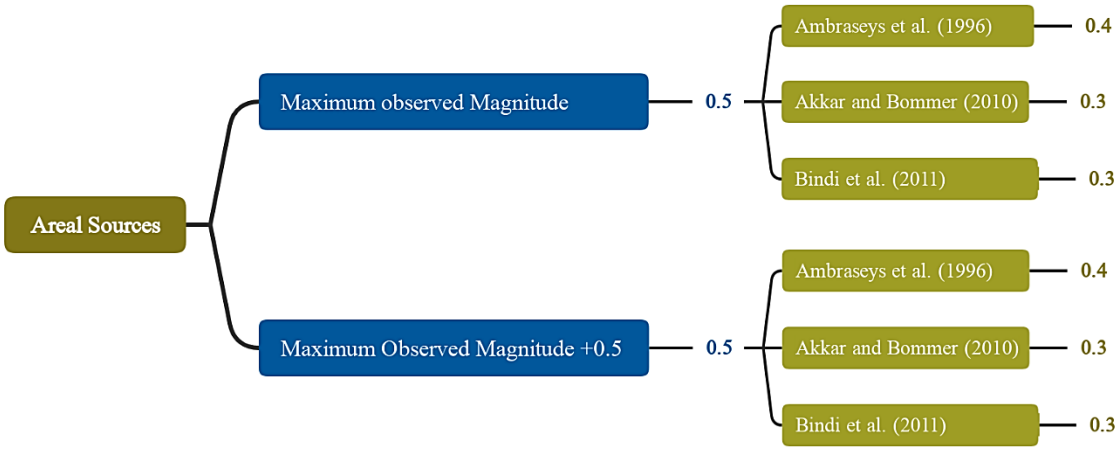

Fig. IV. 3: Parameters and weighting factors adopted in the logic tree

All steps towards the seismic hazard assessment are described in a flowchart (Fig. III. 4).

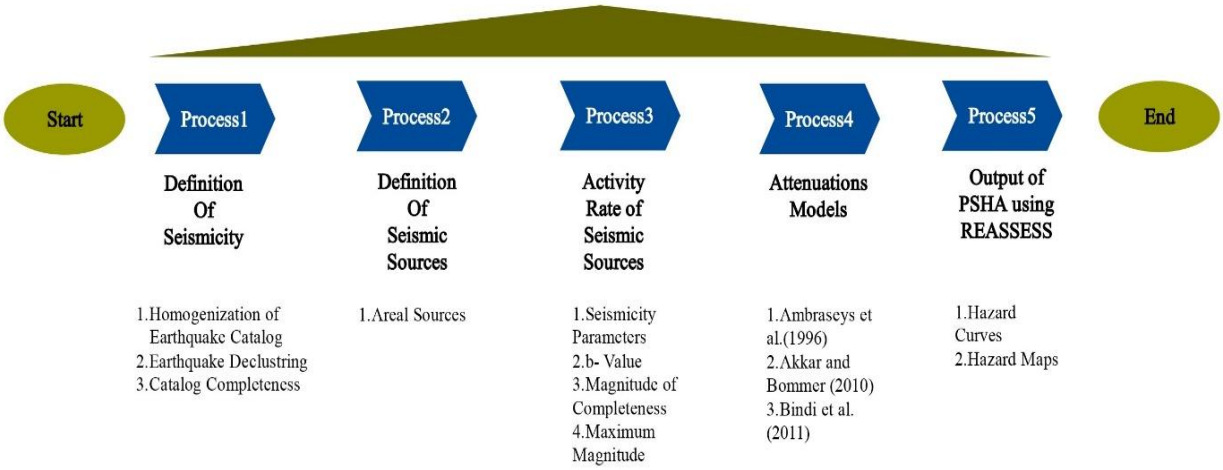

Fig. IV. 4: Steps Followed in Executing Probabilistic Seismic Hazard Analysis (PSHA) for the Northeastern Region of Algeria.

2.4 PSHA Results

The seismic hazard assessment for Northeast Algeria involved dividing the study area into a grid system, with each cell measuring 0.1° × 0.1° (approximately 11 km × 11 km). A total of 1,275 grid points were analyzed. At each grid point, Peak Ground Acceleration (PGA) and Spectral Acceleration (Sa) values, corresponding to periods of 0.1 seconds and 1 second, were calculated at the bedrock level for return periods of 100 and 475 years. The results include Uniform Hazard Spectra (UHS) alongside hazard maps presented in terms of PGA and Sa.

Over the past forty years, various computer software programs have been developed to facilitate PSHA, such as EQRISK (McGuire, 1976), SEISRISK III (Bender & Perkins, 1987), OpenSHA (Field et al., 2003), Ez-frisk software, and CRISIS (Ordaz et al., 2013). To address the need for an engineering-oriented tool integrating recent advancements in PSHA, a new standalone software called REgionAl, Single SitE and Scenario-based Seismic hazard analysis (REASSESS) with a user-friendly interface has been developed by Chioccarelli et al. (2019). The software was used recently to conduct PSHA and other related studies(Caruso et al., 2021; Chioccarelli et al., 2021; Forte et al., 2019; Gabbianelli et al., 2023; Nettis et al., 2024). In this study, REASSESS V2.0 is utilized to generate hazard curves and maps.

2.5 Earthquake hazard maps

2.5.1 Hazard maps in terms of peak ground acceleration (PGA)

Seismic hazard maps for Northeast Algeria were generated using refined grid systems. Fig. IV. 5 (a and b) illustrate the site-specific hazard maps depicting PGA for return periods of 100 and 475 years. As anticipated, the Babors and Djidjelli regions (Zones 1 and 2 in Fig. 40) exhibit maximum PGAs of 0.20 g and 0.19 g, respectively, for the 475-year return period. In contrast, the remaining areas of the study region display significantly lower acceleration values.

2.5.2 Hazard maps in terms of spectral acceleration (SA)

Fig. IV. 5 (c, d, e, and f) present the hazard maps illustrating Spectral Acceleration (SA) values (in g) for periods of 0.1 seconds and 1 second, corresponding to return periods of 100 and 475 years, respectively.

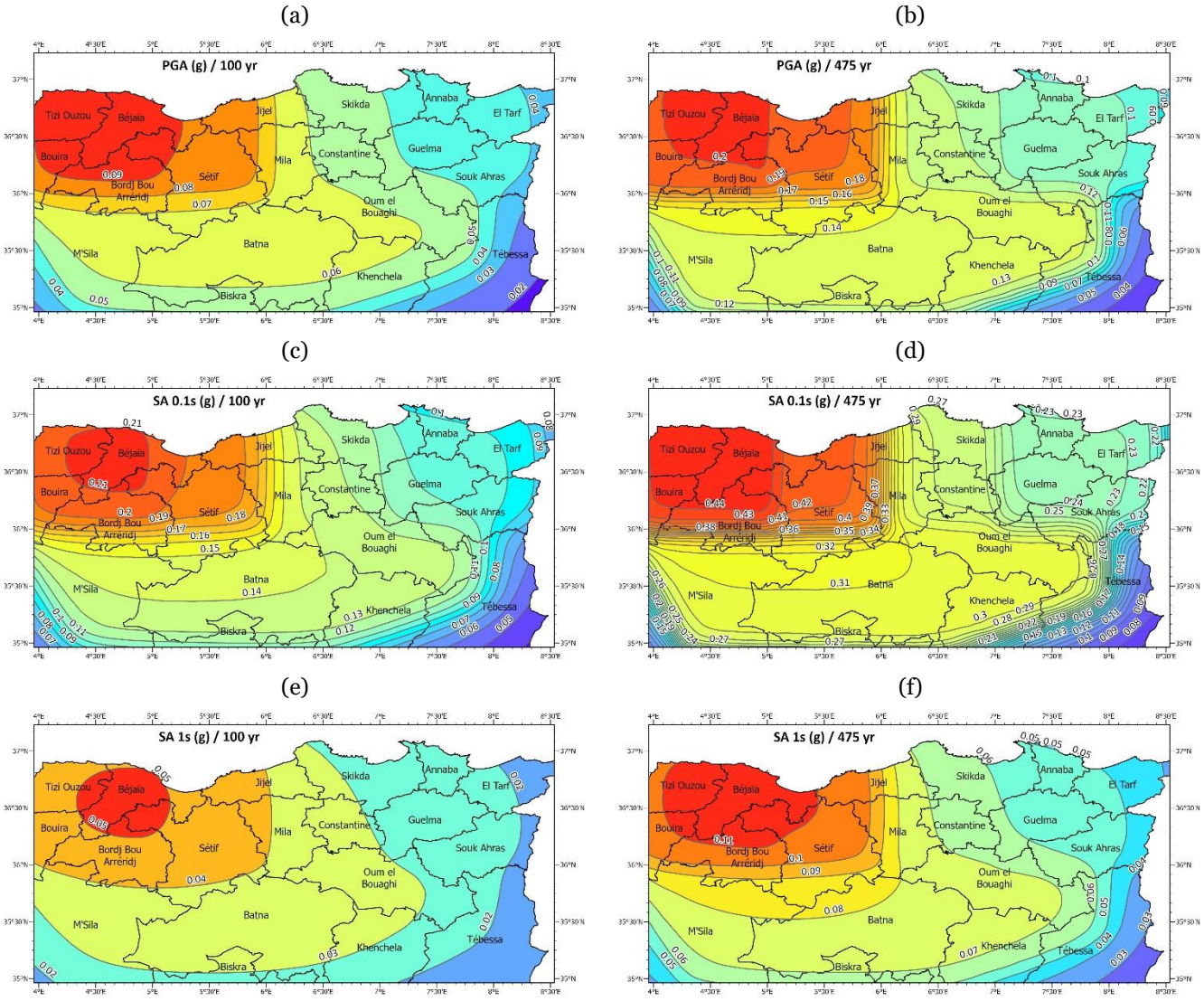

Fig. IV. 5: Seismic hazard map produced in terms of: PGA for return period of a) 100-year, b) 475-year, Spectral Acceleration Sa (0,1s) for return period c) 100-year, d)475-year, and Spectral Acceleration Sa(1s) for return period e) 100-year, f) 475-year

2.5.3 Hazard Curve and Uniform hazard spectra (UHS)

Fig. IV. 6 and 7 display the hazard curves and Uniform Hazard Spectra (UHS) for return periods of 100 and 475 years, specifically for six selected cities within the study area.

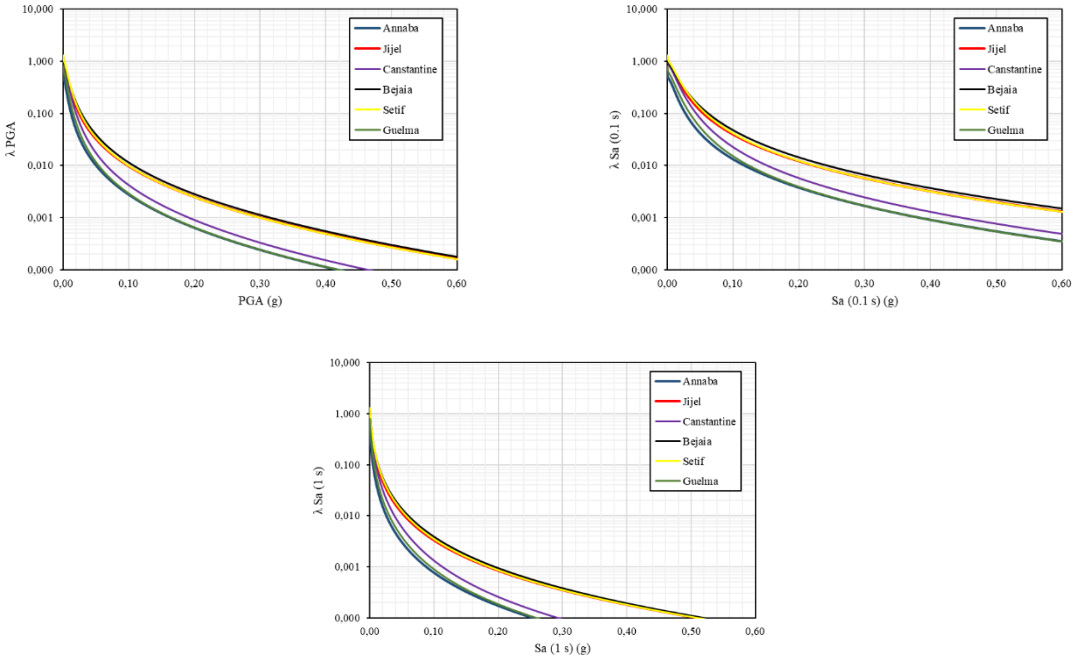

Fig. IV. 6: Hazard Curves for six selected cities (as indicated in each plot) of northeastern Algeria

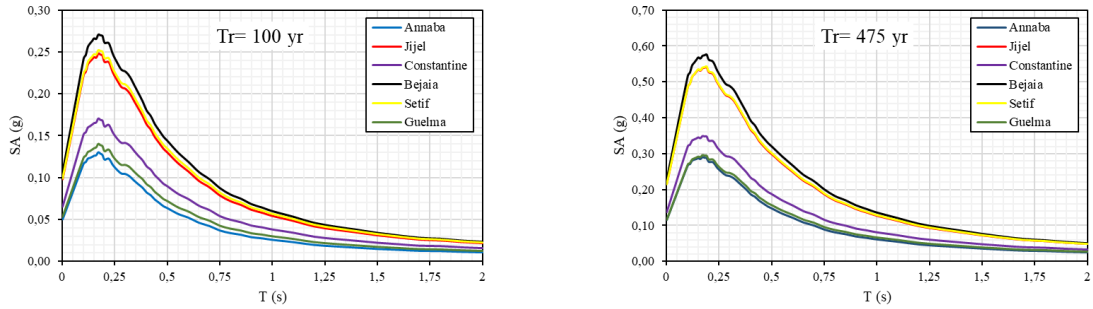

Fig. IV. 7: UHS for the selected cities of northeastern Algeria, computed for a Tr = 100 and 475-year.

2.6 Comparative analysis

Comparing the results of the Probabilistic Seismic Hazard Assessment (PSHA) from this study with previous research is important for several reasons. First, it helps us check how reliable and accurate our findings are by looking at established data from earlier studies. This comparison validates the methods, assumptions, and models used in our research, ensuring that our results are solid (Kumar et al., 2022). Second, a comparative analysis can reveal differences in seismic hazard estimates over time, pointing out any changes in seismic activity or hazard levels in the area. This information is essential for updating and improving seismic hazard assessments, which are critical for disaster preparedness and risk management strategies. Additionally, comparing our PSHA results with past studies helps us understand how consistent and stable these hazard estimates are, allowing us to identify long-term trends and patterns in seismic activity in the region (Kumar et al., 2022). This historical insight is valuable for decision-makers, urban planners, and engineers who need to design infrastructure and buildings that can withstand possible earthquakes.

In this context, Tables IV. 2 and 3 present the Peak Ground Acceleration (PGA) values from our study alongside those from previous research for bedrock conditions.

For a 100-year return period, our study reports a lower PGA of 0.087 g compared to Montilla et al. (2003) and Hamidatou et al. (2021), but it is similar to Hamdache et al. (2012). In Constantine, our reported PGA of 0.057 g is comparable to Hamdache et al. (2012) and Montilla et al. (2003) but significantly lower than Hamidatou et al. (2021). For Guelma, our study shows a lower PGA of 0.047 g compared to all other studies, while for Bejaia, we report a higher PGA of 0.094 g

compared to the other research. Additionally, our study shows a significantly higher PGA of 0.086 g for Jijel than in other studies, and a value that is similar to Hamdache et al. (2012) but lower than Hamidatou et al. (2021) for Annaba.

Table IV. 2: Comparison of the estimated PGA(g) results from this study for a return period of 100 years with other studies.

Cities	(Montilla et al., 2003)	(Hamdache et al., 2012)	(Hamidatou et al., 2021)	Present Study
Setif	0.120	0.090	0.160	0.087
Constantine	0.062	0.050	0.250	0.057
Gulma	0.071	0.064	0.140	0.047
Bejaia	0.071	0.070	0.080	0.094
Jijel	0.055	0.051	/	0.086
Annaba	/	0.040	0.070	0.043

For the 475-year return period, the Peak Ground Acceleration (PGA) reported in the present study for Setif is 0.190 g, which falls between the values found in previous research. In Constantine, our study shows a slightly lower PGA of 0.121 g compared to Montilla et al. (2003) and others, and significantly lower than Hamidatou et al. (2021). In Guelma, the present study indicates a slightly lower PGA of 0.102 g compared to all other studies. Conversely, for Bejaia, our findings reveal a higher PGA of 0.200 g compared to Montilla et al. (2003), Hamdache et al. (2012), and Hamidatou et al. (2021), but still lower than Hamlaoui et al. (2017).

For Jijel, the current study presents a higher PGA of 0.095 g than that reported by Montilla et al. (2003) and Hamdache et al. (2012), yet it remains lower than the figure provided by Hamlaoui et al. (2017). Lastly, in Annaba, our study shows a slightly higher PGA of 0.100 g compared to other studies.

Table IV. 3: Comparison of the estimated PGA(g) results from this study for a return period of 475 years with other studies.

Cities	(Montilla et al., 2003)	(Hamdache et al., 2012)	(Hamlaoui et al., 2017)	(Hamidatou et al., 2021)	Present Study
Setif	0.247	0.207	0.160	0.170	0.190
Constantine	0.137	0.128	0.140	0.270	0.121
Gulma	0.120	0.119	0.110	0.160	0.102
Bejaia	0.117	0.114	0.230	0.100	0.200
Jijel	0.095	0.079	0.250	/	0.190
Annaba	/	0.080	0.090	0.090	0.100

In conclusion, significant discrepancies exist in the Peak Ground Acceleration (PGA) values between our study and previous research for both the 100-year and 475-year return periods. Several factors contribute to these differences:

1. Data Sources: Variations in seismic data stem from how the earthquake catalog is managed, including the application of improved techniques and clearer criteria for data inclusion. Additionally, our study incorporates new data collected up to 2023, which may not be reflected in earlier studies.
2. Seismic Activity: The differences in hazard results for cities like Jijel and Bejaia can be linked to heightened seismic activity observed in recent years, influencing the current assessments.
3. Methodologies: Disparities in the software and Ground Motion Prediction Equations (GMPE) utilized for seismic hazard calculations also play a significant role in the variations observed in the results.

Overall, these factors highlight the evolving nature of seismic hazard assessments and the importance of using the latest data and methodologies to ensure accuracy and reliability.

2.6.1 Comparison with the Seismic Zonation of RPA 2024

a) Overview of the RPA 2024 Seismic Zonation

The *Règlement Parasismique Algérien (RPA 2024)* represents the most recent seismic design code in Algeria. It updates the RPA 99/2003 by incorporating a probabilistic seismic hazard approach that reflects new seismological data and recent earthquake events such as Béjaïa 2021 and Mila 2020. The seismic zonation is based on a return period of 475 years, using PGA as the principal hazard parameter. The country is divided into seven seismic zones (0 to VI), each associated with a reference acceleration coefficient Ak corresponding to soil type S1 (rock conditions). The values range from 0.07g in Zone I to 0.30g in Zone VI, with elastic response spectra (Type 1 or 2) assigned based on the dominant magnitude contributing to the hazard at each location (RPA 2024, Chapter 2).

A comparative table of PGA Values from This Study vs. RPA 2024 is given below

Table IV. 4 PGA values from this study vs. RPA2024

Wilaya	PGA in This Study (g)	RPA 2024 Zone	RPA 2024 Ak (g)	Discrepancy
Guelma	~0.09 – 0.10	Zone V	0.25	Underestimated
Skikda	~0.11 – 0.12	Zone V	0.25	Underestimated
Annaba	~0.10	Zone IV–V	0.20 – 0.25	Underestimated
El Tarf	~0.10	Zone IV–V	0.20 – 0.25	Underestimated
Souk Ahras	~0.07 – 0.09	Zone IV	0.20	Underestimated
Constantine	~0.12 – 0.13	Zone V	0.25	Underestimated
Mila	~0.14	Zone IV	0.20	Slightly underestimated
Jijel	~0.18 – 0.20	Zone V–VI	0.25 – 0.30	Underestimated
Sétif	~0.16 – 0.18	Zone IV	0.20	Slightly underestimated
Batna	~0.14	Zone III	0.15	Consistent
Oum El Bouaghi	~0.11 – 0.12	Zone IV	0.20	Underestimated
Khenchela	~0.12 – 0.13	Zone III–IV	0.15 – 0.20	Slightly underestimated
Tébessa	~0.05 – 0.07	Zone II–III	0.10 – 0.15	Underestimated
Biskra	~0.11 – 0.12	Zone III	0.15	Slightly underestimated

b) Interpretation and Discussion of Discrepancies

The comparative analysis highlights a **systematic underestimation of PGA values** in several wilayas—especially in **Guelma, Skikda, Constantine, and Jijel**—where the RPA 2024 classifies the hazard in **Zone V or higher (Ak = 0.25g or more)**, while the current study reports significantly lower PGA values.

Several factors may explain this discrepancy:

c) GMPEs:

The RPA 2024 does not disclose the specific GMPEs used in its hazard assessment, whereas the present study uses a logic-tree of peer-reviewed, regionally calibrated GMPEs. Differences in the attenuation models—especially if RPA 2024 adopts more conservative or global GMPEs—can directly affect PGA estimates.

d) Source Characterization and Seismicity Assumptions:

The RPA likely incorporates broader safety margins, possibly using worst-case fault scenarios or regional source zones with higher activity rates. In contrast, this study relies on refined seismotectonic models and updated catalog homogenization, which may produce lower but more physically justified estimates in some areas.

e) Local Amplification and Site Conditions:

The RPA 2024 Ak values are for rock conditions (S1), but actual site conditions may vary. If the RPA incorporated indirect amplification effects into its zonation (e.g., urban amplification potential), this could lead to higher Ak assignments even for S1.

f) Hazard Aggregation Methodology:

RPA 2024 likely integrates national-level hazard scenarios using deterministic overlays or higher epistemic safety factors, while this study focuses on probabilistic modeling at a regional scale with uncertainty quantification, which may produce more realistic yet less conservative estimates.

2.6.2 Conclusion

While the PGA values obtained in this study are consistent with RPA 2024 in certain regions (e.g., Batna, Sétif), a clear underestimation is observed in high-hazard zones such as **Guelma, Skikda, and Constantine**. These differences underscore the importance of understanding the assumptions embedded in national codes. The study highlights the benefits of transparent, regionally calibrated PSHA, but also recognizes the need to consider regulatory frameworks that prioritize safety margins in engineering applications.

General Conclusion

This thesis advances the field of seismic hazard assessment for northeastern Algeria by delivering a robust, data-driven evaluation that integrates the latest methodologies in earthquake catalog refinement. In response to the limitations of previous studies and national zoning frameworks, this work develops a unified moment magnitude catalog, enhancing the quality and reliability of seismic data essential for probabilistic seismic hazard assessment (PSHA). This catalog, carefully curated based on regional empirical relationships using rigorous statistical techniques such as the General Orthogonal Regression (GOR) method with appropriate value of the error variance ratio, marks a significant contribution to seismic data processing in Algeria.

Through a comprehensive assessment that combines geological, tectonic, historical, and instrumental evidence, this study precisely identifies and characterizes seismic source zones across the region. The hazard maps generated—quantified in terms of Peak Ground Acceleration (PGA) and spectral acceleration for critical return periods—provide essential tools for understanding seismic risk. Specifically, the results highlight that the PGA values with a 10% probability of exceedance in 50 years (475-year return period) could reach up to 0.2g, underscoring the importance of updated building standards for earthquake resilience.

This thesis not only addresses regional seismic hazard with heightened accuracy but also establishes a benchmark for future research and policy development. The findings support an urgent need to update Algeria's national building code to better reflect the seismic realities of the northeastern region, thereby enhancing the resilience of critical infrastructure against potential earthquake impacts.

Ultimately, this thesis provides a comprehensive framework for regional seismic hazard assessment that can serve as a valuable resource for seismologists, engineers, urban planners, and policymakers. It lays the groundwork for further studies in seismic hazard analysis and building code adaptation, supporting a future where northeastern Algeria is more resilient, better prepared, and informed by rigorous, state-of-the-art scientific analysis.

References:

Abacha, I. (2018). *Étude de la sismicité de la région Nord-Est de l'Algérie*

Abacha, I., Boulahia, O., Yelles-Chaouche, A., Bendjama, H., Fossen, H., Chabou, M. C., Roubeche, K., Rahmani, S. T.-E., Tikhamarine, E.-M., & Mohammedi, Y. (2023). The 24 January 2020 Mw 5.0 El Aouana Earthquake, Northeastern Algeria: Insights into a New NW–SE Right-Lateral Bejaia-Babors Shear Zone. *Pure and Applied Geophysics*, *180*(6), 1945-1971.

Adcock, R. J. (1878). A problem in least squares. *The Analyst*, *5*(2), 53-54.

Aki, K. (1963). *Some problems in statistical seismology*. Hawaii Institute of Geophysics, University of Hawaii.

Aki, K. (1965). Maximum likelihood estimate of b in the formula log N= a-bM and its confidence limits. *Bull. Earthquake Res. Inst., Tokyo Univ.*, *43*, 237-239.

Aki, K. (1969). Analysis of the seismic coda of local earthquakes as scattered waves. *Journal of geophysical research*, *74*(2), 615-631.

Akkar, S., & Bommer, J. J. (2010). Empirical equations for the prediction of PGA, PGV, and spectral accelerations in Europe, the Mediterranean region, and the Middle East. *Seismological Research Letters*, *81*(2), 195-206.

Ambraseys, N. (1990). Uniform magnitude re-evaluation of European earthquakes associated with strong-motion records. *Earthquake engineering & structural dynamics*, *19*(1), 1-20.

Ambraseys, N. N., Simpson, K. u., & Bommer, J. J. (1996). Prediction of horizontal response spectra in Europe. *Earthquake engineering & structural dynamics*, *25*(4), 371-400.

Anderson, T. W. (1984). Estimating linear statistical relationships. *The Annals of statistics*, *12*(1), 1-45.

Aoudia, A., Vaccari, F., Suhadolc, P., & Meghraoui, M. (2000). Seismogenic potential and earthquake hazard assessment in the Tell Atlas of Algeria. *Journal of Seismology*, *4*, 79-98.

Athmani, A., & Ademovic, N. (2023). Site effect influence on the seismic vulnerability of unreinforced masonry buildings in low to moderate seismic urban areas in Algeria. *Multidiscipline Modeling in Materials and Structures*, *19*(6), 1057-1086.

Baker, J., Bradley, B., & Stafford, P. (2021). *Seismic hazard and risk analysis*. Cambridge University Press.

Bakun, W. H. (1984). Magnitudes and moments of duration. *Bulletin of the Seismological Society of America*, *74*(6), 2335-2356.

Bakun, W. u., & Wentworth, C. (1997). Estimating earthquake location and magnitude from seismic intensity data. *Bulletin of the Seismological Society of America*, *87*(6), 1502-1521.

Balouch, M., Nemati, M., Bagheripour, M. H., & Rashidi, A. (2023). A probabilistic seismic hazard analysis in SE Iran; case study: Kerman province. *Journal of Iberian Geology*, *49*(3), 257-274.

Beldjoudi, H. (2011). *Etude de la sismicité du Nord Algerien* Université de Tlemcen-Abou Bekr Belkaid].

Beldjoudi, H., Guemache, M., Kherroubi, A., Semmane, F., Yelles-Chaouche, A., Djellit, H., Amrani, A., & Haned, A. (2009). The Lâalam (Béjaïa, north-east Algeria) moderate earthquake (M w= 5.2) on March 20, 2006. *Pure and Applied Geophysics*, *166*, 623-640.

Bellalem, F. (2007). *Aléa sismique en un site, méthodologie et application* Boumerdes].

Bellalem, F., Talbi, A., & Maouche, S. (2022). A unified MW parametric earthquake catalog for Algeria and adjacent regions (PECAAR). *Mediterranean Geoscience Reviews*, *4*(4), 427-443.

Benbelkacem, N., Ousadou, F., & Ayadi, A. (2022). Empirical calibration of earthquake magnitudes for the Tell Atlas (Northern Algeria). *Mediterranean Geoscience Reviews*, *4*(4), 445-452.

Bender, B., & Perkins, D. M. (1987). *SEISRISK III: a computer program for seismic hazard estimation*. US Government Printing Office.

Benouar, D., Aoudia, A., Maouche, S., & Meghraoui, M. (1994). The 18 August 1994 Mascara (Algeria) earthquake—a quick-look report. *Terra Nova*, *6*(6), 634-638.

Bernardi, F., Braunmiller, J., Kradolfer, U., & Giardini, D. (2004). Automatic regional moment tensor inversion in the European-Mediterranean region. *Geophysical Journal International*, *157*(2), 703-716.

Bethmann, F., Deichmann, N., & Mai, P. M. (2011). Scaling relations of local magnitude versus moment magnitude for sequences of similar earthquakes in Switzerland. *Bulletin of the Seismological Society of America*, *101*(2), 515-534.

Bindi, D., Pacor, F., Luzi, L., Puglia, R., Massa, M., Ameri, G., & Paolucci, R. (2011). Ground motion prediction equations derived from the Italian strong motion database. *Bulletin of Earthquake Engineering*, *9*, 1899-1920.

Bindi, D., Spallarossa, D., Eva, C., & Cattaneo, M. (2005). Local and duration magnitudes in northwestern Italy, and seismic moment versus magnitude relationships. *Bulletin of the Seismological Society of America*, *95*(2), 592-604.

Bommer, J. J. (2002). Deterministic vs. probabilistic seismic hazard assessment: an exaggerated and obstructive dichotomy. *Journal of earthquake engineering*, *6*(spec01), 43-73.

Bommer, J. J., Douglas, J., Scherbaum, F., Cotton, F., Bungum, H., & Fah, D. (2010). On the selection of ground-motion prediction equations for seismic hazard analysis. *Seismological Research Letters*, *81*(5), 783-793.

Boore, D. M., & Atkinson, G. M. (2008). Ground-motion prediction equations for the average horizontal component of PGA, PGV, and 5%-damped PSA at spectral periods between 0.01 s and 10.0 s. *Earthquake spectra*, *24*(1), 99-138.

Boore, D. M., Stewart, J. P., Seyhan, E., & Atkinson, G. M. (2014). NGA-West2 equations for predicting PGA, PGV, and 5% damped PSA for shallow crustal earthquakes. *Earthquake spectra*, *30*(3), 1057-1085.

Borman, P. (2021). Earthquake, magnitude. In *Encyclopedia of Solid earth geophysics* (pp. 243-254). Springer.

Bormann, P., & Khalturin, V. (1975). Relations between different kinds of magnitude determinations and their regional variations. *Proceed. XIVth General Assembly of the European Seismological Commission, Trieste, 16-22 September 1974*, 27-39.

Bormann, P., Liu, R., Ren, X., Gutdeutsch, R., Kaiser, D., & Castellaro, S. (2007). Chinese national network magnitudes, their relation to NEIC magnitudes, and recommendations for new IASPEI magnitude standards. *Bulletin of the Seismological Society of America*, *97*(1B), 114-127.

Bormann, P., Liu, R., Xu, Z., Ren, K., Zhang, L., & Wendt, S. (2009). First application of the new IASPEI teleseismic magnitude standards to data of the China National Seismographic Network. *Bulletin of the Seismological Society of America*, *99*(3), 1868-1891.

Bormann, P., Wendt, S., & DiGiacomo, D. (2013). Seismic sources and source parameters. In *New manual of seismological observatory practice 2 (NMSOP2)* (pp. 1-259). Deutsches GeoForschungsZentrum GFZ.

Boulahia, O., Abacha, I., Yelles-Chaouche, A., Bendjama, H., Kherroubi, A., Mohammedi, Y., Aidi, C., & Chami, A. (2021). Recent seismic activity in the Bejaia–Babors region (Northeastern Algeria): the case of the 2012–2013 Bejaia Earthquake Sequences. *Pure and Applied Geophysics*, *178*, 1253-1279.

Brune, J. N., & Engen, G. R. (1969). Excitation of mantle Love waves and definition of mantle wave magnitude. *Bulletin of the Seismological Society of America*, *59*(2), 923-933.

Cabañas, L., Rivas-Medina, A., Martínez-Solares, J., Gaspar-Escribano, J., Benito, B., Antón, R., & Ruiz-Barajas, S. (2015). Relationships between M w and other earthquake size parameters in the spanish IGN seismic catalog. *Pure and Applied Geophysics*, *172*, 2397-2410.

Carroll, R., & Ruppert, D. (1996). The use and misuse of orthogonal regression in linear errors-in-variables models. *The American Statistician*, *50*(1), 1-6.

Caruso, M., Pinho, R., Bianchi, F., Cavalieri, F., & Lemmo, M. T. (2021). Integrated economic and environmental building classification and optimal seismic vulnerability/energy efficiency retrofitting. *Bulletin of Earthquake Engineering*, *19*(9), 3627-3670.

Castellaro, S., & Bormann, P. (2007). Performance of different regression procedures on the magnitude conversion problem. *Bulletin of the Seismological Society of America*, *97*(4), 1167-1175.

Castellaro, S., Mulargia, F., & Kagan, Y. Y. (2006). Regression problems for magnitudes. *Geophysical Journal International*, *165*(3), 913-930.

Castello, B., Olivieri, M., & Selvaggi, G. (2007). Local and duration magnitude determination for the Italian earthquake catalog, 1981–2002. *Bulletin of the Seismological Society of America*, *97*(1B), 128-139.

Chioccarelli, E., Adriana, P., & Iunio, I. (2021). Italian Seismic Risk Maps Based on Code-Compliant Design. *Proceedings of the 31st European Safety and Reliability Conference (ESREL 2021)*.

Chioccarelli, E., Cito, P., Iervolino, I., & Giorgio, M. (2019). REASSESS V2. 0: software for single-and multi-site probabilistic seismic hazard analysis. *Bulletin of Earthquake Engineering*, *17*, 1769-1793.

Choy, G. L., & Boatwright, J. L. (1995). Global patterns of radiated seismic energy and apparent stress. *Journal of Geophysical Research: Solid Earth*, *100*(B9), 18205-18228.

Cornell, C. A. (1994). Statistical analysis of maximum magnitudes. *The earthquakes of stable continental regions*, *1*, 5.1-5.27.

Das, R., Wason, H., Gonzalez, G., Sharma, M. L., Choudhury, D., Lindholm, C., Roy, N., & Salazar, P. (2018). Earthquake magnitude conversion problem. *Bulletin of the Seismological Society of America*, *108*(4), 1995-2007.

Das, R., Wason, H., & Sharma, M. L. (2011). Global regression relations for conversion of surface wave and body wave magnitudes to moment magnitude. *Natural hazards*, *59*, 801-810.

Das, R., Wason, H., & Sharma, M. L. (2012). Magnitude conversion to unified moment magnitude using orthogonal regression relation. *Journal of Asian Earth Sciences*, *50*, 44-51.

Das, R., Wason, H., & Sharma, M. L. (2013). General orthogonal regression relations between body-wave and moment magnitudes. *Seismological Research Letters*, *84*(2), 219-224.

Das, R., Wason, H., & Sharma, M. L. (2014). Unbiased estimation of moment magnitude from body-and surface-wave magnitudes. *Bulletin of the Seismological Society of America*, *104*(4), 1802-1811.

Deichmann, N. (2006). Local magnitude, a moment revisited. *Bulletin of the Seismological Society of America*, *96*(4A), 1267-1277.

Durand, D. M. (1969). Mise au point sur la structure du Nord-Est de la Berbérie. *Bull Serv Carte Géol Agérie NS*, *39*, 89-131.

Dziewonski, A. M., Chou, T. A., & Woodhouse, J. H. (1981). Determination of earthquake source parameters from waveform data for studies of global and regional seismicity. *Journal of Geophysical Research: Solid Earth*, *86*(B4), 2825-2852.

Ekström, G., & Dziewonski, A. M. (1988). Evidence of bias in estimations of earthquake size. *Nature*, *332*(6162), 319-323.

Ferdi, S., & Harbi, A. (2014). Roman literary and epigraphic sources for the study of historical seismicity in Algeria circa 42–420 AD. *Journal of Seismology*, *18*, 277-287.

Field, E. H., Jordan, T. H., & Cornell, C. A. (2003). OpenSHA: A developing community-modeling environment for seismic hazard analysis. *Seismological Research Letters*, *74*(4), 406-419.

Forte, G., Chioccarelli, E., De Falco, M., Cito, P., Santo, A., & Iervolino, I. (2019). Seismic soil classification of Italy based on surface geology and shear-wave velocity measurements. *Soil Dynamics and Earthquake Engineering*, *122*, 79-93.

Fuller, W. A. (2009a). *Measurement error models*. John Wiley & Sons.

Fuller, W. A. (2009b). *Measurement error models* (Vol. 305). John Wiley & Sons.

Gabbianelli, G., Milanesi, R. R., Gandelli, E., Dubini, P., & Nascimbene, R. (2023). Seismic vulnerability assessment of steel storage tanks protected through sliding isolators. *Earthquake engineering & structural dynamics*, *52*(9), 2597-2618.

Gardner, J., & Knopoff, L. (1974). Is the sequence of earthquakes in Southern California, with aftershocks removed, Poissonian? *Bulletin of the Seismological Society of America*, *64*(5), 1363-1367.

Gasperini, P., & Ferrari, G. (2000). Deriving numerical estimates from descriptive information: the computation of earthquake parameters.

Gasperini, P., Lolli, B., & Vannucci, G. (2013a). Body-wave magnitude mb is a good proxy of moment magnitude M w for small earthquakes (m b< 4.5–5.0). *Seismological Research Letters*, *84*(6), 932-937.

Gasperini, P., Lolli, B., & Vannucci, G. (2013b). Empirical calibration of local magnitude data sets versus moment magnitude in Italy. *Bulletin of the Seismological Society of America*, *103*(4), 2227-2246.

Gasperini, P., Lolli, B., Vannucci, G., & Boschi, E. (2012). A comparison of moment magnitude estimates for the European—Mediterranean and Italian regions. *Geophysical Journal International*, *190*(3), 1733-1745.

Glaister, P. (2005). The use of orthogonal distances in generating the total least squares estimate. *Mathematics and Computer Education*, *39*(1), 21.

Grünthal, G. (1998). European macroseismic scale 1998 (EMS-98).

Grünthal, G., & Wahlström, R. (2003). An M w based earthquake catalogue for central, northern and northwestern Europe using a hierarchy of magnitude conversions. *Journal of Seismology*, *7*, 507-531.

Gupta, I. (2002). The state of the art in seismic hazard analysis. *ISET J Earthq Technol*, *39*(4), 311-346.

Gürboğa, Ş., & Sarp, G. (2013). Application of deterministic seismic hazard analysis on the area of 1970 Gediz earthquake. *International Journal of Engineering and Applied Sciences*, *5*(2), 18-37.

Gusev, A. (1991). Intermagnitude relationships and asperity statistics. *Pure and Applied Geophysics*, *136*, 515-527.

Gutdeutsch, R., Kaiser, D., & Jentzsch, G. (2002). Estimation of earthquake magnitudes from epicentral intensities and other focal parameters in Central and Southern Europe. *Geophysical Journal International*, *151*(3), 824-834.

Gutenberg, B. (1945). Magnitude determination for deep-focus earthquakes. *Bulletin of the Seismological Society of America*, *35*(3), 117-130.

Gutenberg, B., & Richter, C. (1955). Magnitude and energy of earthquakes. *Nature*, *176*(4486), 795-795.

Gutenberg, B., & Richter, C. F. (1936). Magnitude and energy of earthquakes. *Science*, *83*(2147), 183-185.

Gutenberg, B., & Richter, C. F. (1944). Frequency of earthquakes in California. *Bulletin of the Seismological Society of America*, *34*(4), 185-188.

Hainzl, S., Scherbaum, F., & Beauval, C. (2006). Estimating background activity based on interevent-time distribution. *Bulletin of the Seismological Society of America*, *96*(1), 313-320.

Hamdache, M., Bezzeghoud, M., & Mokrane, A. (1998). Estimation of seismic hazard parameters in the northern part of Algeria. *Pure and Applied Geophysics*, *151*, 101-117.

Hamdache, M., Peláez, J., Talbi, A., Mobarki, M., & López Casado, C. (2012). Ground-motion hazard values for Northern Algeria. *Pure and Applied Geophysics*, *169*, 711-723.

Hamidatou, M., Yahia, M., Yelles-Chaouche, A., Thallak, I., Stromeyer, D., Lebdioui, S., Cotton, F., Hallal, N., & Khemici, O. (2021). Seismic hazard analysis of surface level, using topographic condition in the Northeast of Algeria. *Pure and Applied Geophysics*, *178*, 823-846.

Hamlaoui, M., Vanneste, K., Baddari, K., Louail, L., Vleminckx, B., & Demdoum, A. (2017). Probabilistic seismic hazard assessment in the northeastern part of Algeria. *Arabian Journal of Geosciences*, *10*, 1-14.

Hanks, T. C., & Kanamori, H. (1979). A moment magnitude scale. *Journal of Geophysical Research: Solid Earth*, *84*(B5), 2348-2350.

Harbi, A., Benouar, D., & Benhallou, H. (2003). Re-appraisal of seismicity and seismotectonics in the north-eastern Algeria Part I: Review of historical seismicity. *Journal of Seismology*, *7*, 115-136.

Harbi, A., Maouche, S., & Ayadi, A. (1999). Neotectonics and associate seismicity in the Eastern Tellian Atlas of Algeria. *Journal of Seismology*, *3*, 95-104.

Harbi, A., Peresan, A., & Panza, G. F. (2010). Seismicity of Eastern Algeria: a revised and extended earthquake catalogue. *Natural hazards*, *54*, 725-747.

Heaton, T. H., Tajima, F., & Mori, A. W. (1986). Estimating ground motions using recorded accelerograms. *Surveys in Geophysics*, *8*(1), 25-83.

Helffrich, G. R. (1997). How good are routinely determined focal mechanisms? Empirical statistics based on a comparison of Harvard, USGS and ERI moment tensors. *Geophysical Journal International*, *131*(3), 741-750.

Jaeger, J., Cook, N., & Zimmerman, R. (2007). Fundamentals of rock mechanics, Blackwell Publishing. In: Oxford.

Johnston, A. C. (1996). Seismic moment assessment of earthquakes in stable continental regions—I. Instrumental seismicity. *Geophysical Journal International*, *124*(2), 381-414.

KADİRİOĞLU, F. T., & Kartal, R. F. (2016). The new empirical magnitude conversion relations using an improved earthquake catalogue for Turkey and its near vicinity (1900-2012). *Turkish Journal of Earth Sciences*, *25*(4), 300-310.

Kagan, Y. Y. (2003). Accuracy of modern global earthquake catalogs. *Physics of the Earth and Planetary Interiors*, *135*(2-3), 173-209.

Kanamori, H. (1977). The energy release in great earthquakes. *Journal of geophysical research*, *82*(20), 2981-2987.

Kanamori, H., & Anderson, D. L. (1975). Theoretical basis of some empirical relations in seismology. *Bulletin of the Seismological Society of America*, *65*(5), 1073-1095.

Khemis, A., & Athmani, A. (2023). Regional relations converting the surface and body wave magnitudes to moment magnitude for Northern Algeria using the general orthogonal regression method. *Acta Geophysica*, *71*(6), 2747-2762.

Kijko, A. (2004). Estimation of the maximum earthquake magnitude, m max. *Pure and Applied Geophysics*, *161*, 1655-1681.

Kijko, A., & Singh, M. (2011). Statistical tools for maximum possible earthquake magnitude estimation. *Acta Geophysica*, *59*, 674-700.

Knopoff, L. (1964). The statistics of earthquakes in Southern California. *Bulletin of the Seismological Society of America*, *54*(6A), 1871-1873.

Kolathayar, S., & Sitharam, T. (2018). *Earthquake hazard assessment: India and adjacent regions*. CRC press.

Kramer, S. L. (1996). *Geotechnical earthquake engineering* (W. J. Hall, Ed.). Prentice-Hall International Series in Civil Engineering and Engineering Mechanics.

Krystek, M., & Anton, M. (2008). A weighted total least-squares algorithm for fitting a straight line. *Measurement Science and Technology*, *19*(7), 079801.

Kumar, S., Sengupta, A., Hermanns, R., Dehls, J., Bhasin, R. K., Penna, I., & Gupta, V. (2022). Probabilistic Seismic Hazard Analysis (PSHA) to estimate the input ground motions for Co-seismic landslide hazard assessment: A case study on Himalayan highways, Sikkim India. *Physics and Chemistry of the Earth, Parts A/B/C*, *127*, 103157.

Laouami, N., Slimani, A., & Larbes, S. (2018). Ground motion prediction equations for Algeria and surrounding region using site classification based H/V spectral ratio. *Bulletin of Earthquake Engineering*, *16*, 2653-2684.

Li, H. C. (1984). A generalized problem of least squares. *The American Mathematical Monthly*, *91*(2), 135-137.

Lofi, J., Déverchère, J., Gaullier, V., Gillet, H., Gorini, C., Guennoc, P., Loncke, L., Maillard, A., Sage, F., & Thinon, I. (2011). *Seismic atlas of the Messinian Salinity Crisis markers in the Mediterranean and Black Seas* (Vol. 179). Société Géologique de France.

Lolli, B., & Gasperini, P. (2012). A comparison among general orthogonal regression methods applied to earthquake magnitude conversions. *Geophysical Journal International*, *190*(2), 1135-1151.

Lolli, B., Gasperini, P., & Vannucci, G. (2014). Empirical conversion between teleseismic magnitudes (mb and M s) and moment magnitude (M w) at the Global, Euro-Mediterranean and Italian scale. *Geophysical Journal International*, *199*(2), 805-828.

Lolli, B., Randazzo, D., Vannucci, G., Biondini, E., & Gasperini, P. (2023). Homogenization of magnitudes of the ISC Bulletin. *Geophysical Journal International*, *234*(3), 1771-1785.

Lolli, B., Randazzo, D., Vannucci, G., & Gasperini, P. (2020). The homogenized instrumental seismic catalog (HORUS) of Italy from 1960 to present. *Seismological Society of America*, *91*(6), 3208-3222.

Madansky, A. (1959). The fitting of straight lines when both variables are subject to error. *Journal of the american statistical association*, *54*(285), 173-205.

Marsan, D., & Lengline, O. (2008). Extending earthquakes' reach through cascading. *Science*, *319*(5866), 1076-1079.

Mazari, O. S., Sebaa, A., Amaro-Mellado, J.-L., & Martínez-Álvarez, F. (2023). Creating a homogenized earthquake catalog for Algeria and mapping the main seismic parameters using a geographic information system. *Journal of African Earth Sciences*, *201*, 104895.

McGuire, R. K. (1976). *FORTRAN computer program for seismic risk analysis* (2331-1258).

McGuire, R. K. (2001). Deterministic vs. probabilistic earthquake hazards and risks. *Soil Dynamics and Earthquake Engineering*, *21*(5), 377-384.

Meghraoui, M. (1988). Géologie des zones sismiques du nord de l'Algérie: Paléosismologie, tectonique active et synthese sismotectonique (Geology of seismic zones at northern Algeria: Paleoseismology, active tectonics and seismotectonics synthesis. Doctorat thesis Univ. Paris XI (Orsay), pp 356.

Mezcua, J. (2002). Seismic engineering course. *Madrid: Universidad Politécnica de Madrid*.

Mobarki, M., & Talbi, A. (2022). Spatio-temporal analysis of main seismic hazard parameters in the Ibero–Maghreb region using an Mw-homogenized catalog. *Acta Geophysica*, *70*(3), 979-1001.

Molchan, G., & Dmitrieva, O. (1992). Aftershock identification: methods and new approaches. *Geophysical Journal International*, *109*(3), 501-516.

Montilla, J. A. P., Hamdache, M., & Casado, C. L. (2003). Seismic hazard in Northern Algeria using spatially smoothed seismicity. Results for peak ground acceleration. *Tectonophysics*, *372*(1-2), 105-119.

Mouloud, H., & Badreddine, S. (2017). Probabilistic seismic hazard assessment in the Constantine region, Northeast of Algeria. *Arabian Journal of Geosciences*, *10*, 1-20.

Mueller, C. S. (2010). The influence of maximum magnitude on seismic-hazard estimates in the central and eastern United States. *Bulletin of the Seismological Society of America*, *100*(2), 699-711.

Nettis, A., Raffaele, D., & Uva, G. (2024). Seismic risk-informed prioritisation of multi-span RC girder bridges considering knowledge-based uncertainty. *Bulletin of Earthquake Engineering*, *22*(2), 693-729.

Nuttli, O. W. (1972). Magnitude, intensity and ground motion relations for earthquakes in the central United States. Proceedings of the International Conference on Microzonation for Safer Construction Research and Application,

Okal, E. A., & Talandier, J. (1989). Mm: A variable-period mantle magnitude. *Journal of Geophysical Research: Solid Earth*, *94*(B4), 4169-4193.

Okal, E. A., & Talandier, J. (1990). M m: Extension to Love waves of the concept of a variable-period mantle magnitude. *Pure and Applied Geophysics*, *134*(3), 355-384.

Ordaz, M., Martinelli, F., D'Amico, V., & Meletti, C. (2013). CRISIS2008: A flexible tool to perform probabilistic seismic hazard assessment. *Seismological Research Letters*, *84*(3), 495-504.

Peláez, J. A., Hamdache, M., & Casado, C. L. (2005). Updating the probabilistic seismic hazard values of northern Algeria with the 21 May 2003 M 6.8 Algiers earthquake included. *Pure and Applied Geophysics*, *162*, 2163-2177.

Petrova, N. V., & Gabsatarova, I. P. (2020). Depth corrections to surface-wave magnitudes for intermediate and deep earthquakes in the regions of North Eurasia. *Journal of Seismology*, *24*(1), 203-219.

Poggi, V., Garcia-Peláez, J., Styron, R., Pagani, M., & Gee, R. (2020). A probabilistic seismic hazard model for North Africa. *Bulletin of Earthquake Engineering*, *18*(7), 2917-2951.

Pondrelli, S., Salimbeni, S., Morelli, A., Ekström, G., Postpischl, L., Vannucci, G., & Boschi, E. (2011). European–Mediterranean regional centroid moment tensor catalog: solutions for 2005–2008. *Physics of the Earth and Planetary Interiors*, *185*(3-4), 74-81.

Real, C. R., & Teng, T.-L. (1973). Local Richter magnitude and total signal duration in southern California. *Bulletin of the Seismological Society of America*, *63*(5), 1809-1827.

Reasenberg, P. (1985). Second-order moment of central California seismicity, 1969–1982. *Journal of Geophysical Research: Solid Earth*, *90*(B7), 5479-5495.

Reiter, L. (1990). Earthquake hazard analysis: issues and insights. *(No Title)*.

Richter, C. F. (1935). An instrumental earthquake magnitude scale. *Bulletin of the Seismological Society of America*, *25*(1), 1-32.

Richter, C. F. (1958). ELEMENTARY SEISMOLOGY.

Ristau, J. (2009). Comparison of magnitude estimates for New Zealand earthquakes: moment magnitude, local magnitude, and teleseismic body-wave magnitude. *Bulletin of the Seismological Society of America*, *99*(3), 1841-1852.

Rydelek, P. A., & Sacks, I. S. (1989). Testing the completeness of earthquake catalogues and the hypothesis of self-similarity. *Nature*, *337*(6204), 251-253.

Sadigh, K., Chang, C., Abrahamson, N., Chiou, S., & Power, M. (1993). Specification of long-period ground motions: updated attenuation relationships for rock site conditions and adjustment factors for near-fault effects. Proc. ATC-17-1 Seminar on Seismic Isolation, Passive Energy Dissipation, and Active Control,

Saouma, V. E., & Hariri-Ardebili, M. A. (2021). *Aging, Shaking, and Cracking of Infrastructures: From Mechanics to Concrete Dams and Nuclear Structures*. Springer Nature.

Sawires, R., Peláez, J., Fat-Helbary, R., & Ibrahim, H. (2016). Updated probabilistic seismic-hazard values for Egypt. *Bulletin of the Seismological Society of America*, *106*(4), 1788-1801.

Sawires, R., Peláez, J. A., Fat-Helbary, R. E., Panzera, F., Ibrahim, H. A., & Hamdache, M. (2017). Probabilistic seismic hazard deaggregation for selected Egyptian cities. *Pure and Applied Geophysics*, *174*, 1581-1600.

Sawires, R., Peláez, J. A., & Hamdache, M. (2020). Probabilistic Seismic Hazard Assessment for United Arab Emirates, Qatar and Bahrain. *Applied Sciences*, *10*(21), 7901.

Scariano, S. M., & Barnett II, W. (2003). Contrasting total least squares with ordi nary least squares part I: Basic ideas and results. *Mathematics and Computer Education*, *37*(2), 141.

Scherbaum, F., & Kuehn, N. M. (2011). Logic tree branch weights and probabilities: Summing up to one is not enough. *Earthquake spectra*, *27*(4), 1237-1251.

Scholz, C. H. (2019). *The mechanics of earthquakes and faulting*. Cambridge university press.

Scordilis, E. (2006). Empirical global relations converting MS and mb to moment magnitude. *Journal of Seismology*, *10*, 225-236.

Sieberg, A. (1912). Über die makroseismische Bestimmung der Erdbebenstärke. *Gerl. Beitr. Geophys*, *11*, 227-239.

Sieberg, A. H., & Gutenberg, B. (1923). *Geologische, physikalische und angewandte Erdbebenkunde*. G. Fischer.

Sponheuer, W. (1964). *7. Tagung der Europäischen Seismologischen Kommission vom 24.9. bis 30.9. 1962 in Jena, DDR* (Vol. 77). Walter de Gruyter GmbH & Co KG.

Stein, S., & Wysession, M. (2009). *An introduction to seismology, earthquakes, and earth structure*. John Wiley & Sons.

Stepp, J. (1972). Analysis of completeness of the earthquake sample in the Puget Sound area and its effect on statistical estimates of earthquake hazard. Proc. of the 1st Int. Conf. on Microzonazion, Seattle,

Stromeyer, D., Grünthal, G., & Wahlström, R. (2004). Chi-square regression for seismic strength parameter relations, and their uncertainties, with applications to an M w based earthquake catalogue for central, northern and northwestern Europe. *Journal of Seismology*, *8*, 143-153.

Sucuoğlu, H., Akkar, S., Halûk, S., & Sinan, A. (2014). Basic earthquake engineering. *Basic Earthquake Engineering*.

Tang, C. C., Zhu, L., & Huang, R. (2016). Empirical Mw–ML, mb, and Ms conversions in western China. *Bulletin of the Seismological Society of America*, *106*(6), 2614-2623.

Thenhaus, P. C., Campbell, K. W., Chen, W., & Scawthorn, C. (2003). Seismic hazard analysis. *Earthquake engineering handbook*, *8*, 1-50.

Tinti, S., & Mulargia, F. (1985). An improved method for the analysis of the completeness of a seismic catalogue. *Lettere al Nuovo Cimento (1971-1985)*, *42*, 21-27.

Tsuboi, S., Abe, K., Takano, K., & Yamanaka, Y. (1995). Rapid determination of Mw from broadband P waveforms. *Bulletin of the Seismological Society of America*, *85*(2), 606-613.

Tsuboi, S., Whitmore, P. M., & Sokolowski, T. J. (1999). Application of M wp to deep and teleseismic earthquakes. *Bulletin of the Seismological Society of America*, *89*(5), 1345-1351.

Uhrhammer, R. (1986). Characteristics of northern and central California seismicity. *Earthquake Notes*, *57*(1), 21.

van Stiphout, T., Zhuang, J., & Marsan, D. (2012). Seismicity declustering. *Community online resource for statistical seismicity analysis*, *10*(1), 1-25.

Vanek, J. (1962). Standardization of magnitude scales. *Bulletin of the Academy of Sciences of the USSR Geophysics Series*, *2*, 108.

Vannoli, P., & Console, R. (2023). Improving seimic hazard assessment in the Mediterranean Region. *Annals of Geophysics*.

Vicente de Julián-Ortiz, J., Pogliani, L., & Besalu, E. (2010). Two-variable linear regression: modeling with orthogonal least-squares analysis. *Journal of chemical education*, *87*(9), 994-995.

Vila, J.-M. (1980). La chaîne alpine de l'Algérie orientale et des confins algéro-tunisiens. *These de Doctorat-es-sciences, Universite Pierre et Marie curie*.

Wang, Z. (2009). Seismic hazard vs. seismic risk. *Seismological Research Letters*, *80*(5), 673-674.

Wason, H., Das, R., & Sharma, M. (2018). Regression relations for magnitude conversion for the Indian region. *Advances in Indian Earthquake Engineering and Seismology: Contributions in Honour of Jai Krishna*, 55-66.

Wason, H., Das, R., & Sharma, M. L. (2012). Magnitude conversion problem using general orthogonal regression. *Geophysical Journal International*, *190*(2), 1091-1096.

Wells, D. L., & Coppersmith, K. J. (1994). New empirical relationships among magnitude, rupture length, rupture width, rupture area, and surface displacement. *Bulletin of the Seismological Society of America*, *84*(4), 974-1002.

Wheeler, R. L. (2009). *Methods of Mmax estimation east of the Rocky Mountains*. US Department of the Interior, Geological Survey.

Wiemer, S., & Wyss, M. (2000). Minimum magnitude of completeness in earthquake catalogs: Examples from Alaska, the western United States, and Japan. *Bulletin of the Seismological Society of America*, *90*(4), 859-869.

Woessner, J., & Wiemer, S. (2005). Assessing the quality of earthquake catalogues: Estimating the magnitude of completeness and its uncertainty. *Bulletin of the Seismological Society of America*, *95*(2), 684-698.

Wood, H. O., & Neumann, F. (1931). Modified Mercalli intensity scale of 1931. *Bulletin of the Seismological Society of America*, *21*(4), 277-283.

Yelles-Chaouche, A., Aidi, C., Beldjoudi, H., Abacha, I., Chami, A., Boulahia, O., Mohammedi, Y., Chimouni, R., Kherroubi, A., & Alilli, A. (2022). The recent seismicity of northern Algeria: the 2006–2020 catalogue. *Mediterranean Geoscience Reviews*, *4*(4), 407-426.

Yelles-Chaouche, A., Boudiaf, A., Djellit, H., & Bracene, R. (2006). Active tectonics in northern Algeria. *COMPTES RENDUS GEOSCIENCE*, *338*(1-2), 126-139.

Zaliapin, I., Gabrielov, A., Keilis-Borok, V., & Wong, H. (2008). Clustering analysis of seismicity and aftershock identification. *Physical review letters*, *101*(1), 018501.

Zhuang, J., Ogata, Y., & Vere-Jones, D. (2002). Stochastic declustering of space-time earthquake occurrences. *Journal of the american statistical association*, *97*(458), 369-380.

Appendix

Table II. 9: a sample of the homogenized catalog for magnitude range $M_w \geq 5,5$

Year	Month	Day	Hour	Min	Sec	Lat	Long	Depth	M_w
1719	3	6	0	0	0	37,1	8,5	/	5,956
1748	9	22	9	30	0	37,4	6	/	5,956
1750	5	9	0	0	0	37,2	7	/	5,956
1850	2	9	0	0	0	36,3	4,8	/	5,956
1859	3	9	19	0	0	37,2	7,4	/	5,956
1860	9	27	0	0	0	36,3	4,5	/	5,956
1862	8	22	17	0	0	37,2	5,1	/	5,956
1885	1	30	9	30	0	35,71	4,53	/	5,956
1891	10	23	20	45	0	36,57	4,31	/	5,956
1935	3	6	3	30	0	36,9	8,87	/	5,956
1942	3	2	22	23	27	36,5	5,2	/	5,956
1946	9	9	17	26	26	36,4	4,1	/	5,956
1949	2	17	21	1	0	36,52	5,24	/	5,956
1956	6	26	1	51	15	36	8,1	/	5,956
1957	11	13	19	16	24	36,28	5,41	3	5,956
1960	12	1	15	14	10	36,5	6	/	5,956
1962	3	20	19	15	0	36,9	8	/	5,956
1963	9	4	5	6	46	35,936	5,2968	25	5,677
1963	3	14	15	0	0	36,2	6,1	/	5,956
1964	10	21	19	17	44	36,23	4,38	5	5,956
1965	2	21	2	20	52	35,5	6,5	/	5,956
1965	8	7	6	18	2	35,2	4,7	/	5,956
1966	2	25	0	0	0	36,7	5,55	/	5,956
1967	4	5	8	31	10	35,5	4,9	/	5,956
1973	11	24	15	22	8	36,090	4,4238	3,7	5,5458
1973	11	24	15	22	6	36,06	4,47	8	5,956
1974	6	28	11	9	38	36,57	5,26	20	5,956
1974	7	28	0	0	0	36,25	5,48	0	5,956
1974	11	9	12	15	10	36,4	5	33	5,956
1975	7	11	7	18	47	36,3	5,37	33	5,956
1975	10	17	8	54	6	36,35	4,49	17	5,956
1976	12	1	1	33	9	36,5	8,6	0	5,956
1977	1	19	20	46	53	36,55	8,43	21	5,956
1977	2	9	13	55	3	36,42	8,47	41	5,956
1977	4	14	7	17	10	36,43	5,71	18	5,956
1980	12	21	0	59	32	36,34	7,58	10	5,956
1985	10	27	19	35	1	36,419	6,7794	24,6	5,8
2000	11	10	20	10	55	36,468	4,8213	19,1	5,7
2000	11	10	20	10	56	36,61	4,84	33	5,7

2006	3	20	19	44	25	36,71	5,32	10	5,956
2013	5	19	9	7	27	36,768	5,3109	6	5,6118
2021	3	18	0	4	6	36,92	5,21	10	6
2021	3	18	0	4	8	36,93	5,24	0	6
2021	3	18	0	17	5	36,910	5,3143	10	5,5757

Table II. 10: Number of earthquakes reported in each decade.

	Number of Earthquakes in a magnitude range								
	Gardner and Knopoff (1974)			Uhrhammer (1976)			Reasenberg (1985)		
Time in year	**2,5-3,5**	**3,51-4,5**	**4,51-6**	**2,5-3,5**	**3,51-4,5**	**4,51-6**	**2,5-3,5**	**3,51-4,5**	**4,51-6**
2014-2023	547	125	35	697	157	61	767	169	35
2004-2013	1245	278	29	1641	385	43	1694	378	27
1994-2003	229	150	25	333	188	30	360	199	26
1984-1993	15	29	7	15	35	7	15	33	7
1974-1983	3	50	21	3	65	27	3	70	27
1964-1973	2	25	19	3	32	20	3	34	19
1954-1963	15	39	21	15	47	21	15	52	24
1944-1953	9	48	5	11	55	5	12	55	5
1934-1943	2	24	7	2	29	7	2	34	7
1924-1933	1	23	7	1	26	7	1	28	7
1914-1923	4	21	6	4	21	6	4	21	7
1904-1913	9	28	2	10	30	2	8	30	2
1894-1903	2	6	2	2	6	2	2	6	2
1884-1893	1	7	6	1	7	6	1	7	7
1874-1883	1	7	0	1	7	0	1	7	0
1864-1873	4	7	0	4	6	0	4	6	0
1854-1863	0	7	6	0	7	6	0	7	6
1844-1853	0	0	2	0	0	2	0	0	2
1834-1843	0	0	0	0	0	0	0	0	0
1824-1833	0	0	0	0	0	0	0	0	0
1814-1823	0	0	0	0	0	0	0	0	0
1804-1813	0	0	0	0	0	0	0	0	0
1794-1803	0	0	0	0	0	0	0	0	0
1784-1793	0	0	0	0	0	0	0	0	0
1774-1783	0	0	0	0	0	0	0	0	0
1764-1773	0	0	0	0	0	0	0	0	0
1754-1763	0	1	0	0	1	0	0	1	0
1744-1753	0	0	2	0	0	2	0	0	2
1734-1743	0	0	0	0	0	0	0	0	0
1724-1733	0	0	0	0	0	0	0	0	0
1714-1723	0	0	1	0	0	1	0	0	1

1704-1713	0	0	0	0	0	0	0	0	0
1694-1603	0	0	0	0	0	0	0	0	0
1684-1693	0	0	0	0	0	0	0	0	0
1674-1683	0	0	0	0	0	0	0	0	0
1664-1673	0	0	0	0	0	0	0	0	0
1654-1663	0	0	0	0	0	0	0	0	0
1644-1653	0	0	0	0	0	0	0	0	0
1634-1643	0	0	0	0	0	0	0	0	0
1624-1633	0	0	0	0	0	0	0	0	0
1614-1623	0	0	0	0	0	0	0	0	0
1504-1613	0	0	0	0	0	0	0	0	0
1594-1603	0	0	0	0	0	0	0	0	0
1584-1593	0	0	1	0	0	1	0	0	1
1574-1583	0	0	0	0	0	0	0	0	0
1564-1573	0	0	0	0	0	0	0	0	0
1554-1563	0	0	0	0	0	0	0	0	0
1544-1553	0	0	0	0	0	0	0	0	0
1534-1543	0	0	0	0	0	0	0	0	0
1524-1533	0	0	0	0	0	0	0	0	0
1514-1523	0	0	0	0	0	0	0	0	0
1504-1513	0	1	0	0	1	0	0	1	0

Table II. 11: Earthquake distribution by time and magnitude

	Gardner and Knopoff (1974)						
Time period	T	2,5-3,5		3,51-4,5		4,51-6	
		N	N/T(λ)	N	N/T(λ)	N	N/T(λ)
2014-2023	10	547	54,7	125	12,5	35	3,5
2004-2013	20	1792	89,6	403	20,2	64	3,2
1994-2003	30	2021	67,4	553	18,4	89	3
1984-1993	40	2036	50,9	582	14,6	96	2,4
1974-1983	50	2039	40,8	632	12,6	117	2,3
1964-1973	60	2041	34	657	11	136	2,3
1954-1963	70	2056	29,4	696	9,9	157	2,2
1944-1953	80	2065	25,8	744	9,3	162	2
1934-1943	90	2067	23	768	8,5	169	1,9
1924-1933	100	2068	20,7	791	7,9	176	1,8
1914-1923	110	2072	18,8	812	7,4	182	1,7
1904-1913	120	2081	17,3	840	7	184	1,5
1894-1903	130	2083	16	846	6,5	186	1,4
1884-1893	140	2084	14,9	853	6,1	192	1,4
1874-1883	150	2085	13,9	860	5,7	192	1,3

1864-1873	160	2089	13,1	867	5,4	192	1,2
1854-1863	170	2089	12,3	874	5,1	198	1,2
1844-1853	180	2089	11,6	874	4,9	200	1,1
1834-1843	190	2089	11	874	4,6	200	1,1
1824-1833	200	2089	10,4	874	4,4	200	1
1814-1823	210	2089	9,9	874	4,2	200	1
1804-1813	220	2089	9,5	874	4	200	0,9
1794-1803	230	2089	9,1	874	3,8	200	0,9
1784-1793	240	2089	8,7	874	3,6	200	0,8
1774-1783	250	2089	8,4	874	3,5	200	0,8
1764-1773	260	2089	8	874	3,4	200	0,8
1754-1763	270	2089	7,7	875	3,2	200	0,7
1744-1753	280	2089	7,5	875	3,1	202	0,7
1734-1743	290	2089	7,2	875	3	202	0,7
1724-1733	300	2089	7	875	2,9	202	0,7
1714-1723	310	2089	6,7	875	2,8	203	0,7
1704-1713	320	2089	6,5	875	2,7	203	0,6
1694-1603	330	2089	6,3	875	2,7	203	0,6
1684-1693	340	2089	6,1	875	2,6	203	0,6
1674-1683	350	2089	6	875	2,5	203	0,6
1664-1673	360	2089	5,8	875	2,4	203	0,6
1654-1663	370	2089	5,6	875	2,4	203	0,5
1644-1653	380	2089	5,5	875	2,3	203	0,5
1634-1643	390	2089	5,4	875	2,2	203	0,5
1624-1633	400	2089	5,2	875	2,2	203	0,5
1614-1623	410	2089	5,1	875	2,1	203	0,5
1504-1613	420	2089	5	875	2,1	203	0,5
1594-1603	430	2089	4,9	875	2	203	0,5
1584-1593	440	2089	4,7	875	2	204	0,5
1574-1583	450	2089	4,6	875	1,9	204	0,5
1564-1573	460	2089	4,5	875	1,9	204	0,4
1554-1563	470	2089	4,4	875	1,9	204	0,4
1544-1553	480	2089	4,4	875	1,8	204	0,4
1534-1543	490	2089	4,3	875	1,8	204	0,4
1524-1533	500	2089	4,2	875	1,8	204	0,4
1514-1523	510	2089	4,1	875	1,7	204	0,4
1504-1513	520	2089	4	876	1,7	204	0,4
	Uhrhammer (1976)						
Time period	T	2,5-3,5		3,51-4,5		4,51-6	
		N	N	N	N/T(λ)	N	N/T(λ)
2014-2023	10	697	157	61	6,1	35	3,5

2004-2013	20	2338	542	104	5,2	64	3,2
1994-2003	30	2671	730	134	4,5	89	3
1984-1993	40	2686	765	141	3,5	96	2,4
1974-1983	50	2689	830	168	3,4	117	2,3
1964-1973	60	2692	862	188	3,1	136	2,3
1954-1963	70	2707	909	209	3	157	2,2
1944-1953	80	2718	964	214	2,7	162	2
1934-1943	90	2720	993	221	2,5	169	1,9
1924-1933	100	2721	1019	228	2,3	176	1,8
1914-1923	110	2725	1040	234	2,1	182	1,7
1904-1913	120	2735	1070	236	2	184	1,5
1894-1903	130	2737	1076	238	1,8	186	1,4
1884-1893	140	2738	1083	244	1,7	192	1,4
1874-1883	150	2739	1090	244	1,6	192	1,3
1864-1873	160	2743	1096	244	1,5	192	1,2
1854-1863	170	2743	1103	250	1,5	198	1,2
1844-1853	180	2743	1103	252	1,4	200	1,1
1834-1843	190	2743	1103	252	1,3	200	1,1
1824-1833	200	2743	1103	252	1,3	200	1
1814-1823	210	2743	1103	252	1,2	200	1
1804-1813	220	2743	1103	252	1,1	200	0,9
1794-1803	230	2743	1103	252	1,1	200	0,9
1784-1793	240	2743	1103	252	1,1	200	0,8
1774-1783	250	2743	1103	252	1	200	0,8
1764-1773	260	2743	1103	252	1	200	0,8
1754-1763	270	2743	1104	252	0,9	200	0,7
1744-1753	280	2743	1104	254	0,9	202	0,7
1734-1743	290	2743	1104	254	0,9	202	0,7
1724-1733	300	2743	1104	254	0,8	202	0,7
1714-1723	310	2743	1104	255	0,8	203	0,7
1704-1713	320	2743	1104	255	0,8	203	0,6
1694-1603	330	2743	1104	255	0,8	203	0,6
1684-1693	340	2743	1104	255	0,8	203	0,6
1674-1683	350	2743	1104	255	0,7	203	0,6
1664-1673	360	2743	1104	255	0,7	203	0,6
1654-1663	370	2743	1104	255	0,7	203	0,5
1644-1653	380	2743	1104	255	0,7	203	0,5
1634-1643	390	2743	1104	255	0,7	203	0,5
1624-1633	400	2743	1104	255	0,6	203	0,5
1614-1623	410	2743	1104	255	0,6	203	0,5
1504-1613	420	2743	1104	255	0,6	203	0,5
1594-1603	430	2743	1104	255	0,6	203	0,5

1584-1593	440	2743	1104	256	0,6	204	0,5
1574-1583	450	2743	1104	256	0,6	204	0,5
1564-1573	460	2743	1104	256	0,6	204	0,4
1554-1563	470	2743	1104	256	0,5	204	0,4
1544-1553	480	2743	1104	256	0,5	204	0,4
1534-1543	490	2743	1104	256	0,5	204	0,4
1524-1533	500	2743	1104	256	0,5	204	0,4
1514-1523	510	2743	1104	256	0,5	204	0,4
1504-1513	520	2743	1105	256	0,5	204	0,4
	Reasenberg (1985)						
Time period	**T**	2,5-3,5		3,51-4,5		4,51-6	
		N	N/T(λ)	N	N/T(λ)	N	N/T(λ)
2014-2023	10	767	76,7	169	16,9	35	3,5
2004-2013	20	2461	123,1	547	27,4	62	3,1
1994-2003	30	2821	94	746	24,9	88	2,9
1984-1993	40	2836	70,9	779	19,5	95	2,4
1974-1983	50	2839	56,8	849	17	122	2,4
1964-1973	60	2842	47,4	883	14,7	141	2,4
1954-1963	70	2857	40,8	935	13,4	165	2,4
1944-1953	80	2869	35,9	990	12,4	170	2,1
1934-1943	90	2871	31,9	1024	11,4	177	2
1924-1933	100	2872	28,7	1052	10,5	184	1,8
1914-1923	110	2876	26,1	1073	9,8	191	1,7
1904-1913	120	2884	24	1103	9,2	193	1,6
1894-1903	130	2886	22,2	1109	8,5	195	1,5
1884-1893	140	2887	20,6	1116	8	202	1,4
1874-1883	150	2888	19,3	1123	7,5	202	1,3
1864-1873	160	2892	18,1	1129	7,1	202	1,3
1854-1863	170	2892	17	1136	6,7	208	1,2
1844-1853	180	2892	16,1	1136	6,3	210	1,2
1834-1843	190	2892	15,2	1136	6	210	1,1
1824-1833	200	2892	14,5	1136	5,7	210	1,1
1814-1823	210	2892	13,8	1136	5,4	210	1
1804-1813	220	2892	13,1	1136	5,2	210	1
1794-1803	230	2892	12,6	1136	4,9	210	0,9
1784-1793	240	2892	12,1	1136	4,7	210	0,9
1774-1783	250	2892	11,6	1136	4,5	210	0,8
1764-1773	260	2892	11,1	1136	4,4	210	0,8
1754-1763	270	2892	10,7	1137	4,2	210	0,8
1744-1753	280	2892	10,3	1137	4,1	212	0,8
1734-1743	290	2892	10	1137	3,9	212	0,7

1724-1733	300	2892	9,6	1137	3,8	212	0,7
1714-1723	310	2892	9,3	1137	3,7	213	0,7
1704-1713	320	2892	9	1137	3,6	213	0,7
1694-1603	330	2892	8,8	1137	3,4	213	0,6
1684-1693	340	2892	8,5	1137	3,3	213	0,6
1674-1683	350	2892	8,3	1137	3,2	213	0,6
1664-1673	360	2892	8	1137	3,2	213	0,6
1654-1663	370	2892	7,8	1137	3,1	213	0,6
1644-1653	380	2892	7,6	1137	3	213	0,6
1634-1643	390	2892	7,4	1137	2,9	213	0,5
1624-1633	400	2892	7,2	1137	2,8	213	0,5
1614-1623	410	2892	7,1	1137	2,8	213	0,5
1504-1613	420	2892	6,9	1137	2,7	213	0,5
1594-1603	430	2892	6,7	1137	2,6	213	0,5
1584-1593	440	2892	6,6	1137	2,6	214	0,5
1574-1583	450	2892	6,4	1137	2,5	214	0,5
1564-1573	460	2892	6,3	1137	2,5	214	0,5
1554-1563	470	2892	6,2	1137	2,4	214	0,5
1544-1553	480	2892	6	1137	2,4	214	0,4
1534-1543	490	2892	5,9	1137	2,3	214	0,4
1524-1533	500	2892	5,8	1137	2,3	214	0,4
1514-1523	510	2892	5,7	1137	2,2	214	0,4
1504-1513	520	2892	5,6	1138	2,2	214	0,4